Implementing a new optically stimulated luminescence dosimetry system

A thesis submitted in partial fulfilment of the requirements for the degree of Master of Applied Science

Clement F. Conheady

B.Sc.

School of Applied Sciences

College of Science, Engineering and Health.

RMIT University

July 2013

Declaration

I certify that except where due acknowledgement has been made, the work is that of the author alone; the work has not been submitted previously, in whole or in part, to qualify for any other academic award; the content of the thesis is the result of work which has been carried out since the official commencement date of the approved research program; any editorial work, paid or unpaid, carried out by a third party is acknowledged; and, ethics procedures and guidelines have been followed.

Clement F Conheady

2013-07-04

Acknowledgments

I would like to thank my Supervisors past and present: Professor James Macnae (RMIT), Dr Trevor Ackerly (WBRC), Professor Peter Johnston (ARPANSA) and Ms Thu Tran (Barwon Health) for their suggestions, guidance and for patiently answering the same questions another time.

I also thank my colleges at William Buckland Radiotherapy Centre Frank, Matthew, Chris, Vanessa, Ryan, Janet, Sam, Craig, Sarah and Rob for the many unscheduled, unsolicited brainstorming sessions. Special thanks go to Frank Gagliardi for finding the worst of the logical and writing errors in each chapter before my supervisors saw them. Custom phantoms and jigs were constructed by Mr Neil Brouwer at WBRC. I acknowledge his fine technical assistance and thank him for his advice.

I must acknowledge the very timely input of Mr Leon Dunn from the Australian Clinical Dosimetry Service and thank him for sharing his techniques and experience at a time when the project was stalling. Mr Phil Francis (RMIT) provided irreplaceable assistance with the scanning electron microscope.

Thank you to Jeff Crosbie for reminding me that the cat sat on the mat.

Finally, to my Principessa, thank-you for the love and support you have shown me during the project. I promise not to do a PhD any time soon.

Table of contents

Declaration ii

Acknowledgments iii

Table of contents iv

Symbols v

Terms and abbreviations vi

1. Abstract 1

2. Background 4

3. Common materials and equipment 16

4. Common methods 26

5. SEM investigation of OSLDs 33

6. Reader internal calibration 41

7. Ambient light 46

8. Read routine inconsistency 52

9. Carousel wobble 65

10. Accumulated dose since last bleaching 79

11. Dose rate and irradiation angle 85

12. Calibration and measurement method 91

13. Conclusions 97

Appendix A. Uncertainty budget 100

Appendix B. Excluded influence quantities 102

References 105

Symbols

D_W	Delivered dose (Gy). The absorbed dose to water at the site of a dosimeter.
D_{CALC}	Calculated dose (Gy). The estimate of the dose delivered calculated using the method proposed in this project.
$N_{D,W}$	Absorbed dose to water calibration factor. A single value for a calibration batch of OSLDs (Gy/counts)
M	Dosimeter reading calculated from equation 2.1 (counts)
S	Raw signal (counts). The raw output from the PMT. Raw signal is calculated from equation 6.2.
S_{offset}	Residual reader dose offset (mrad).
S_{mrad}	Reader dose (mrad). The reader software's estimate of delivered dose using the internal calibration.
k_{ECF}	Element correction factor. Correction factor for the different sensitivities of individual OSLDs (dimensionless).
k_W	Wobble correction factor.
k_T	The read routine correction factor. Corrects for the change in dose reported between read routines. May be calculated differently during each experiment.
k_L	Non-linearity correction factor. Corrects for the change sensitivity with dose delivered since last bleaching.
a, b, ...	Curve fitting parameters (a, b, c, d, e, f, g). Defined differently in each experiment.
i,j	Indices. Defined differently in each experiment.
σ_X	Standard deviation in quantity X.
$\bar{X}$	Mean of quantity X.
p	Significance level

Some other symbols are defined in chapter 4 or locally within chapters.

Terms and abbreviations

Absorbed dose to water	The ratio of deposited energy to mass (BIPM 2006).
Anneal	A process that frees charge carriers from deep traps in the OSL or TL material (p 14).
Beam	A term for the radiation produced by a particular accelerating energy on treatment machine (e.g. 6 MV on TU2, Filter 1 on SXRT unit).
Bleach	A process that frees charge carriers from the dosimetric traps in the OSL or TL material (p 14).
DCF	Dose correction factor (p 17)
DCRC	Dosimeter calibration reference conditions (p 9).
Depression	A depression in a slab of solid water used to hold OSLDs (p 24).
Dose signal	The information stored in dosimetric traps in the Al_2O_3:C. This information cannot be directly accessed but can be estimated by observing OSL.
Expose	Refers to exposure to visible light.
Field	A particular combination of energy, collimation, MU.
Hole	A positive charge carrier, the absence of an electron in a crystal lattice.
IAEA	International Atomic Energy Agency.
Irradiate	Refers to exposure to ionising radiation.
LINAC	Radiotherapy linear accelerator (p 16).
MU	Monitor unit (p 17).
OSL	Optically stimulated luminescence.
OSLD	Disk shaped Al_2O_3:C OSL dosimeter supplied with the OSL system.
OSL system	The OSL reader and OSLD together.
PMT	Photomultiplier tube.
QA	Quality assurance (p 8).
Reader	The Bluelight OSL reader.
Read routine	The automated process in which the OSL reader optically stimulates and observes the OSL from each OSLD in turn.
RO	Radiation oncologist; a doctor specialising in radiotherapy.
SAD	Source-axis distance. The distance from the source along the beam's central axis.
SCRC	Source calibration reference conditions (p 8)
SXRT	Superficial x-ray radiotherapy (p 17).
TL/TLD	Thermoluminescence/thermoluminescent dosimeter.
TU1/2/3, LA4	LINAC names at WBRC (p 16)
WBRC	William Buckland Radiotherapy Centre, Alfred Hospital, Melbourne, Australia.

1. Abstract

The William Buckland Radiotherapy Centre (WBRC) purchased a new dosimetry system (OSL system) using Al_2O_3:C optically stimulated luminescence dosimeters (OSLD) for in vivo dosimetry on patients receiving megavoltage photon external beam radiotherapy. The primary aim of this project was to move from the OSL system's simple internal dose calculation method to a method that considers all the OSLD system's influence quantities.

The secondary aim of this project was to uncover the practical considerations, such as the effect of ambient light, which would guide the safe and accurate use of the OSLD system in the clinic.

An investigation was conducted into the structure of the OSLDs by using scanning electron microscopy (SEM) equipment at the RMIT Microscopy and Microanalysis Facility, Melbourne. The expectation was that this insight might inform later investigations into dosimetry using the OSLDs.

The development of a calculation method began with a compilation of possible influence quantities including: accumulated dose since last bleaching, individual OSLD sensitivity, dose rate, photon energy, dose signal fading at room temperature, and dose history. The need for further corrections for carousel wobble, and read routine inconsistency were discovered. It was determined that the reader software applies a constant calibration factor as well as a residual reader dose offset. The reader's internal calibration was therefore reverse engineered so calculation could be made using the raw signal from the PMT.

Conclusions of the experiments were that:

Exposing the OSLDs to room light for two minutes reduced the mean raw signal by 3.3 ± 2.9 %. There was no statistically significant difference between OSLDs stored in the dark and OSLDs covered by a single layer of black plastic and exposed to room light for two hours.

Raw signal values were observed to change significantly in repeated read routines where the values should be approximately the same. Slippage of the hub on the spindle at the beginning of some read routines; and therefore loss of stimulation at the periphery of OSLDs; was determined to be the dominant cause of inconsistency.

Readout after irradiation of forty-nine OSLDs with the same dose produced a pattern of raw signal values that suggested the reader's carousel wobbled as it rotated during the read routine. The pattern was modelled in order to correct for the wobble.

The relationship between raw signal and accumulated dose since last bleaching was modelled by delivering repeated 2 Gy irradiations to OSLDs up to 22 Gy. While the relationship was observed to be non-linear between 4 Gy and 22 Gy a function was found that modelled the relationship accurately.

Dose rate dependence was measured by varying the monitor units (measure of dose delivered by a radiotherapy linear accelerator) per minute. No statistically significant dose rate dependence was observed.

In order to investigate angular dependence, two groups of ten OSLDs were irradiated. One group was positioned perpendicular and the other group positioned parallel to the beam's central axis. There was no statistically significant difference between the raw signal values of the two groups.

Fading and energy corrections were found to be unimportant compared to the read routine inconsistency. Any need for dose history correction was eliminated in the proposed calibration method, as it is recommended that all OSLDs be calibrated before each use.

A method was devised which allows the calculation of an unknown dose from the values reported by the reader and incorporates a number of necessary corrections. Patient doses calculated via the OSL system's internal method or with the more comprehensive set of corrections devised in this project have significant uncertainty and may potentially lead to incorrect dose monitoring. An error in an in vivo dosimetry estimate may lead to an ill-informed clinical decision.

Therefore the OSL system should not be used clinically until the issues of read routine inconsistency and carousel wobble can be fully resolved. This recommendation and the above conclusions apply only to the specific devices used at WBRC and do not necessarily apply to other products by the same manufacturer or others.

2. Background

2.1. Introduction

In June 2012 the William Buckland Radiotherapy Centre (WBRC) took delivery of a Gammasonics Bluelight OSL Reader (Gammasonics Institute for Medical Research Pty Ltd Five Dock, NSW) and carbon-doped aluminium oxide (Al_2O_3:C) based optically stimulated luminescence dosimeters (OSLDs). This OSL system was intended to replace a thermoluminescent dosimetry (TLD) system for in vivo dosimetry on patients receiving megavoltage photon external beam radiotherapy.

The primary aim of this project was to move from the OSL system's simple internal dose calculation method to a method that considers all the OSLD system's influence quantities. The secondary aim of this project was to uncover the practical considerations, such as the effect of ambient light, which would guide the safe and accurate use of the OSLD system in the clinic.

Other dosimeters used in the radiotherapy clinic, such as ionisation chambers, thermoluminescent dosimeters, diodes and radiosensitive films, are well characterised in the literature. The OSL system is new and the characteristics were unknown.

The new method takes as its model the International Atomic Energy Agency's formalism for absorbed dose to water D_W, measured with a dosimeter (IAEA 2000a):

$$D_W = M \; N_{D,W} \tag{2.1}$$

where $N_{D,W}$ is the absorbed dose to water calibration factor and M is the dosimeter reading. For a batch of OSLDs in this project $N_{D,W}$ is obtained by cross-calibration with another dosimeter and M is calculated by:

$$M = S \prod k_X \tag{2.2}$$

where S is the raw signal from the photomultiplier tube (PMT) in the reader and k_X are factors to correct for various phenomena on which the raw signal depends. Combining equations 2.1 and 2.2 gives:

$$D_W = N_{D,W} \; S \; \prod k_X \qquad (2.3)$$

To convert the reader dose values, S_{mrad}, in the reader's dose report back to raw signal values, the reader's internal calibration method had to be reverse engineered

The phenomena on which the raw signal was expected to depend were: accumulated dose since last bleaching (k_I), individual OSLD sensitivity (k_{ECF}), dose rate (k_R), irradiation angle (k_A), photon energy (k_E), dose signal fading at room temperature (k_F), and dose history (k_H). The need for further corrections for carousel wobble (k_W), and read routine inconsistency (k_T) were discovered. All calibration factors were calculated so as to be applied via multiplication to the raw signal.

All calibration factors were calculated so as to be applied via multiplication to the raw signal.

Accuracy is very important to in vivo dosimetry estimates because large uncertainty or errors may lead to an incorrect dose being reported to the treating radiation oncologist (RO). An inaccurate in vivo dosimetry estimate may lead to an ill-informed clinical decision which will adversely affect the outcome of the patient's radiotherapy.

2.2. Radiotherapy

2.2.1. Introduction

Ionising radiation is utilised in many medical treatments because it can kill human cells (Hall & Giaccia 2006). Radiotherapy has a role in the radical treatment of malignant and benign cancers (Dark 2013); suppression of the immune system before bone marrow transplantations (Roberts, Chen & Seropian 2008); and pain management in palliative care (Faull et al. 2012). The most common radiotherapy source is a medical linear accelerator (LINAC) which delivers high energy electrons directly to the patient or to a metal target to produce high energy photons (Karzmark, Nunan & Tanabe 1993). Other radiotherapy sources include x-ray tubes, external gamma-emitters, internal radioactive sealed sources (brachytherapy) and radiopharmaceuticals (Khan 2003; Bushberg et al. 2002).

A necessary consequence of killing target cells is that many non-targeted cells will also be killed or damaged. Side-effects from non-target cell damage range from skin reddening,

tissue necrosis and organ failure up to cancer induction and death. Side-effects may appear immediately or may occur many years after treatment.

The likelihood of an effective radiotherapy treatment increases with increased radiation dose but so does the likelihood and severity of radiation side-effects although this may occur in different proportions (Marks et al. 2010). A Radiation Oncologist - with input from international guidelines, peer reviewed literature, other medical staff and the patient - must balance the probabilities and prescribe a dose of radiation.

Radiation dose is measured and prescribed in units of Gy (BIPM 2006). A course of radiotherapy is usually delivered in equal fractions, for example, 50 Gy in twenty-five 2 Gy daily doses on Monday to Friday for 5 weeks (Hoskin 2012).

2.2.2. Clinical risk management

Health care providers are expected to minimise clinical risk (Department of Health 2011). Risk can be quantified by the product of the likelihood of an adverse event and the consequence of the adverse event (Yoe 2011). Adverse events for a radiotherapy patient could be sub-optimal selection of treatment parameters (judgement errors) or incorrect delivery of the radiotherapy (treatment errors).

The likelihood of judgement errors can be reduced by training, research and clinical trials. The likelihood of treatment errors can be reduced by a range of quality assurance checks throughout the radiotherapy process (Millar et al. 1996).

Consequences of adverse events include over dosing or under dosing tissues with radiation. Over dosing patients with radiation can cause severe side-effects and death while under dosing can dramatically reduce the chance of treatment success.

According to ORH information notice 2005-01 (NYC DOHMH 2005) a patient in New York was severely overdosed in March 2005 when a software error corrupted MLC data and caused the MLC to wrongly be in the open position during three five-field IMRT treatments. Other examples of treatment accidents can be found in a report by the International Atomic Energy Agency (IAEA 2000b).

The likelihood and severity of consequences of some of these accidents may have been reduced if an independent indication of the accuracy of the treatment such as in vivo

dosimetry were included in the quality assurance. In the context of radiotherapy, in vivo dosimetry is a measurement of radiation dose in the patient (or just outside the patient surface) during the delivery of radiation.

High-quality in vivo dosimetry is part of a defence-in-depth strategy as suggested in IAEA's basic safety standards (IAEA 1996). In vivo dosimetry is valuable for detecting patient positioning errors; machine faults between routine checks; corruption of plan data; and unknown inaccuracies in monitor unit calculations.

2.2.3. Radiotherapy process at WBRC

A simple description of the radiotherapy process as conducted at WBRC is given in **Figure 2.1**. After diagnosis, the RO outlines the benefits and risks of radiotherapy and the patient decides if they want radiotherapy. The RO chooses a technique and fractionation then orders a course of treatment.

The patient's anatomy is simulated. Most patients in Australia are simulated using a CT scanner (Van Dyk & Taylor 1999; RANZCR 2011). The planner then makes a "plan" which contains the location and orientation of sources relative to the anatomy; the length of exposure; and the use of radiation beam modifiers (Barrett et al. 2009).

When the radiotherapy is delivered, much effort is made to position the patient anatomy identically as it was at simulation. Setup notes, immobilisation devices and in-room imaging help to ensure every fraction matches the plan exactly but very small random and systematic errors still occur.

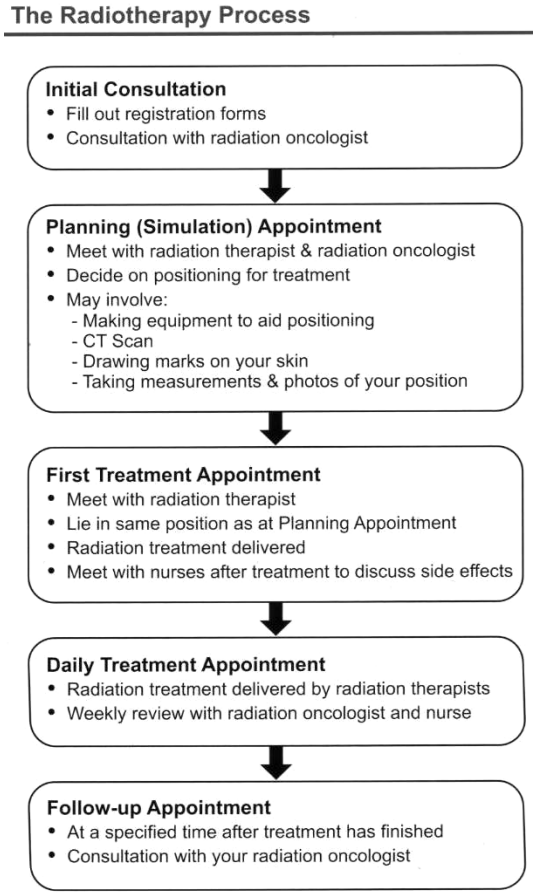

Figure 2.1. The radiation process as explained to WBRC patients (WBRC Patient Information Committee 2013). CC BY-NC-SA 3.0 AU Licence

Radiotherapy clinics operate quality assurance programs to minimise the occurrence of treatment errors (Millar et al. 1996). A quality assurance program will include document checking, equipment testing, patient setup verification, image guidance at treatment and in vivo dosimetry. WBRC are conducting a pilot study in which all external beam photon first treatments will be monitored in vivo with measurement of entrance dose.

2.3. Medical physics calibration

2.3.1. Source calibration reference conditions (SCRC)

When a physicist calibrates a radiation source, they will likely follow an internationally recognised code of practice (Thwaites et al. 1996; Almond et al. 1999; IAEA 2000a). Codes of practice reduce uncertainties and to allow ease of comparison between patient

outcomes in different clinics. Each code specifies the reference conditions, a set of values of influence quantities for which the calibration is valid without need for further correction factors (IAEA 2000a). Dosimeter position; phantom material and geometry; and radiation collimation will influence the calibration, as will temperature, pressure and relative humidity but these can be easily corrected for.

Reference conditions for LINAC photon calibration at WBRC, for example, are based on IAEA TRS 398 (2000a): and are summarised in Table 2.1. A depth of 10 cm is recommended but 5 cm depth is the local practice. LINAC commissioning records show that normalised profiles at 5 cm and 10 cm depth do not vary by more than 1 % within the central part of the 6 MV beam used in this project. SCRC is often approximated using solid water-equivalent phantoms in the place of water for routine source QA.

Table 2.1. Reference conditions for LINAC photon calibration at WBRC

Condition	Detail
Reference dosimeter	0.6 cm^3 graphite cylindrical ionisation chamber
Field size at isocentre	10 cm x 10 cm
Depth	5 cm
Source-to-surface distance	95 cm
Phantom material	Water

Reference conditions for SXRT unit calibration at WBRC are based on the IPEMB code of practice (Klevenhagen et al. 1996) and vary with beam energy.

2.3.2. Dosimeter calibration reference conditions (DCRC)

Dosimeters do not need to be calibrated under SCRC but can be calibrated under any conditions at which the dose is known. Some dosimeters at WBRC are calibrated at SCRC while others are calibrated at the depth of maximum dose (which may not be the surface).

Most experiments within this project are conducted under LINAC photon SCRC approximated using a solid water phantom (see sub-section 3.4). Experiments that utilise the SXRT unit are conducted at the surface of a solid water phantom.

2.3.3. Traceable calibration route

The calibration route for in vivo dosimeters used at WBRC is shown in **Figure 2.2**. Each arrow represents cross-calibration between two dosimeters under the same conditions.

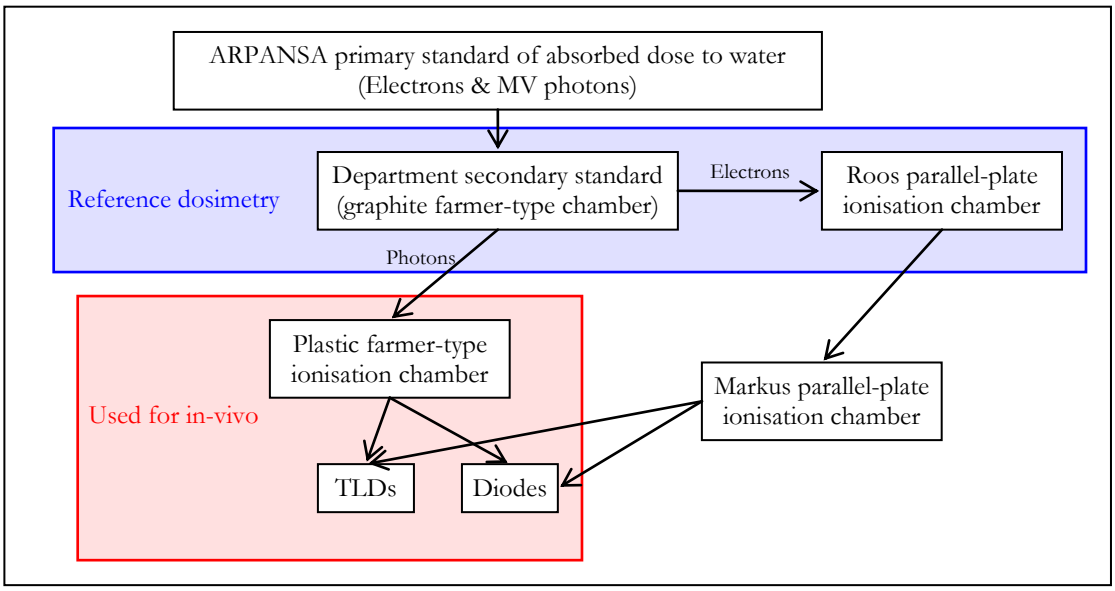

Figure 2.2. Calibration route for in-vivo dosimeters.

2.4. In vivo dosimetry

2.4.1. Ideal in vivo dosimetry

Ideally, every radiotherapy fraction would be accompanied by a real-time measurement of absorbed dose at several points in or on the patient (e.g. target volume, sensitive organs).

Any small discrepancy between the expected and measured dose would trigger the cessation of the fraction and an investigation. The investigation might involve testing of the treatment machine, checking the patient setup and confirming that the correct plan has been imported from planning.

The dose measurement device (dosimeter) would ideally have the characteristics listed in Table 2.2. The most unrealistic but desirable characteristic is the ability to measure dose inside the tissues in question.

Table 2.2. Characteristics of an ideal in vivo dosimeter.

Real-time monitoring/instantaneous results
Small volume to provide point dose instead of volume averaged dose
Ability to be placed inside organs or on without causing damage
High signal to noise ratio (SNR)
Constant response to radiation of all energies
Constant response to radiation in different temperature environments
Constant response to radiation from all incident angles
Constant response to radiation with time and dose history
Radiological equivalence to water
Waterproof housing
Ease of cleaning
Indestructibility
Calibration that is independent from the treatment source
Low cost
Ease of use

2.4.2. Real in vivo dosimetry

In a real radiotherapy clinic, a variety of dosimeters can be used for in vivo dosimetry. Each one has less-than-ideal characteristics that reduce accuracy; require corrections; limit their range of applications; or may skew a cost-benefit analysis towards not conducting in vivo dosimetry at every faction or for every patient. Equipment and personnel costs limit the implementation of vivo dosimetry

Real in vivo dosimetry does not necessarily measure the dose to the target volume or organs directly but measures the dose at a more accessible point. The relationship between doses at the two points is calculated during treatment planning. Therefore the estimate of the target or organ dose is dependent on the plan calculation (Ismail et al. 2009).

In vivo dosimeters are often calibrated using the radiation source that will be used to treat patients. Therefore the estimate of the target or organ dose is also dependent on the source calibration.

Ionisation chambers (Khan 2003; IAEA 2000a) have relatively flat energy response, high SNR and instantaneous results but are large, expensive and fragile. Diodes and MOSFETs (Rosenfeld 2011; Holmes-Siedle 1974; Huyskens et al. 2001) are smaller, cheaper and also offer instantaneous results but are susceptible to angular dependence and changes in sensitivity.

Passive dosimeters such as films (Butson et al. 2003; Niroomand-Rad et al. 1998; Oldham 2007; Williams & Metcalfe 2010), thermoluminescent (TL) dosimeters (Gagliardi et al., 2009, Marinello, 2007) and optically stimulated luminescent dosimeters (OSLD) (see sub-section 2.5) have a lower cost per dosimeter. The main drawback to passive dosimeters is the time delay between the irradiation and the results.

Exotic dosimeters such as gels (Wong et al. 2007), diamonds (Bucciolini et al. 2003), amorphous silicon EPID (back projection) (Piermattei et al. 2006) and plastic scintillator dosimeters (Beddar et al. 2003) have also been suggested as in vivo dosimeters. At present, these dosimeters are either expensive or require extensive in-house development.

2.4.3. Accuracy required

To give an indication of the accuracy required of an in vivo dosimeter, the following are examples of events that the dosimeter should be able to detect.

- → An incident report must be submitted to the Australian Radiation Protection and Nuclear Safety Agency (ARPANSA) via the Victorian Department of Health 'when during administration of a therapeutic dose of radiation from a radiation apparatus or a sealed radioactive source, the dose delivered differs from the total prescribed treatment dose by more than 10 %' (ARPANSA 2011).
- → At WBRC, if the treatment planning system and independent MU check differ by more than 5 % an investigation is required before treatment begins. If no resolution is found, the first fraction may be treated and a third estimate of the MUs required is made via in vivo dosimetry.
- → The daily x-ray output constancy must remain within 3 % (Klein et al. 2009).

Therefore an in vivo dosimeter should ideally have a combined standard uncertainty of less than 3 %. If the uncertainty is greater than 3 %, the dosimeter may still be able to resolve a MU discrepancy or detect a treatment incident but it will be less worth the costs associated with measurement.

2.4.4. Commissioning and quality assurance

International guidelines recommend establishing calibrations for vivo dosimeters in each beam and separately for entrance, exit and special treatments (Huyskens et al. 2001; Yorke et al. 2005; Van Dam and Marinello 2006). At WBRC, separate calibrations for 6

MV and 18 MV (see **Table 3.1**) would be required but only 6 MV is considered in this project.

The TLD system currently used at WBRC is calibrated under LINAC SCRC only. The assumption is made that the response of the TLDs is the same under SCRC and not under SCRC. The same assumption will be made in this project. Calibration at non-reference conditions (e.g. entrance, exit) for specific treatment types could easily be conducted as an extension to this project.

Quality assurance of passive in vivo dosimeters involves regular recalibration. At WBRC, calibration is repeated every three months. If the calibration varies significantly from recent values, the dosimeter may be discarded (Brady 2012).

2.5. Optically stimulated luminescence (OSL)

OSL is a similar process to thermoluminescence (TL) except that light is used instead of heat. TL dosimeters are widely used in Australian radiotherapy clinics. The main potential advantage of OSL is that readout may be repeated many times because the dosimetric information is not destroyed.

Electron-hole pairs are formed by ionising radiation. Under normal conditions, electrons and holes will recombine. The doping in an OSL material causes some charge carriers to become trapped (Metcalfe, Kron & Hoban 2007). At a later time, if the material is illuminated with photons of sufficient energy, the charge carriers can be freed. As the charge carriers fall back to their ground state, energy will be releases as luminescence (Yukihara & McKeever 2011).

WBRC hoped to benefit from of some of the other advantages of OSL dosimetry over TL dosimetry. For example, the turn-around time to reuse a TLD at WBRC is a whole working day because readout partially anneals and a full anneal is required before reuse. Theoretically OSLDs can be reused almost straight away as long as fading and previous irradiations are taken into account. Another advantage is that OSLDs can be enclosed in light-tight plastic cassettes or given protective coatings that would be damaged by the heat of TL.

A disadvantage of TL dosimetry at WBRC is that it requires a supply of high purity nitrogen gas for heating the dosimeters whereas OSL systems do not.

The "depth" of a trap describes how much energy is required to free the charge carrier. Shallow traps may be emptied by thermal vibration energy. So-called dosimetric traps are those that are usually emptied during dose readout. Some traps are so deep that optical stimulation cannot free the charge carriers; heating would be required.

The carbon-doped aluminium oxide crystals in the OSLDs emit blue light when stimulated by the reader's green laser. The light detected by the readers PMT is related to the amount of energy that was deposited by the ionising radiation (absorbed dose).

2.5.1. Clinical Al_2O_3:C OSL dosimetry

In an ESTRO guide on in vivo dosimetry, Van Dam and Marinello (2006, p. 63) stated that 'although further research on their basic characteristics is needed, OSL dosimeters have already been used on patients'. Much work has been published since using Al_2O_3:C OSLDs with (Jursinic 2007; Kim et al. 2012) and without plastic cassettes (Yukihara et al. 2010; Schembri & Heijmen 2007). Most authors concluded that OSL dosimetry is convenient and accurate if appropriate limitations and corrections are taken into account.

Out of field doses have been measured by Schembri and Heijmen (2007) with OSL "films" (Landauer Inc., Glenwood, IL, USA) that were 0.3 mm thick and 7.25 mm in diameter and by Scarboro et al.(2012) with Landauer nanoDots™ (Landauer Inc, Glenwood, IL, USA). Both groups found that correction is necessary to measure out of the field doses.

OSLDs are in use in Australia. According to responses to a post on the Australasian College of Physical Scientists & Engineers in Medicine list-server in May 2013, several radiotherapy clinics have purchased OSL based in vivo dosimetry systems. The Australian Clinical Dosimetry Service* has began using nanoDots™ in its level 1 remote auditing program (Dunn et al. 2013).

OSL can be exploited in near-real-time by OSLD and observing the luminescence via an optical-fibre (Aznar et al. 2004) but the only the passive application are considered in this project.

* http://www.arpansa.gov.au/services/ACDS/index.cfm

3. Common materials and equipment

The following equipment was used in multiple experiments within this project and are described here to aid brevity in later chapters. In later chapters, equipment will be referred to by the section or sub-section heading used in this chapter.

3.1. Sources

3.1.1. LINACs

WBRC maintains four radiotherapy LINACs from Varian Medical Systems (Palo Alto, CA, USA). The three dual-energy LINACS are beam matched which means that they are interchangeable in regards to beam characteristics.

Figure 3.1. Varian Clinac 21EX at WBRC (left) and the setup for an in vivo measurement (right).

The main advantage of megavoltage treatments is that skin is spared a significant portion of the dose delivered to the target volume. Absorbed dose is deposited via many secondary electron scatter events initiated by mostly Compton interactions with the primary beam. The maximum longitudinal range of the scattered electrons is approximately 1.5 cm for a 6 MV beam. Therefore the point of maximum dose in water occurs at approximately this depth (Metcalfe, Kron & Hoban 2007).

Table 3.1. Specifications of LINACs at WBRC. Electron beams are available on TU2, TU3 and LA4. Unless stated, all irradiations were with a 6 MV beam and had an average dose rate of 600 MU/min.

LINAC	Model	SN	Beams	Dose rates (MU/min)	Nominal calibration
TU1	Novalis Classic	1171	6 MV	160, 320, 480, 640, 800	1 cGy/MU
TU2 TU3 LA4	Clinac 21EX Clinac iX Clinac 21EX	2889 3843 2828	6 MV, 18 MV	100, 200, 300, 400, 500, 600	1 cGy/MU

The treatment beam passes through a transmission ionisation chamber (monitor chamber) which provides feedback to the beam steering and dose control circuits (Karzmark, Nunan & Tanabe 1993). The LINAC photon beam geometry is defined by two sets of tungsten jaws[*]. The field size is identified by the field width at 100 cm SAD in the two jaw axes. The "flat" region of the field, where the dose at 10 cm depth is uniform , is marginally smaller than the field width.

A monitor unit (MU) is a measure of dose delivered to a calibration point under reference conditions (Dutreix et al. 1997). The choice of reference conditions and the nominal relationship between dose in Gy and MU varies by clinic (see sub-section 2.3.1).

The actual dose delivered per MU (output) will drift over time but modern LINACs are very stable. In most experiments within this project, only the relative response to different irradiation or read routine conditions was studied, therefore the nominal calibration was used to choose the number of MU required.

In some experiments, a more accurate absolute dose was required. In these cases, the output was measured using a FC65-P ionisation chamber. The ratio of output to nominal calibration (DCF) was calculated and used to scale up or down the MU. Only integer numbers of MUs can be delivered.

3.1.2. SXRT unit

WBRC maintains a Pantak Therapax SXT 150 Series 3 x-ray unit capable of accelerating potentials from 30 to 150 kV (see Figure 3.2 and Table 3.2) for superficial x-ray radiotherapy (SXRT) of skin conditions. The unit is relatively simple and has no monitor

[*] Multileaf collimators downstream from the jaws ultimately define most patient treatment fields but were fully retracted during all experiments in this project.

ionisation chamber. The field is defined by one of several right circular cone-shaped applicator (see Figure 3.2).

There are eight available beams, known as 'filters'. Filters are referred to by their half value layer (HVL) in clinical prescriptions. HVL is the thickness of the specified material required to reduce the air kerma rate of the beam to half its initial value (Klevenhagen et al. 1996) and is an indication of the penetrative power of the beam. Filter 3 is out of clinical service and calibration is not maintained.

Table 3.2. Beams available on the Pantak SXT 150. (may 2012)

Filter no.	HVL	Tube potential (kV)	Filament current (mA)	Surface dose rate (CO) (Gy/min)	Timer correction (min)
1	0.3 mm Al	30	7.6	0.803	0.03
2	0.5 mm Al	40	8.6	0.980	0.03
3	0.4 mm Al	50	30.0	-	-
4	1.2 mm Al	80	4.0	1.010	0.02
5	2.2 mm Al	80	8.0	1.108	0.03
6	4.9 mm Al	100	10.5	1.165	0.03
7	8.4 mm Al	120	11.2	1.132	0.03
8	1.0 mm Cu	150	13.2	1.132	0.04

Planning consists of calculating a treatment time which is entered into the unit console in minutes:

$$\text{treatment time} = \frac{\text{SD}}{\text{CO}} + \text{timer correction} \tag{3.1}$$

where SD is surface dose required in Gy, CO is the current calibrated output in Gy/min (see Table 3.2). The timer correction is required because the unit ramps up to a stable dose rate.

Figure 3.2. The treatment head of theSXRT unit at WBRC. The image shows a 10 cm diameter applicator inserted with a measurement jig (not used in this project).

3.2. Dosimeters

3.2.1. OSLDs

The OSLDs supplied as part of the system are approximately 6 mm in diameter and 0.3 mm thick. The aluminium oxide (Al_2O_3:C) is in a powder form that has been printed on to a polyester substrate and protected on both faces by a coating.

The OSLDs are punched from a larger sheet. The OSLDs are very similar in appearance to the dosimeter inside a nanoDot™ (Landauer Inc., Glenwood, IL, USA) (see Figure 3.3).

Figure 3.3. One OSLD supplied by Gammasonics (bottom left) next to a nanoDot™ (bottom right) taken out of its cassette (top).

Using OSLDs without light-tight cassettes has several potential advantages. Firstly, they can be manufactured in smaller sizes and even cut smaller again by the user although some sensitivity may be lost. The smaller size could enable measurements in smaller radiation fields, inside phantoms or under patient bolus or shielding.

Charles et al. (2012) used measurements and a Monte Carlo model of a nanoDot™ to show that the 0.5 mm air gap within the plastic cassette causes it to under-respond in small stereotactic fields.

Another potential advantage is that OSLDs sealed by their protective coating may be able to be washed, or even sterilised between in vivo measurements.

The main advantage of light-tight cassettes is that they allow handling, measurements, storage and loading into the reader to be done in ordinary workplace lighting. Another is that bar-codes can be printed on the cassettes to eliminate the constant possibility of mixing up dosimeters.

OSLDs in this project are often assigned temporary numbers but these apply only for the current experiment. For a description of the SEM examination of the OSLDs see chapter 5.

3.2.2. Ionisation chambers

Ionisation chambers were used in this project to measure or monitor the output of a LINAC. The two chambers used were a farmer-type FC65-P (SN 2133) and a CC13 (SN 5676) both made by IBA Dosimetry GmbH (Schwarzenbruck, Germany).

The FC65-P is regularly cross calibrated against a reference ionisation chamber with a calibration traceable to the Australian primary standard. An expected value of charge per 200 MU is maintained for each beam. Stability checks are conducted regularly on the FC65-P using a ^{90}Sr source.

At WBRC the CC13 is cross calibrated against a non-reference farmer-type chamber but no stability checks are conducted. In this project, the CC13 is only used for monitoring output stability.

Figure 3.4. Two cylindrical ionisation chambers, a CC13 (top) with a FC65-P (bottom).

3.2.3. Electrometer

The ionisation chambers were used in conjunction with either of two interchangeable Dose 1 electrometers (SN 10056 and 15384) made by IBA Dosimetry GmbH (Schwarzenbruck, Germany). The electrometers are regularly compared and checked for stability.

Figure 3.5. Dose 1 electrometer.

3.3. Reader

Reader for this project was a Gammasonics Bluelight OSL Reader (Gammasonics Institute for Medical Research Pty Ltd Five Dock, NSW: SN OBL-C6-001). The reader is still under active development; therefore the findings of this project cannot necessarily be applied to other readers of the same model or from the same manufacturer.

The reader arrived with a dedicated computer which controls movement of the reader's parts. The software keeps a database of results as reader dose values. The database is stored using Microsoft® Access 2002. Results can be viewed directly via Access, via the

in-software database interface or exported as a comma separated values (.csv) file from the software.

The OSLDs can sit in any of the forty-nine numbered recesses in the reader's carousel (Figure 3.6 a and b). The carousel has fifty recesses but recess 1 must remain empty. Each recess has a 4 mm diameter gap in the bottom through which the OSLD is stimulated. The top of each recess is open.

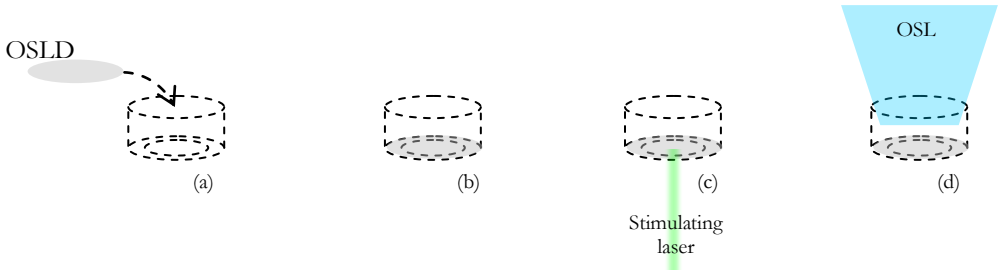

Figure 3.6. Placement and stimulation of OSLDs inside a recess. The dashed cylinder represents one recess in the carousel. The dashed circle in the bottom of the recess represents the 4 mm diameter gap.

The carousel is placed into the tray (Figure 3.7 top left). Before a read routine, the carousel is automatically retracted into the reader and onto a hub. The hub (Figure 3.7 top right) sits atop a spindle which, with the help of a stepper motor, rotates the hub and carousel (Figure 3.7 bottom left). The hub is secured to the spindle via three grub screws running perpendicular to the spindle rotation axis.

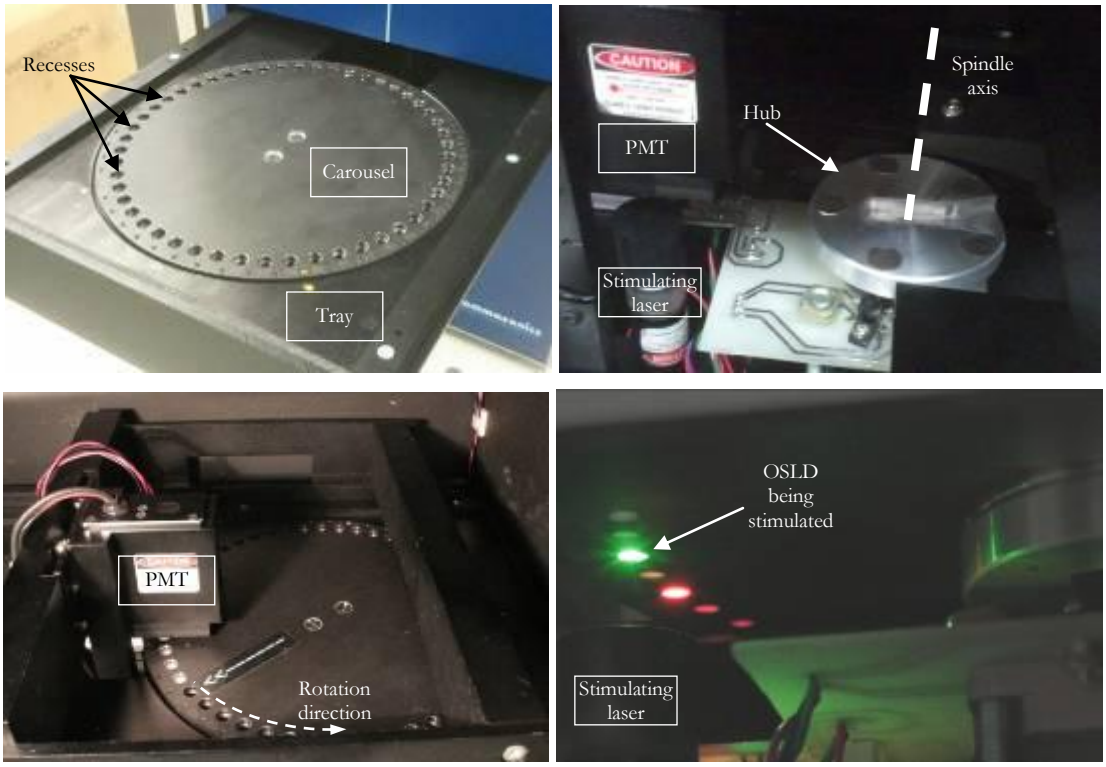

Figure 3.7. Photos showing various parts and functions of the reader.

Running a read routine activates a series of processes: (1) identify which recesses contain OSLDs; (2) take a dark count PMT reading; and (3) stimulate each OSLD (Figure 3.7 bottom right) and record the PMT signal. Each OSLD is positioned in turn between the PMT and stimulating laser by one-fiftieth revolutions (7.2°) of the spindle. A read routine of forty-nine OSLDs takes approximately 4.5 minutes.

Before any tray movement and before a read routine, the spindle zero position is re-established. The zero position is the only angle at which the carousel can slide onto the hub without jamming the tray. The zero position also provides a constant starting point for each read routine.

Through observation of the reader in operation, it has been concluded that an independent feedback system is used to determine which position of the stepper motor is zero while the spindle makes one or more revolutions. The red light visible in Figure 3.7 (bottom right) is presumed to be part of this system.

3.4. Solid water

All irradiations of OSLDs in this project were conducted in a RW3 "solid water" slab phantom (PTW-Freiburg, Freiburg, Germany). RW3 is polystyrene with titanium oxide incorporated, which produces a white colour. RW3 is not radiologically water equivalent at superficial x-ray energies (Hill, Kuncic & Baldock 2010) but dose accuracy is not required at superficial energies in this experiment.

The RW3 is slightly denser than water (Seco & Evans 2006). Therefore 5 cm depth in solid water is approximately equal to 5.2 $g.cm^{-2}$ (i.e. 5.2 cm depth in water). In a 6 MV beam on LA4, absorbed dose is 1.2 % lower at 5.2 $g.cm^{-2}$ than at 5.0 $g.cm^{-2}$ depth. This must be considered when cross-calibrating dosimeters.

Most of the experiments in this project relay on comparison of S_{mrad}, S or M values from groups of OSLDs under different conditions (irradiation conditions, timings, reader conditions). The error introduced to these comparisons by the density of solid water is minimal. Therefore, solid water was assumed to have density of 1.000 $g.cm^{-3}$ for these experiments.

The phantom comprises of many general-use 1 cm thick slabs, a range of thinner slabs with various thicknesses (1 mm to 5 mm), and several specialised slabs with cavities for detectors. All slabs are 30 cm wide and 30 cm long.

Two general-use slabs were modified by milling a grid of twenty-five 0.3 mm deep depressions into the centre of the front face of both slabs. The depressions were milled in five rows, 1.5 cm apart and each row contained five depressions 1.5 cm apart. Therefore all twenty five OSLDs can be irradiated within a 6.6 cm x 6.6 cm square.

3.5. Bleaching light-chamber

OSLDs were bleached using an in-house manufactured fluorescent tube light-chamber. Two Crompton (Padstow, NSW) LFD10 linkable fluorescent fittings were attached to the inside-top of a wooden box. The tubes each put out approximately 500 lumens at 6500K (daylight). The tubes can be left on for days without heating up.

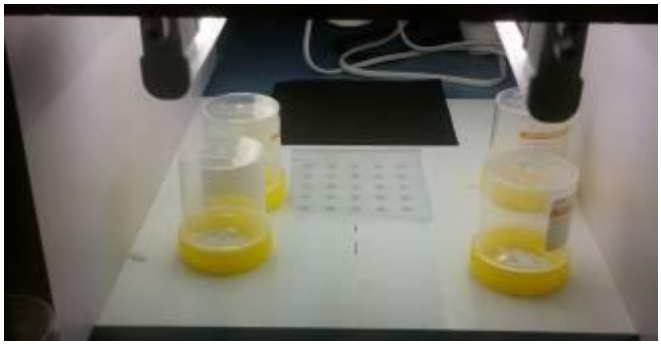

Figure 3.8. OSLDs were bleached in the light-chamber in the solid water slab and in specimen jars.

4. Common methods

4.1. Experimental

4.1.1. Read routine timing

Various investigators (Reft 2009; Danzer et al. 2007; Dunn et al. 2013) have observed that the decay of the OSL signal from Al_2O_3:C stabilises within approximately 15 minutes after irradiation. All read routines are run between 30 minutes and approximately two hours after irradiation. See Appendix B for more discussion of time effects.

4.1.2. Bleaching

A distinction must be made between bleaching and annealing. In this project, bleaching means to empty dosimetric traps so that the reader will report effectively zero dose. Annealing refers to emptying much deeper traps that require heating. No annealing was conducted in this project.

The manufacturer of the reader verbally advised reusing the OSLDs and subtracting previous measurements without bleaching. The manufacturer also suggested that bleaching was possible and that they may supply a bleaching device in the future.

One consequence of not bleaching between uses is that the OSLDs must be kept in the dark; even while resealing them after a read routine in preparation for the next irradiation. Another consequence is that dose signal will fade at room temperature. In addition to the small loss of dose signal from laser stimulation, correcting subsequent raw signals for several partially-faded previous irradiations may be very difficult.

The consequences of bleaching between uses are the possible change in sensitivity and the time taken to bleach the OSLDs. To bleach OSLDs, they were placed in the light chamber (see section 3.5). OSLDs were usually bleached for several days, after which a read routine was run to check that they have negligible residual dose. A raw signal value less than 100 counts is considered negligible because this represents less than 0.1 % of the raw signal from a 1 Gy irradiation.

For each experiment, unless stated, all OSLDs were bleached since their previous use or were being used for the first time since delivery from the vendor. In either case, a read

routine was run to check that they have negligible residual dose. Bleaching usually occurred for several days but twenty hours as a minimum.

4.1.3. OSLD handling

OSLDs were handled with MacIndoe forceps, vacuum tweezers or gloved hands. All handling was done in the dark unless exposure to light is specified.

4.1.4. Equipment warm-up

Before each irradiation for this project, radiation sources were warmed up with several typically-sized irradiations. The electrometer (if used) was switched on for several hours and ionisation chambers were plugged in and placed in the treatment room within phantoms to come to room temperature. A pre-irradiation of 1000 MU and background signal measurement were conducted for each experiment. The reader was also allowed to warm up for several hours before any read routines were run.

4.2. Calculation

4.2.1. Microsoft® Office Excel

Most of the analysis required for this thesis was conducted using Microsoft® Office Excel 2003 (11.8169.8172) SP3. Excel functions were validated against the methods and equations described below.

4.2.2. Standard deviation

The standard deviation was frequently calculated as a measure of the spread of the distribution of results. The Excel function STDEV() was used frequently in this project.

$$\sigma_X = \sqrt{\frac{\sum(X - \bar{X})^2}{n - 1}} \tag{4.1}$$

4.2.3. Linear regression

Linear regression is a technique in which a straight line of best fit through measured data is calculated. The straight line helps to determine if two variables X and Y are correlated. The following equations from Mould (1989) give characteristics of the straight line:

$$\text{Y-axis intercept} = \frac{\sum X \sum XY - \sum X^2 \sum Y}{(\sum X)^2 - N(\sum X^2)} \tag{4.2}$$

$$\text{Gradient} = \frac{\sum X \sum Y - N \sum XY}{(\sum X)^2 - N(\sum X^2)} \tag{4.3}$$

$$r^2 = \left(\frac{\sum [(X - \bar{X})(Y - \bar{Y})]}{\sqrt{[\sum (X - \bar{X})^2][\sum (Y - \bar{Y})]}} \right)^2 \tag{4.4}$$

The r^2 value is the coefficient of determination and gives an indication of correlation between X and Y. A value of 1 (or -1) indicates perfect positive (or negative) correlation. A value of 0 indicates no correlation. The r^2 is an indirect measure of goodness-of-fit.

In this project, linear regression and curve fitting is calculated using the LINEST() Excel function. LINEST() produces an array so the required values are accessed via the INDEX() function.

4.2.4. Curve fitting

Non-linear curve fitting was calculated using TableCurve™ 2D (Windows version 4.06, AISN Software Inc.). The values of the dependent and independent variables were transfered into TableCurve™ and the fit equation was selected from a list ranked by r^2 value. The selected equation and corresponding fit parameters were then transferred out of Tablecurve™ and the modelled values of the dependent variable were calculated in Excel.

The help files for Tablecurve™ dos not give an equation for r^2 but several trials show the values to be very similar to those calculated using the Excel function.

4.2.5. Test for plausibility of a normal model

To test if a sample of n results or a population has a normal distribution a histogram can be plotted but the shape is dependent on choice of counting interval unless n is very high.

Alternatively, the results X can be sorted into ascending order and paired with ascending normal scores m_i:

$$m_i = P\left(i \times \frac{1}{n+1}\right) \tag{4.5}$$

where P(ζ) is the area under the standard normal curve between ζ and −∞. The Excel function NORMSINV() was used to calculate P.

The normal scores are the idealised n-sized sample from the standard normal distribution (Johnson & Bhattacharayya 1992). If the plot of X vs m_i is a straight line then the results are normally distributed. The gradient of the line of best fit is σ_X and the m-axis intercept is $\bar{X}$. The r^2 value of the gives an indication of the normal distribution

The normal scores can be converted into the idealised sample from with the same mean and standard deviation using:

$$X_{ideal} = m_i \times \sigma_X + \bar{X} \tag{4.6}$$

The goodness-of-fit between the ideal and real results can be established with a χ^2 test (see sub-section 4.4.3).

4.3. Uncertainty

Uncertainty was calculated using the ISO Guide to the Expression of Uncertainty in Measurement (BIPM 2008) with guidance from Bentley (2003).

Uncertainty is reported using the ± symbol or in a separate column in a table. In both cases the expanded uncertainty is reported. The expanded uncertainty is the interval that is estimated to contain the measurand with 95 % probability.

$$\text{Expanded uncertainty} = \text{standard uncertainty} \times \text{coverage factor} \tag{4.7}$$

The coverage factor depends on the degrees of freedom, υ. Values were taken from Bentley (2003).

4.4. Hypothesis testing

Table 4.1 is a generalised schedule for hypothesis testing based on a schedule by Mould (1989). A variety of hypothesis tests have been developed. The way these tests were used in this project are described briefly in this section.

Table 4.1. Generalised schedule for hypothesis testing.

1	Consider the problem to be studied.
2	State the hypothesis, H_0.
3	Ensure that the chosen test is valid for testing H_0.
4	Chose a significance level.
5	Calculate the test statistic using the formula appropriate for the test.
6	Consult a table of values of the test statistic stated in terms of probability levels (p-value) and degrees of freedom.
7	Compare the probability level derived from the test with the significance level to accept or reject H_0.

The schedule in Table 4.1 is simplified in this project for several reasons. Firstly, each test is used in only one way (see Table 4.2). Secondly, Excel functions give the derived probability level without first calculating the test statistic.

Table 4.2. Hypothesis tests used in this project.

Test	**Samples**	**H_0**
t	Two un-paired samples	Both samples were taken from the same population
ANOVA	More than two samples/groups	All groups were taken from the same population
χ^2	Expected and observed results	There is no difference between the model and the observed results

A p-value below the significance level suggests rejection of H_0. The significance level represents the risk of falsely rejecting H_0. A significance level of 0.05 has been chosen uniformly for this project but the p-value is given to show if H_0 would still be rejected at a different significance level.

A p-value above the significance level does not confirm the null hypothesis but a high p-value represents a low risk of falsely accepting the null hypothesis. The exact risk is dependent on the sample size and underlying population.

Good experimental design considers the sample size required to conclusively prove or disprove H_0. Sample size is sometimes limited by the number of OSLDs available or by the limit of forty-nine OSLDs that can be examined in the same read routine.

4.4.1. Student's t-test

The t-test is a hypothesis test suitable for small samples taken from a normally distributed population (Mould 1989).

$$t = \frac{\text{Difference in means}}{\text{Standard error of the difference in means}} \tag{4.8}$$

To test the null hypothesis in Table 4.1 the formula for two unpaired samples with equal variance is used via the Excel function TTEST() with two tails and homoscedastic samples.

4.4.2. Analysis of variance (ANOVA)

The single factor ANOVA analysis tool in Excel was used as a generalisation of the t-test to more than two groups. The i-th result in group j (X_{ij}) can be broken down into the overall mean plus the deviation between groups plus residual deviation (Mould 1989). i.e.:

$$X_{ij} = \bar{\bar{X}} + (\bar{X}_j - \bar{\bar{X}}) + (X_{ij} - \bar{X}_j) \tag{4.9}$$

The F-statistic is calculated by comparing variance between groups and residual variance:

$$F = \frac{\text{Mean square between groups}}{\text{residual mean square}} = \frac{n\sum_j(\bar{X}_j - \bar{\bar{X}})^2}{\sum_j\sum_i(X_{ij} - \bar{X}_j)^2} \frac{\upsilon_1}{\upsilon_2} \tag{4.10}$$

where n is the number in each group, υ_1 is the degrees of freedom between groups and υ_2 is the residual degrees of freedom (total degrees of freedom − υ_1).

4.4.3. Chi-squared (χ^2) test

The chi-squared statistic (Mould 1989) of two paired samples (e.g. the expected results from a model and the observed results) relates to the difference between each pair:

$$\chi^2 = \sum \frac{(\text{Observation}_i - \text{Expectation}_i)^2}{\text{Expectation}_i} \tag{4.11}$$

The chi-squared test was used in this project to test a models goodness-of-fit with the observed results. A sample of expected results to pair with the observed results was

produced from the model. The CHITEST() function in Excel was used on the two samples.

5. SEM investigation of OSLDs

5.1. Introduction

The aim of this investigation was to provide useful insight into the structure of the OSLDs by using scanning electron microscopy (SEM) equipment at the RMIT Microscopy and Microanalysis Facility, Melbourne. The expectation was that this insight might inform later investigations into dosimetry using the OSLDs.

SEM is a well established technique that allows investigators to quickly determine the size, shape and composition of structures on the centimetre to nanometre scale (Vladár & Postek 2008). A very thin (in the order of nanometres) beam of electrons is accelerated to tens of kiloelectron volts in a vacuum and raster scanned across the surface of the sample being investigated. A variety of signals emanate from the sample including backscattered, secondary and auger electrons; characteristic x-rays; visible, ultraviolet, and infrared light; transmitted electrons; and current between the sample and ground. Each signal provides different information about the matter immediately surrounding the impact site of the electron beam. Electron microscopes are fitted with a number of detectors in order to detect a variety of signals.

The images in this investigation were created by capturing the secondary electron signals. Secondary electrons have energies lower than 50 electron volts and therefore can only emanate from the 5 to 50 nm closest to the surface (Vladár & Postek 2008).

Chemical element information was obtained by energy dispersive spectroscopy (EDS). EDS provides a spectrum of characteristic x-ray line intensities across the energy range. (Leng 2009). EDS is a valuable tool in a wide range of applications from analysing historic oil paintings in order to inform their conservation and protection (Şerifaki et al. 2009) to determining Cu/Fe atomic ratios in corrosion of aluminium alloys (Boag et al. 2011).

Relative concentrations of chemical elements are calculated using the signal from the detector and assumptions and corrections (in software). Uncertainty is larger for lighter

elements (Leng 2009). Rough surfaces and non-bulk samples can cause quantitative measures to be in error.

5.2. Materials and methods

The investigation was carried out on a FEI Quanta 200 environmental scanning electron microscope (FEI Company, Hillsboro, Oregon, USA) fitted with an energy dispersive spectroscopy module incorporating a Si(Li) detector (EDAX Inc., Mahwah, N,J U.S.A.) and EDS control software (also EDAX Inc.). The EDS module cannot detect elements lighter than carbon (Z = 6).

A single OSLD was removed from the vendor's packaging and placed on the microscope stage (Figure 5.1). The sample chamber was pumped down to high vacuum (2×10^{-4} Torr). Build-up of charge on the surface of the OSLD obscured most of the detail in the images. Therefore low vacuum mode (0.5 Torr) was employed for subsequent images and analysis. Water vapour was introduced into the sample chamber to remove some of the charge from the OSLD's insulating surface. Low vacuum mode offers less contrast but the same spatial resolution (same spot size).

Several images were captured of the surface of OSLD. Particular attention was paid to the edges of OSLD because more features were visible at the edges. EDS analysis was conducted on a region well clear of the edge.

Figure 5.1. Left: FEI Quanta 200 ESEM; and right: removing the top layer of the OSLD. The Si(Li) detector (labelled "EDAX") is visible at the back of the microscope.

The top layer of the OSLD was removed with a sharp blade Figure 5.2. Further images were captured to show the structure under the top layer of the OSLD. EDS was also conducted on a region well clear of the edge in order to compare elemental composition with and without the top layer of the OSLD.

Figure 5.2. Removing the top layer of the OSLD.

5.3. Results

The top face of the OSLD is flat and featureless as shown in Figure 5.3. In contrast, the edges reveal what appear to be layers, fibres and crystals. Interpretation of SEM images can be complicated by foreign objects, surface charging and volume averaging. The OSLD is irregular in shape; the centre image of Figure 5.3 shows a burr sticking out of the edge by approximately 0.3 mm.

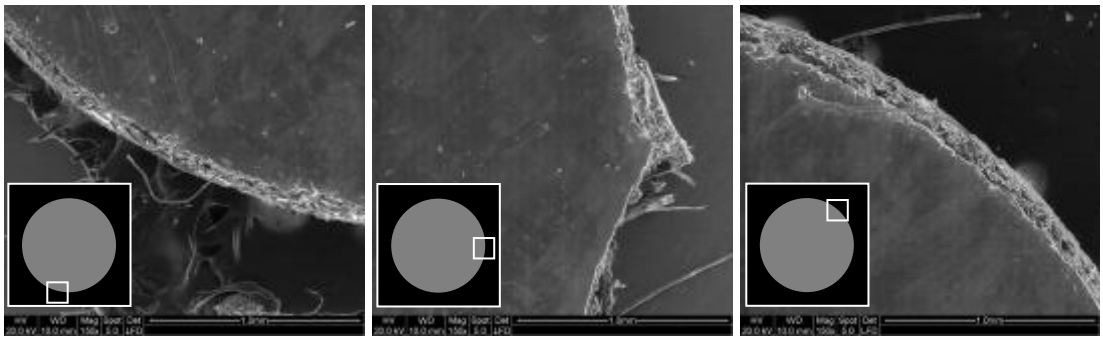

Figure 5.3. SEM images of the OSLD edge. The inset for each image is a diagram showing the approximate position of the view compared to the whole OSLD. The OSLD is sitting on a piece of conducting carbon tape which appears black in the left and right images.

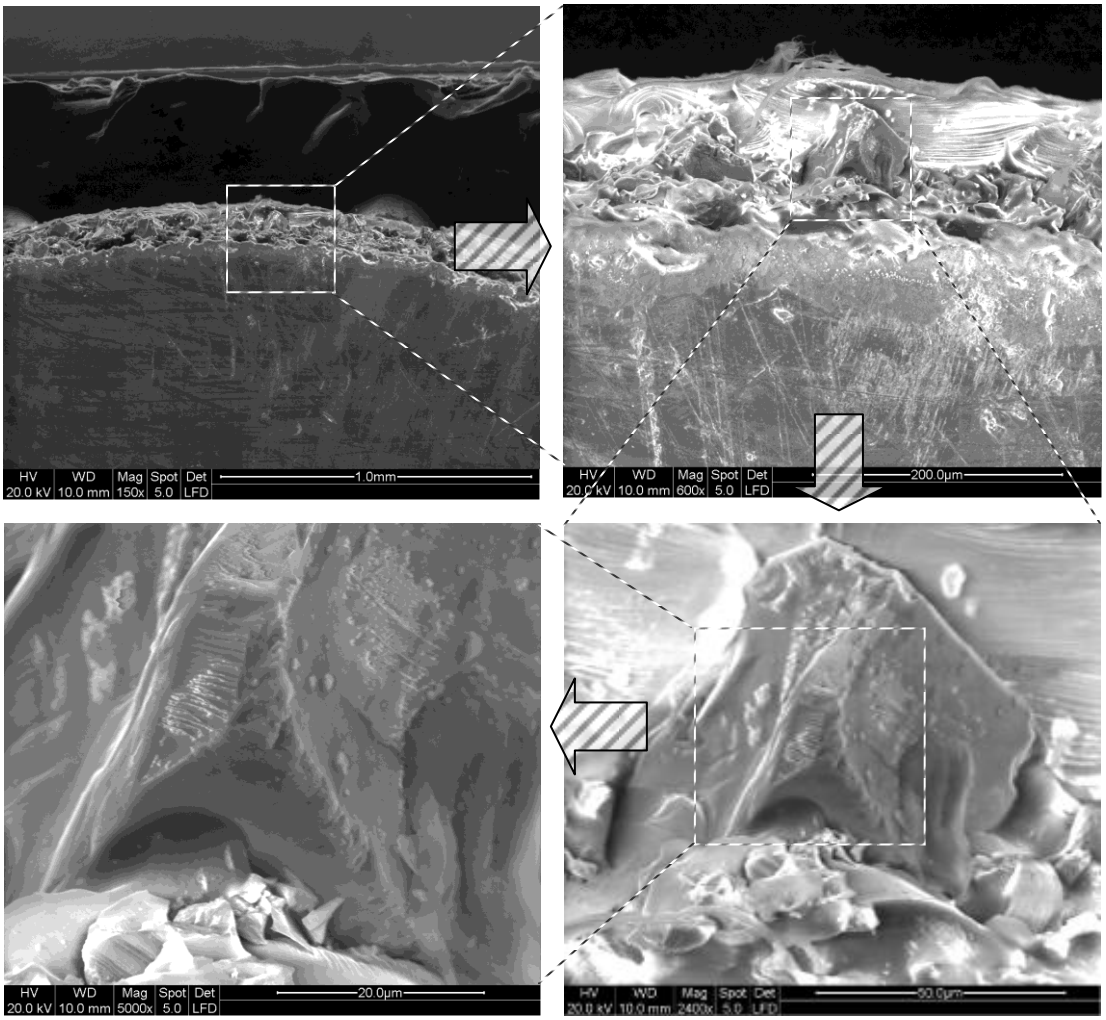

Figure 5.4. SEM images of a feature protruding from the OSLD edge. In each image, the dashed box is the outline of the next image in the series. Even in low vacuum mode, charge from the electron beam builds up on the surface and causes bright patches in the image.

A series of images of a feature protruding from the OSLD edge are presented in Figure 5.4 with progressively higher magnification. The feature appears to be a block of a separate material to the substrate. The composition of the block is unknown but it is presumed to be a crystal of Al_2O_3:C. Even in low vacuum mode, charge from the electron beam builds up on the surface and causes bright patches in the images.

With the top layer of the OSLD removed, more detailed internal structure was visible (Figure 5.5). Many features similar to the block shown in Figure 5.4 can be seen. The blocks appear to be of different sizes (typically 1-12 μm wide) and randomly spaced, at least on the plane made visible.

It is not known if what appear to be cavities in Figure 5.5 previously existed or were caused by the removal of the top layer of the OSLD. It is also not known if removal of the top layer of the OSLD caused the distribution of blocks in size and position.

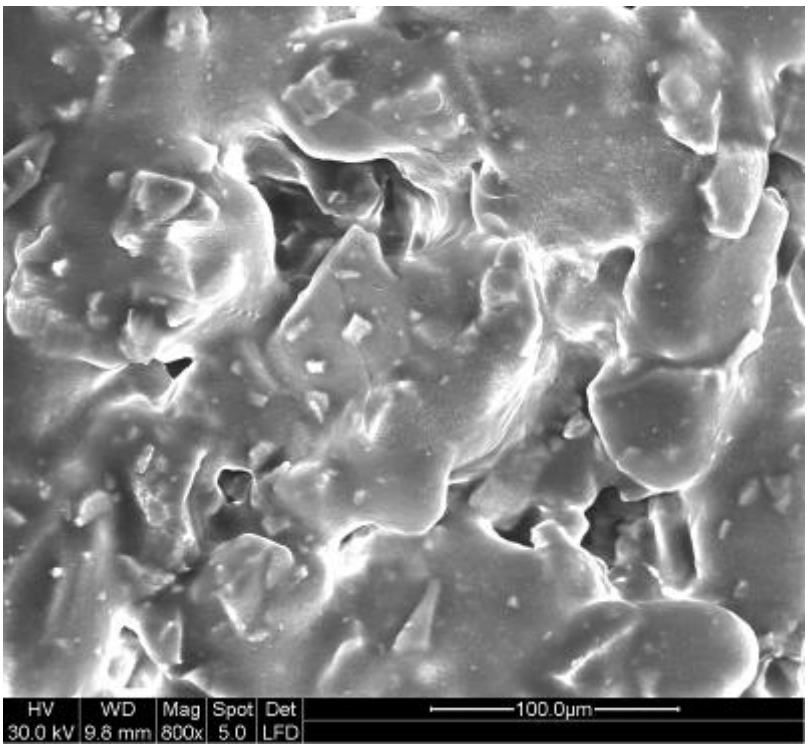

Figure 5.5. 800x SEM image of OSLD with top layer removed.

The EDS analysis from the surface of the OSLD indicates the presence of carbon and oxygen and offers some evidence for the presence of aluminium. The EDS spectrum is shown in Figure 5.6. The EDS software facilitates detection of characteristic x-ray peaks

and a search for their corresponding elements from a database. Each peak is labelled with its corresponding elements and energy level transition (e.g. Al Kα) (Halliday, Resnick & Walker 2001).

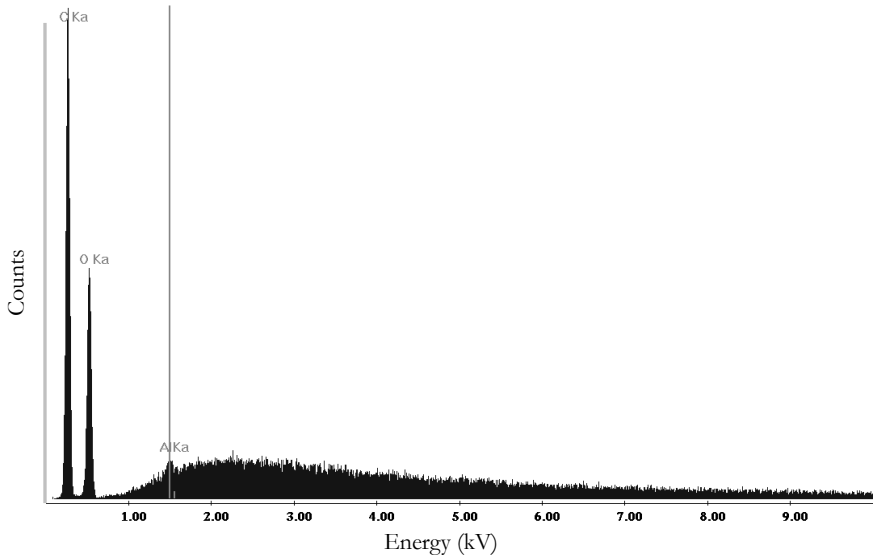

Figure 5.6. Energy dispersive spectroscopy spectrum of the OSLD top layer. The horizontal axis is the energy (in keV) of characteristic x-rays emanating from the region in question while the vertical axis is relative intensity of x-rays of each energy.

Figure 5.7 shows that removing the top layer of the OSLD reveals distinct peaks corresponding to aluminium and silicon. The relative composition by weight estimated by the software is 40 % carbon, 49 % oxygen, 7 % aluminium and 3 % silicon.

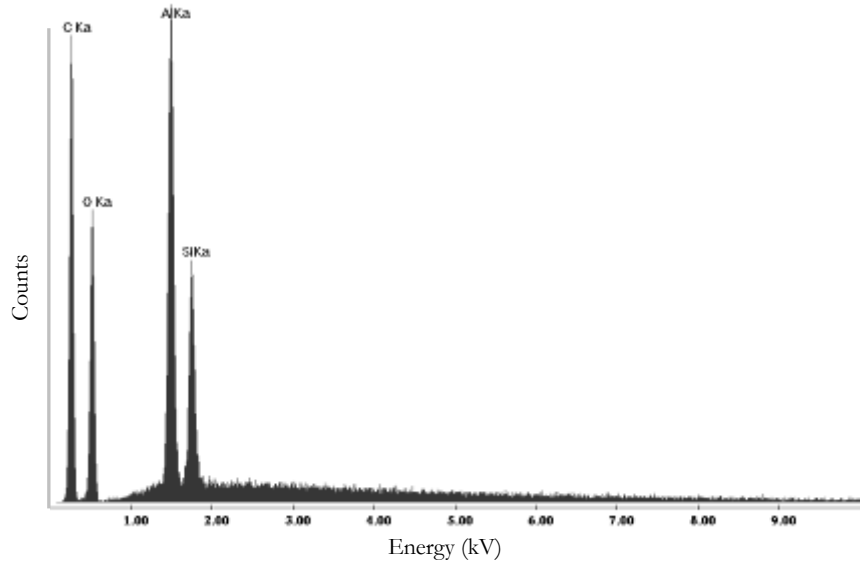

Figure 5.7. Energy dispersive spectroscopy spectrum of the OSLD with top layer removed. The horizontal axis is the energy (in keV) of characteristic x-rays emanating from the region in question while the vertical axis is relative intensity of x-rays of each energy.

5.4. Discussion

SEM images of the edge of the OSLD explain three observations that had been noted while using the OSLDs in previous investigations. Firstly, the OSLDs are cut to shape roughly. Therefore, they do not drop consistently into the bottom of the numbered recesses in the reader's carousel but frequently sit at an angle. External mechanical assistance is often required to ensure that the OSLD is parallel with the carousel plane.

Secondly, the edges of the OSLDs are not sealed. Darkening at the edges of the OSLDs has been noticed through repeated used and handling. The darkening is likely due to contamination sticking to the rough edge. It is unknown if contaminants could enter the OSLD and alter its performance. If the OSLDs were used to make measurements in a water phantom, it is also not known if water would enter the OSLD. As a precaution, OSLDs should be discarded if the edges became darkened.

Thirdly, the build up of charge on the surface of the OSLD shows that the surface is an excellent insulator. It has been observed that the OSLDs frequently stick to blocks of solid water and other plastic items. The electrostatic attraction is usually stronger than the force of gravity on the OSLDs. Again, some gentle external mechanical assistance is required.

The blocks seen in Figure 5.4 and Figure 5.5 are presumed to be crystals of Al_2O_3:C because they are 'regular polyhedral form[s]' (Howard n.d., pt 1) and because the alternative, that the Al_2O_3:C crystals are smaller and unseen and that the blocks are some other material, would seem unreasonable.

The top face of the OSLD is smooth and contains somewhat less aluminium than the inside of the OSLD. Both facts point to an absence of Al_2O_3:C crystals on the top face of OSLD. The depth at which Al_2O_3:C crystals are present may be relevant for surface dose measurements or measurement of radiation with very low penetration.

5.5. Conclusions

The SEM images and EDS analysis presented above give insight into the composition and structure of the OSLDs. The above results suggest that the OSLDs are likely to be unsuitable for water phantom measurements due to infiltration by water or contaminants.

The lack of Al_2O_3:C crystals on the OSLD surface may need to be considered if using the OSLDs to measure surface dose or if measuring very low energy radiation.

Finally, the distribution of Al_2O_3:C crystals suggests that if the OSLDs were cut down to smaller size or another shape, there may be a greater sensitivity difference between OSLDs.

6. Reader internal calibration

6.1. Introduction

The reader software automatically applies a simple raw signal to reader dose conversion. A dose report (comma separated values file) exported from the software contains reader dose values only. In later chapters, the quantity of interest is the raw signal, S (in counts), not the reader dose, S_{mrad} (in nominal millirads). Therefore it is useful to understand how the reader is calibrated and how to reverse the conversion to reader dose.

The reader software's internal calibration assumes a linear response to delivered dose, a constant non-zero residual raw signal and a uniform response across all OSLDs and recesses.

The reader Software User's & Service Manual (Shin 2012) sets out a method for calibration. In summary, groups of three OSLDs are irradiated to different doses (same dose within each group) spanning the expected clinical dose range and a calibration routine was run. The user inputs the delivered doses and the software calculates calibration parameters. The calibration is then automatically applied to subsequent measurements.

6.2. Materials and methods

6.2.1. Perform calibration

Calibration of the reader was conducted using nine OSLDs in accordance with the user's manual (Shin 2012) with groups irradiated to 0 Gy, 1 Gy and 4 Gy (equal to 0 mrad, 100,000 mrad and 400,000 mrad respectively). The calibration entry was exported as a comma separate values (CSV) file for analysis. The delivered doses were plotted against the corresponding raw signal values.

6.2.2. Reverse engineer calibration

When operated in engineering mode, the reader software displays the raw signal on screen as each OSLD is stimulated. The reader dose is written to the database as usual. To exploit this, another twenty-five OSLDs were irradiated under SCRC with doses

ranging from 0 Gy to 5.5 Gy. As the OSLDs were stimulated, the raw signal was observed on-screen and recorded. Three read routines were conducted to give more values for analysis. The database entries were exported as CSV files.

The reader doses were potted against the corresponding raw signal values and a linear fit calculated using the LINEST() function in Microsoft® Excel.

6.3. Results

The following results only apply for work with the calibration established on 7/11/2012. If the calibration were re-established, new results would be required.

6.3.1. Perform calibration

The "new cal factor" given in the header of the calibration CSV file was 1.42. The gradient in of the straight line between the mean of the 0 Gy data and the 4 Gy data was 1.42×10^{-5} Gy/counts as shown in Figure 6.1. The average of the raw signal values for the 0 Gy group multiplied by the calibration factor equals 77.63 mrad. This value can be interpreted as the reader's estimate of the residual reader dose on the OSLDs which must be subtracted from every subsequent result.

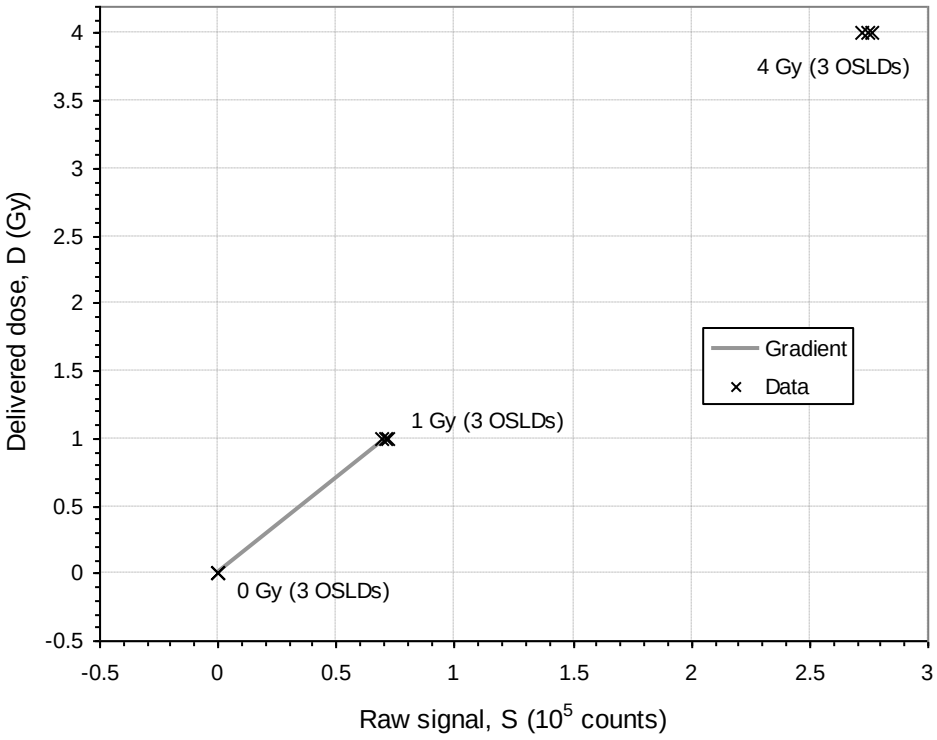

Figure 6.1. Graph showing delivered doses plotted against the corresponding raw signal values. Groups of three OSLDs are identified by their delivered dose in Gy. The grey line represents the straight line between the average of the 0 Gy group and the average of the 1 Gy group.

6.3.2. Reverse engineer calibration

The plot of reader doses vs. raw signal values is shown in Figure 6.2.

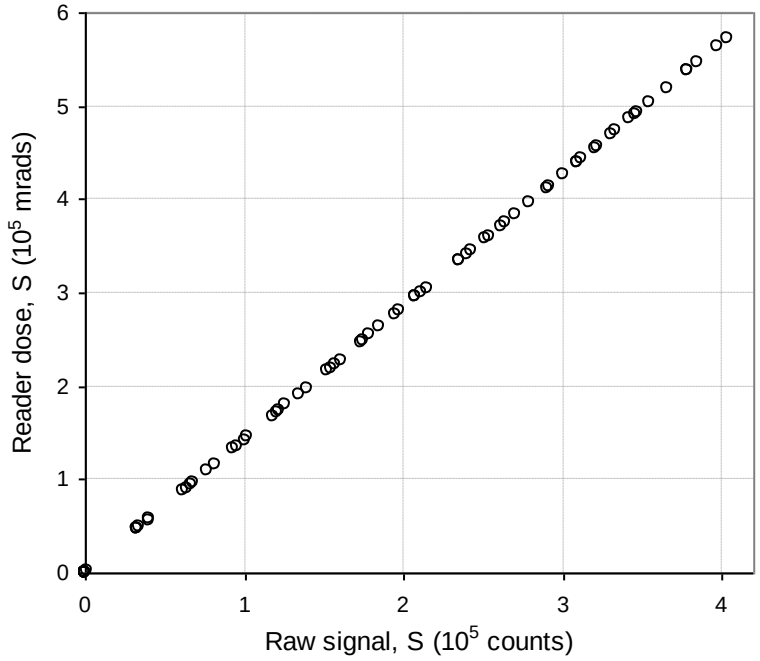

Figure 6.2. Plot of reader dose against raw signal. Seventy-five raw signal values were observed on-screen and matched with their corresponding reader dose values as written to the database.

The linear fit of reader doses vs. raw signal values was assumed to take the form:

$$S_{mrad} = S \times f_{cal} + S_{offset} \quad (6.1)$$

The gradient of the linear fit, f_{cal}, was 1.42 mrad/counts. The intercept of the linear fit with a reader dose axis (S_{offset}) was −77.63 mrad. The reader does not report negative doses. Instead, any raw signal values under 55 counts are reported as 0 mrad. The coefficient of determination (r^2) for the fit was 1.00 which indicates perfect correlation between the fit and the data.

6.4. Discussion

The reader software assumes linearity as shown by the straight line in Figure 6.2. Unsurprisingly the calibration factor is equal to the gradient of the linear fit of reader doses vs. raw signal values. The calibration factor is also equal to $G_{0,1}$. From this it can be gathered that the reader software only uses raw signal values for the non-irradiated OSLDs and the irradiated OSLDs with the lowest delivered dose to calculate the calibration parameters.

The reader dose axis intercept (S_{offset}) is equal and opposite the value obtained by multiplying the average raw signal values for the 0 Gy group by the calibration factor (77.63 mrad).

Evidentially the software takes the gradient $G_{0,lowest}$ as the calibration factor and multiplies it by the average raw signal values for the 0 Gy group to get S_{offset}.

At any time, the values for the calibration factor can be obtained from the file header and S_{offset} can be obtained from the raw signals of the 0 Gy group in the calibration file. Removing the reader internal calibration is a simple matter of rearranging equation 6.1:

$$S = \frac{S_{mrad} + S_{offset}}{f_{cal}} \tag{6.2}$$

The error introduced by not removing S_{offset} for a 1 Gy delivered dose is approximately 0.08 % and less for higher doses. Therefore simply dividing the reader dose by the calibration factor may be an acceptable way of obtaining the raw signal value.

6.5. Conclusions

The first step in determining the calculated dose after a read routine reading will be to remove the internal calibration because the raw signal. The reader dose to raw signal relationship is described above.

It is recommended that the calibration is not repeated because this will change the reader dose to raw signal relationship. The work described above will need to be repeated in the event of recalibration being required due to a software upgrade or failure.

7. Ambient light

7.1. Introduction

The electrons stored in dosimetry traps in Al_2O_3:C crystals can be freed by typical office or laboratory lighting (Yukihara & McKeever, 2011, Jursinic, 2007, Dunn et al., 2013), the effect of which is to reduce the raw signal, S, by an indeterminate amount.

Loading a calibration or experiment set of twenty-five OSLDs into the reader takes at least two minutes. Similarly, unwrapping and loading a small number of OSLDs from a patient dose measurement may easily take two minutes. Two experiments were conducted to determine if significant dose signal is lost while loading the reader in the presence of room lighting.

It is proposed to wrap the OSLDs in thin black plastic after irradiation to prevent loss of dose signal during the return journey to the reader. Therefore another experiment was conducted to test the suitability of an inexpensive, thin black plastic for the aforementioned purpose. The black plastic must be removed before the OSLDs are placed in the reader.

7.2. Materials and methods

7.2.1. Typical room lighting

An initial experiment was conducted to investigate the effect of typical office or laboratory lighting on raw signal. Twenty OSLDs were irradiated with 100 MU under SCRC on LINAC TU2 and left in the solid water phantom.

At the times given in Table 7.1, three groups of OSLDs were exposed to room lighting. In this way, four groups of five OSLDs were exposed to ten, five, two and zero minutes of room light. At one hour post- irradiation a read routine was run using all twenty OSLDs.

Table 7.1. Three groups of OSLDs were exposed to room lighting at the times given.

Time post-irradiation	Action
31 min	First group exposed
36 min	Second group exposed
39 min	Third group exposed
41 min	All OSLDs covered
60 min	Read routine

7.2.2. Two minutes

A follow-up experiment was conducted to determine if the difference in S between OSLDs exposed to two minutes and zero minutes of room lighting is statistically significant. Another set of twenty OSLDs were irradiated with 200 MU under SCRC on TU2 and left in the solid water phantom.

Approximately thirty minutes post-irradiation, only half of the OSLDs were exposed to room lighting for two minutes. At one hour post- irradiation a read routine was run using all twenty OSLDs.

7.2.3. Black plastic

Fifteen OSLDs were irradiated with 100 MU under SCRC on TU2 and left in the solid water phantom.

A 5 cm x 5 cm square piece of black plastic approximately 0.02 mm thick was cut from a Kwikmaster 65 litre all-purpose garbage bag (Bunzl Catering Supplies, Enfield, NSW). One group of five OSLDs were wrapped in the piece of black plastic. The black plastic was folded over and taped to ensure a single layer of plastic covered the OSLDs.

Another group of five OSLDs were kept in the dark in a light-tight box. The remaining five OSLDs were placed uncovered in the light in a single layer on a table next to the wrapped OSLDs. The table was under typical office lighting. After two hours two read routines were run using all fifteen OSLDs.

7.3. Results

7.3.1. Typical room lighting

The reduction in mean S caused by exposure to room light is given in Table 7.2 and expressed as a percentage of mean S for exposure of zero minutes. The uncertainty was

calculated using the ISO Guide to the Expression of Uncertainty in Measurement. The expanded uncertainty is the interval that is estimated to contain the measurand with 95 % probability. The coverage factor for the interval is 2.78.

Table 7.2. The reduction in mean S caused by exposure to room light.

Exposure to light	Reduction in S	Expanded uncertainty
10 min	15 %	13 %
5 min	8.8 %	12 %
2 min	2.7 %	14 %

Loading OSLDs into the reader will take at least two minutes but the effect of two minutes exposure to room light is unclear from the above table due to considerable uncertainty of measurement. A two-tailed t-test (two-sample unequal variance) on the zero and two minute exposure groups shows that the difference in the means is not statistically significant ($p = 0.51$).

Although the uncertainties expressed above are high, a qualitative illustration of the effect of room lighting on the reader can be obtained from Figure 7.1. The decrease in mean S dose with increased exposure to room light is evident.

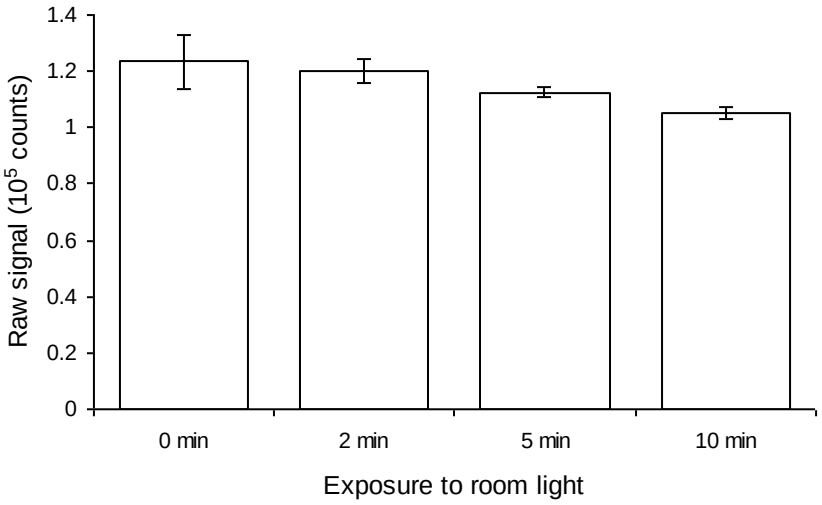

Figure 7.1. Mean S values for OSLDs exposed to room light. The vertical bars represent one standard deviation of S.

7.3.2. Two minutes

The difference in mean S between the group exposed to two minutes of room light and the group not exposed to room light is demonstrated in Figure 7.2.

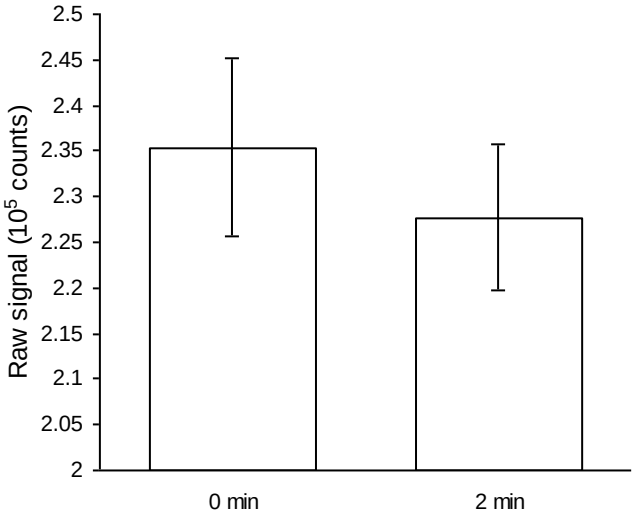

Figure 7.2. Mean S values for OSLDs, half exposed to room light for 2 minutes. The vertical bars represent one standard deviation of S.

A two-tailed t-test (two-sample unequal variance) on the two groups shows that the difference in the means is statistically significant ($p = 0.002$). The difference in the means is 3.3 ± 2.9 percent of the mean of the group not exposed to room light. The expanded uncertainty was calculated as above. The coverage factor is 2.04.

7.3.3. Black plastic

The suitability of the black plastic to protect the OSLDs from room light is demonstrated in Figure 7.3. The mean S for the "light" group is 83 ± 5 percent of mean S of the "dark" group. The expanded uncertainty was calculated as above. The coverage factor is 2.26.

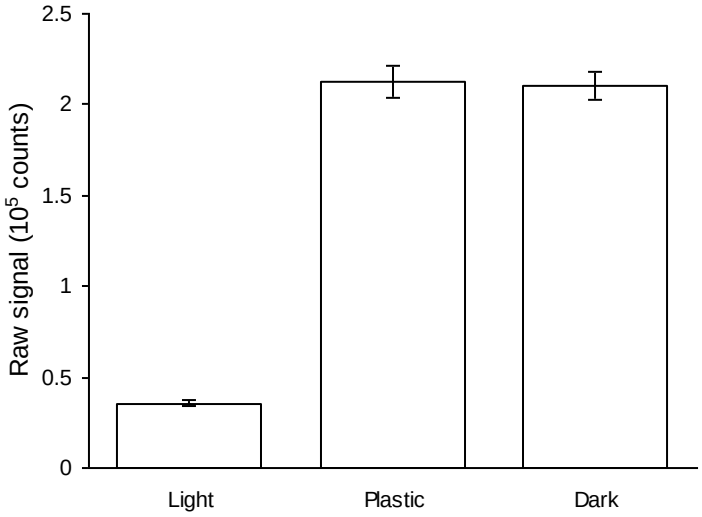

Figure 7.3. Mean raw signal for OSLDs in different light conditions for 2 hours. Five OSLDs were exposed to room light, five were wrapped in black plastic and five were kept in complete darkness.

A two-tailed t-test (two-sample unequal variance) on S values for the "light" and "plastic" groups shows that the difference in the means of two groups is not statistically significant ($p = 0.59$).

7.4. Discussion

The reductions in S due to room light calculated above are not intended to be used to correct for known exposure to room light because there would be large errors in estimating the time and relative intensity of the room light. Instead, the results are intended to inform decisions regarding OSLD handling.

It is clear from sub-section 7.3.2 that only two minutes exposure to room light will make a significant difference to D_{calc} because it is proportional to S. Although the expanded uncertainty is large compared to the difference in the means, it is reasonable to expect that loading the reader with irradiated OSLDs in the presence of room light could introduce a 5 % error in the calculated dose. Therefore the reader's carousel should be loaded in a darkened room and covered while placing it into the reader.

The inexpensive, thin black plastic in sub-section 7.3.3 prevented room light from bleaching dose signal from the OSLDs. The OSLDs used for in vivo measurements in a busy clinic might easily wait two hours before their read routine and change hands

several times. The plastic will ensure no error is introduced due to room light so long as the OSLDs are unwrapped in a darkened room as described above.

The plastic used can be folded over and sealed on three sides with an impulse sealer. The resulting package is effectively light-tight and would provide a barrier between patient and OSLD. The assumption that 0.02 mm thick plastic will not effect dose distribution in patient is reasonable.

7.5. Conclusions

Typical office or laboratory lighting can have a significant effect on S. Just two minutes exposure to room light can introduce a 5 % error in D_{calc}. Avoiding room light is critical.

An inexpensive black plastic was found to be suitable to protect the dose signal from room light. There was no significant difference in S between OSLDs wrapped in black plastic and OSLDs kept in complete darkness.

8. Read routine inconsistency

8.1. Introduction

The original aim of this investigation was twofold: (1) to observe the distribution of k_{ECF}; and (2) to observe any changes in raw signal, S, when the same OSLDs were repeatedly used. As the investigation began, the dose response to the same delivered dose was extremely inconsistent between read routines.

To investigate, the reader service door was opened and the manual command to find spindle zero position was sent several times. The zero position appeared to change, sometimes overshooting or undershooting the position assumed to be zero.

The hypothesis was formed that the changes in response were caused by a mechanical fault in the reader whereby the grub screws in the hub did not hold onto the spindle tightly enough. It follows that after finding the zero position, the hub may slip on the spindle. Therefore when the stepper motor returned to zero, the carousel may not have, i.e. the starting point for the read routine will not be constant.

There was no evidence that the small 7.2º rotations which progress the carousel to the next OSLD do not exert enough torque to cause the hub to slip on the spindle.

This chapter describes three experiments. The first experiment characterised the inconsistent response. The second experiment determined how much of the OSLD is stimulated by the laser. The third experiment tested the above hypothesis, by observing overshoot and undershoot by collimating the stimulating laser and offsetting this collimation by different amounts for different OSLDs.

8.2. Materials and methods

8.2.1. Characterisation of inconsistent response

Twenty-four OSLDs were put through three cycles of irradiation, read routine and bleaching as described in Table 8.1. All irradiations occurred under SCRC on LA4.

Table 8.1. Three cycles of irradiation, read routine and bleaching.

	Irradiate		**Read**		**Bleach**
Day 1	200 MU	→	Four read routines	→	Overnight
Day 2	200 MU	→	Four read routines	→	Overnight
Day 3	200 MU	→	Three read routines	→	Overnight

Collection of results halted because the hub could no longer reliably find its zero position. The carousel mechanism repeatedly became jammed while automatically retracting into the reader. Mechanical repairs were carried out on the reader after the experiment described here in sub-section 8.2.1 but before the experiment described in sub-section 8.2.2. Amongst other things, the hub was replaced. After repairs, changes in the zero position could no longer be seen by observing the hub by eye.

Results from two of the first four read routines were deleted before the intention of this study was defined, because the S values were lower than expected. Therefore results for only nine read routines were preserved. All three irradiations are assumed to be equal because the dose delivered under SCRC per monitor unit does is unlikely to have changed by more than 0.5 % between irradiations.

8.2.2. Quantification of laser stimulation

Twelve apertures were machined from a 0.25 mm thick copper sheet all with outside diameter of 6 mm (the same as the OSLDs) and three different nominal inside diameters: 4 mm, 3 mm and 1 mm. The nominal aperture designates how much of a OSLD can be irradiated. An uncovered "Bare" OSLD is considered to be the forth nominal aperture.

Sixteen OSLDs were arranged in a four-by-four grid on a piece of Gafchromic RTQA2 film (International Specialty Products, Wayne, NJ, USA) in the order shown in Table 8.2. Copper apertures were placed on top of twelve of the OSLDs and four OSLDs remained bare as shown in Figure 8.5.

Table 8.2. Four-by-four grid of OSLDs.

OSLD 1	OSLD 5	OSLD 9	OSLD 13
OSLD 14	OSLD 2	OSLD 6	OSLD 10
OSLD 11	OSLD 15	OSLD 3	OSLD 7
OSLD 8	OSLD 12	OSLD 16	OSLD 4

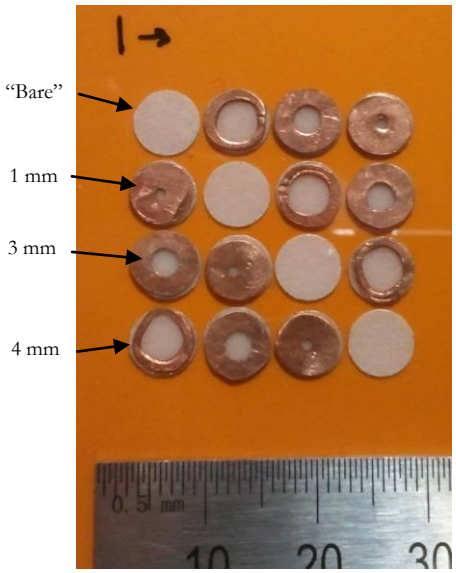

Figure 8.1. OSLDs and copper apertures sitting on film. The sixteen OSLDs were arranged in a four-by-four grid on top of a piece of film. One example of each of the four aperture sizes is labelled.

The film with OSLDs and apertures was placed onto a stack of five 1 cm thick solid water blocks at the opening of the 5 cm applicator of the SXRT unit. The OSLDs were irradiated for 0.48 minutes using filter 1 (approximately 1 Gy surface dose according to the most recent calibration).

Irradiation was conducted in a darkened room and the OSLDs were loaded into the reader under minimal lighting. Eight read routines were run to produce 128 values of S(i,j) where i is the OSLD and j is the read routine.

The mean raw signal for each nominal aperture was calculated using the equations in Table 8.3.

Table 8.3. Equations for the mean S for each of the nominal apertures.

Mean	$\overline{S}_{Bare}$	$\overline{S}_{4mm}$	$\overline{S}_{3mm}$	$\overline{S}_{1mm}$
Equation	$\frac{1}{4\times8}\sum_{i=1}^{4}\sum_{j=1}^{8}S(i,j)$	$\frac{1}{4\times8}\sum_{i=5}^{8}\sum_{j=1}^{8}S(i,j)$	$\frac{1}{4\times8}\sum_{i=9}^{12}\sum_{j=1}^{8}S(i,j)$	$\frac{1}{4\times8}\sum_{i=13}^{16}\sum_{j=1}^{8}S(i,j)$
Equation no.	(8.1)	(8.2)	(8.3)	(8.4)

The proportion of the dose signal that originates from several zones within a typical OSLD was estimated using the equations in Table 8.4. The OSLD was assumed to be

centred on the straight line between the centre of the stimulating laser and the centre of the PMT.

Table 8.4. Proportion of the dose signal that originates from several zones.

Zone	1st (Outer)	2nd	3rd	4th (inner)
Outer/inner radii	6/4 mm	4/3 mm	3/1 mm	1/0 mm
Equation	$\overline{S}_{Bare}-\overline{S}_{4mm}$	$\overline{S}_{4mm}-\overline{S}_{3mm}$	$\overline{S}_{3mm}-\overline{S}_{1mm}$	$\overline{S}_{1mm}$
Equation no.	(8.5)	(8.6)	(8.7)	(8.8)

8.2.3. Observation of overshoot and undershoot

Slit collimators were made by printing five black bars onto an overhead transparency with a Lexmark C544DN office printer (Lexington, Kentucky, USA). The bars were all 4 mm wide and each had a 1 mm wide transparent strip along the long axis.

The strip was centred for one bar and was offset on the other four bars by either 0.5 mm or 1 mm to either the right or the left (five different offsets, see Figure 8.2). The 4 mm bars were wide enough to cover the gap in the bottom of a recess and leave a 1 mm wide slit through which part of the OSLD can be stimulated.

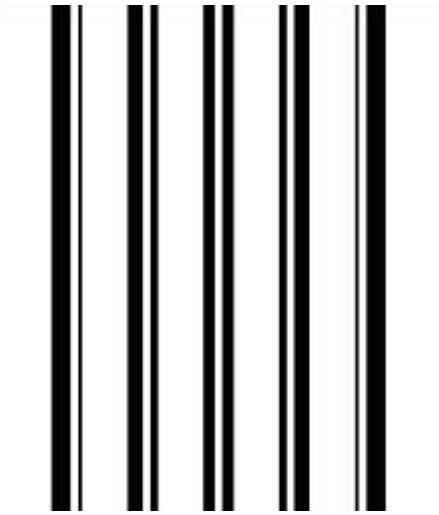

Figure 8.2. Image of five bars to be printed onto an overhead transparency. The transparent trips are offset by 1 mm left, 0.5 mm left, zero, 0.5 mm right and 1 mm right.

The collimators were cut into four 25 mm lengths and taped to the bottom of the carousel as indicated in Table 8.5 and Figure 8.3. An effort was made to cover the gap

with the black bar and to point the slit towards the centre of the carousel. The designation of one direction as "left" and the other as "right" is arbitrary but fixed.

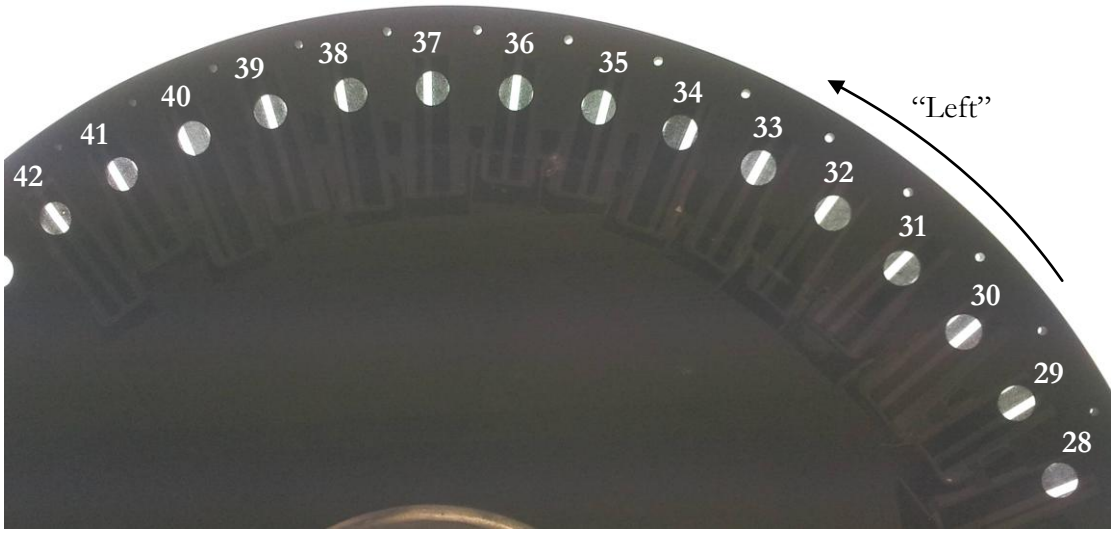

Figure 8.3. Carousel fitted with slit collimators and viewed from below. The positioning of the collimators has an uncertainty of approximately 0.25 mm which is good enough to clearly distinguish between left-offset and right-offset. Left and right are reversed if the carousel is viewed from above or below. Therefore, the direction of increasing recess numbers was arbitrarily chosen as left.

Table 8.5. Collimator offset for each carousel recess.

Carousel recess	28	29	30	31	32	33	34	35	36	37	38	39	40	41	42
Offset (mm)	1	0.5	0	0.5	1	0	1	0.5	0	0.5	1	0	1	0.5	0
Direction	R	R	-	L	L	-	R	R	-	L	L	-	L	L	-

Twenty OSLDs were irradiated with 200 MU under SCRC on LA4 and after one hour were loaded into recesses 26 to 45. Five OSLDs were uncollimated. Without disturbing the collimators the carousel was inserted into the reader and twenty-two consecutive read routines were run over a two hour period.

The read signal values from the five uncollimated OSLDs (recesses 26-27 and 43-45) were used calculate $k_T(j)$ for each read routine j:

$$k_T(j) = \frac{\sum_{i=26}^{27} S(i,1) + \sum_{i=43}^{45} S(i,1)}{\sum_{i=26}^{27} S(i,j) + \sum_{i=43}^{45} S(i,j)} \tag{8.9}$$

where i is the OSLD and j is the read routine.

The dosimeter reading was calculated for each OSLD by modifying equation 2.2:

$$M(i,j) = S(i,j) \cdot k_T(j) \tag{8.10}$$

The mean dosimeter readings for OSLDs with the same collimator offset was calculated using the equations in Table 8.6.

Table 8.6. Equations for mean dosimeter reading for each collimator offset.

Group	Uncollimated	Centred	Left	Right
i =	26,27,43,44,45	30,33,36,39,42	37,38,40,41	28,29,34,35
Mean	$\bar{M}_{uncol}(j)$	$\bar{M}_{centre}(j)$	$\bar{M}_{left}(j)$	$\bar{M}_{right}(j)$
Equation	$\frac{1}{5}\sum_i M(i,j)$	$\frac{1}{5}\sum_i M(i,j)$	$\frac{1}{4}\sum_i M(i,j)$	$\frac{1}{4}\sum_i M(i,j)$
Equation no.	(8.11)	(8.12)	(8.13)	(8.14)

Results from recesses 31 and 32 were discarded in order to have an even number of left and right offsets. For each read routine, the left/right dominance was calculated using:

$$DOM_{LR}(j) = \bar{M}_{right}(j) - \bar{M}_{left}(j) \tag{8.15}$$

A positive value of DOM_{LR} indicates that the right offsets were dominant for the read routine in question. Zero value indicates that the raw signal values from left and right offsets were balanced.

8.3. Results

8.3.1. Characterisation of inconsistent response

The mean raw signal values for the nine read routines are shown in Figure 8.4. Under-response by as much as 97 % of the highest mean raw signal value is observed.

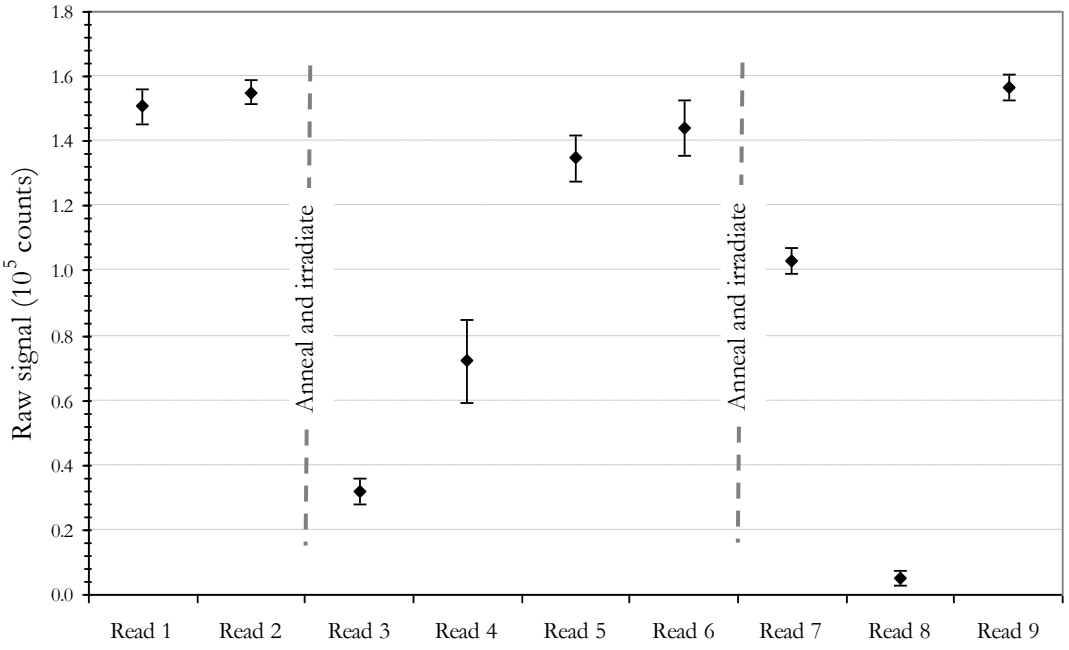

Figure 8.4. The mean raw signal for repeated reads. The error-bars represent one standard deviation above and below the mean for each read.

The standard deviation of the raw signal values within each read routine range from 2.4 % (read routine 2) to 41 % (read routine 8) when expressed as a percentage of the mean of each read routine. When expressed instead as a percentage of the highest mean raw signal value, the standard deviation of the raw signal values within each read routine range from 2.4 % (read routine 2) to 8.2 % (read routine 4).

The standard deviation of the nine mean raw signal values is 36 % when expressed as a percentage of the highest mean raw signal value. Therefore the spread of raw signal values within any read routine is small compared to the spread of the mean raw signal values for each read routine.

8.3.2. Quantification of laser stimulation

A scanned image of the setup film is presented in Figure 8.5.

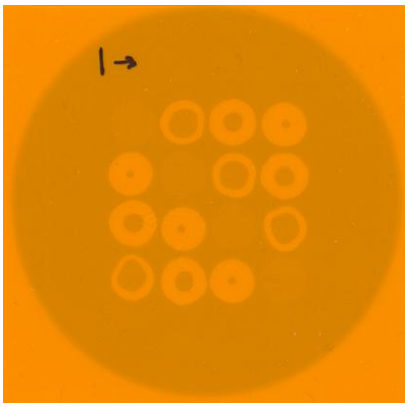

Figure 8.5. The irradiated set-up film. The sixteen OSLDs were arranged in a four-by-four grid on top of a piece of film. The large dark circle is the outline of the SXRT unit's 5 cm applicator. The radiation shadows of the OSLDs and copper apertures placed upstream are visible on the irradiated film.

Mean S values for the bare OSLDs and the three nominal apertures are shown in Figure 8.6 as a percentage of $\overline{S}_{Bare}$.

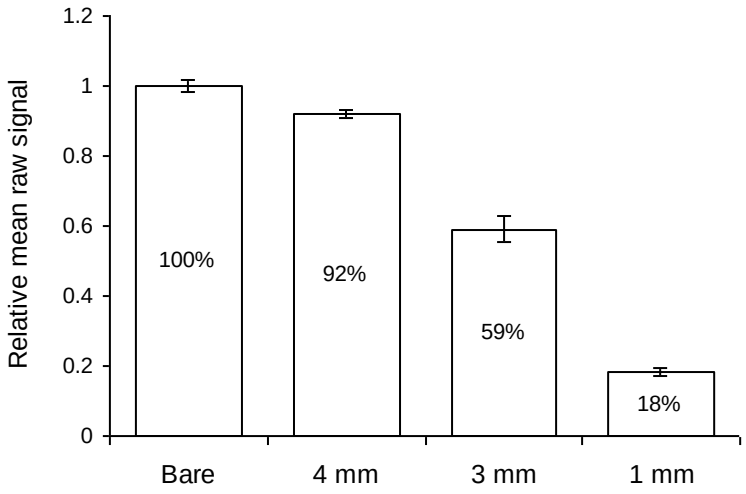

Figure 8.6. Mean S values for the bare OSLDs and the three apertures. The error bars represent the expanded uncertainty as calculated using the ISO Guide to the Expression of Uncertainty in Measurement. The expanded uncertainty is the interval that is estimated to contain the measurand with 95 % probability. The coverage factor for the interval is 2.04.

There was variation in S values between OSLDs with the same nominal aperture because thin copper is difficult to precisely machine and because sensitivity can vary between OSLDs. There was also variation in S values for the same OSLD with read routine. This is reflected in the uncertainty in Figure 8.6.

The proportion of the dose signal that originates from four zones within a typical OSLD is presented as a percentage of $\overline{S}_{Bare}$ in Figure 8.7.

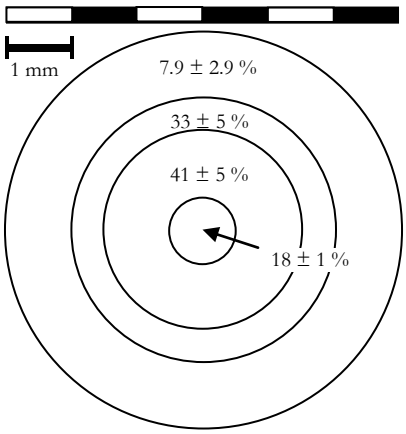

Figure 8.7. Proportion of dose signal originating from each zone of the OSLD.

8.3.3. Observation of overshoot and undershoot

The printed black bars were successful at collimating the stimulating laser. $\overline{M}_{uncol}(1) = 2.1 \times 10^5$ counts and $\overline{M}_{centre}(1) = 0.8 \times 10^5$ counts. A reduction in raw signal of 38 % with slit collimation is consistent with the reduction in read signal with circular shown in Figure 8.7 in the previous sub-section.

Figure 8.8 shows that DOM_{LR} is not constant. Fourteen of the read routines were right-dominant and eight were left dominant.

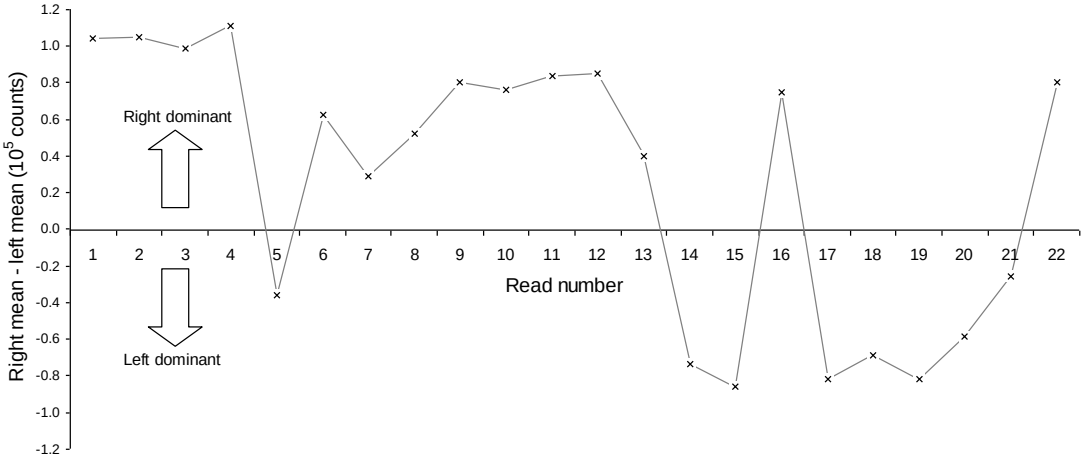

Figure 8.8. Difference between OSLDs with right-offset and left-offset collimators. Values above zero suggest right-dominance and values below zero suggest left-dominance. The dominance is stronger if the value is further from zero.

The ranges of values of M(i,j) for left-offset (i = 37, 38, 40 and 41) and right-offset OSLDs (i = 28, 29, 34 and 35) overlap for four read routines only (j = 5, 7, 13 and 21). These read routines also have weaker right/left dominance (Figure 8.8) and relatively large values of $\overline{M}_{centre}(j)$ (Figure 8.9).

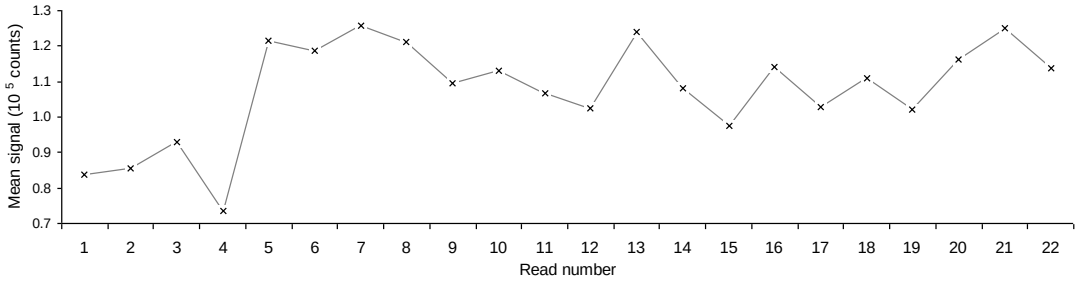

Figure 8.9. Mean raw signal of the five zero-offset collimated OSLDs.

Weak right/left dominance suggests error in the zero position was smaller for that read routine and is confirmed by relatively high values for the mean raw signal of the five OSLDs with zero-offset collimators. Two examples of weak right/left dominance (read routines no. 5 and 7) are shown in Figure 8.10.

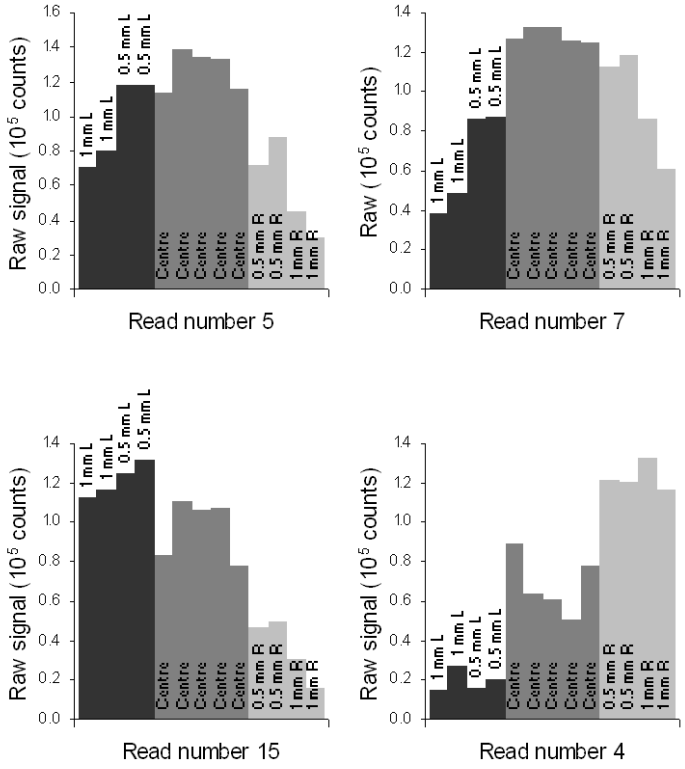

Figure 8.10. A sample of results for OSLDs with collimators from twenty-two read routines. Read numbers 5 and 7 show balance between OSLDs with left and right offset collimators, the centre values (zero offset) are also higher for these read routines. Read number 15 shows higher raw signal values for OSLDs with left-offset collimators and read number 4 shows higher raw signal values for OSLDs with right-offset collimators

The carousel spins in the "right" direction (towards the smaller numbers). Therefore left-dominance suggests that the hub had overshot the zero position at the beginning of the read routine and that the laser was stimulating towards the left side of each OSLD (Figure 8.11 left). Conversely, right-dominance suggests that the hub had undershot the zero position at the beginning of the read routine and that the laser was stimulating towards the right side of each OSLD. Examples of strong left-dominance (read routines no. 15) and strong right-dominance (read routines no. 4) are shown in Figure 8.10.

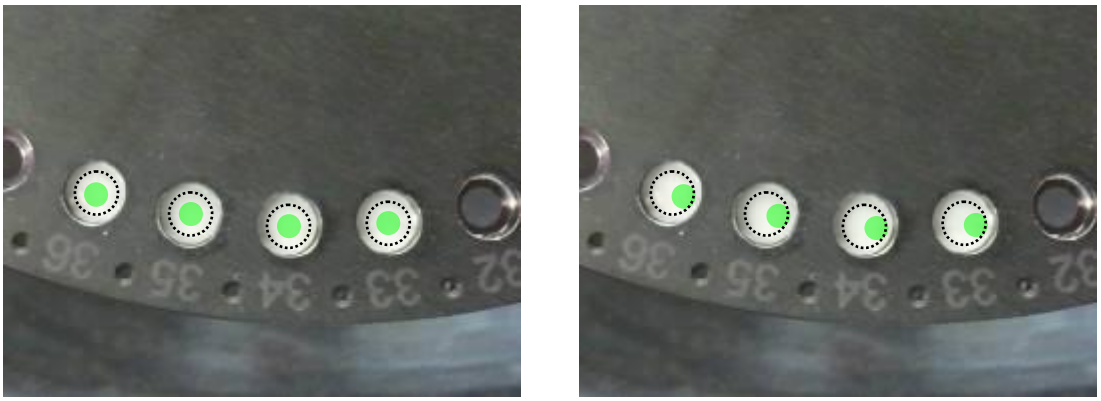

Figure 8.11. Hypothetical illustrations of accurate zero positioning (left) and; undershoot (right). In contrast to Figure 8.3 the carousel is viewed from above here. The dotted circle is the 4 mm diameter circular gap which allows stimulation by the laer from below and the green circle is a representation of the stimulating laser. The size of the green circle is arbitrary.

8.4. Discussion

There are many phenomena that contribute to change in the raw signal between read routines beyond the dose delivered to the OSLDs. Such phenomena include fading, bleaching of OSLDs by room light, bleaching from the stimulating laser as well as inconsistencies in the PMT sensitivity, stimulating laser intensity and positioning of the carousel.

The dominant phenomenon or phenomena that lead to the extreme inconsistency shown in sub-section 8.3.1 sometimes acts to decrease and at other times increase the raw signals relative to the previous read routine. Therefore fading and bleaching can be ruled out as dominant phenomena because these only act to reduce the raw signal.

Additionally the dominant phenomenon or phenomena affected all the OSLDs in a similar way as shown by the relatively small spread of raw signal values within any read routine compared to the spread of the mean raw signal values for each read routine (Figure 8.4). Additionally, raw signal from the left offset OSLDs increase and decrease in concert even though they are spread out across the carousel recesses. Therefore stimulating laser inconstancy can also be ruled out.

The PMT is reactivated and the hub zero position is reset at the beginning of each read routine. Inaccurate hub positioning is the most reasonable explanation for the inconsistency for the following reasons: (1) the hub was shown to overshoot and

undershoot the zero position (sub-section 8.3.3) and; (2) the extreme inconsistency ended after mechanical repairs. Inconsistency in PMT performance cannot be ruled out but it is unlikely because the patterns of response are not entirely random nor do they follow PMT influence factors like age or temperature.

Figure 8.6 and Figure 8.7 show that while the stimulating laser is very narrow, the area of the OSLD that is stimulated is quite extensive. Laser light may reach more peripheral parts of the OSLD via reflection inside the reader or scatter within the OSLD. Such an observation is relevant when considering the possibility of trimming the OSLDs down to smaller sizes (e.g. 1 mm) for use in very small radiotherapy fields with steep dose gradients. The signal to noise ratio would be lower for a trimmed-down OSLD.

The circular gap in the bottom of each numbered recess in the carousel has a diameter of 4 mm. Therefore, there is a 1 mm wide strip around the edge of the OSLD that cannot be directly stimulated by the laser. Taking the difference in raw signal between the bare OSLDs and those with this 1 mm strip covered at irradiation (4 mm copper aperture), the strip was observed to contribute 7.9 ± 2.9 % of the raw signal. Such a high contribution was not expected.

Figure 8.5 shows that the 4 mm copper apertures are irregular in shape and not consistent. The possibility exists that a large part of the 7.9 % is due to unintentionally irradiated areas of the OSLDs.

8.5. Conclusions

The inconsistent behaviour observed in this investigation is of particular interest in the clinical application of the OSLDs for in vivo dosimetry because it introduces errors that may change at any time. Such errors cannot be qualified and corrected for and may invalidate uncertainty estimates based solely on statistics. The extreme inconsistency ended after mechanical repairs but the identified cause, inaccurate hub positioning, still remains. The grub screws may loosen their hold on the spindle over time leading to increasing error. A solution may be to redesign the spindle and hub to allow the screws to thread through the spindle.

9. Carousel wobble

9.1. Introduction

Some pilot experiments were conducted soon after delivery of the OSL system to gain familiarity and to discover which aspects of the system's operation would require more thorough investigation. One such experiment called for uniform irradiation of forty-nine OSLDs. The results suggested that the hub wobbles as it rotates, that is, one point of the hub is always higher. From a fixed vantage point, the closest edge of the hub appears to rise and fall. The wobble is demonstrated in Figure 9.1.

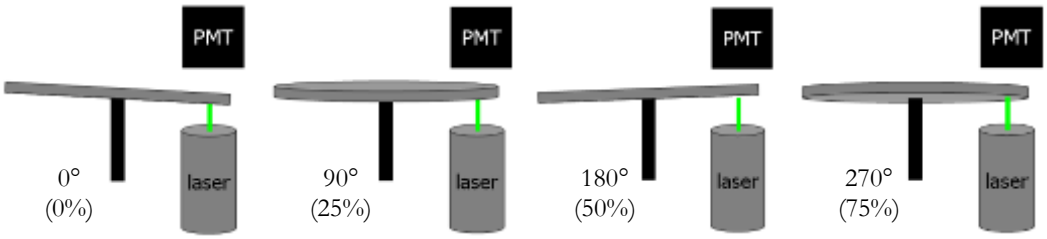

Figure 9.1. Diagrams shows the wobble of the hub at four points in a revolution.

This investigation first covers the discovery of the wobble in a qualitative investigation and then moves on to a characterisation of the effect of the wobble in a quantitative investigation. Characterising the effect of the wobble is not strictly necessary if it remains constant and if OSLDs are always in the same carousel recesses. Neither condition is assured so characterising the effect of the wobble would seem prudent. A wobble factor, k_W, is estimated below for each recess. The wobble factor can be used to convert the reader dose reported for a OSLD to the reader dose which would be reported were it in a different recess.

9.2. Materials and methods

9.2.1. Qualitative investigation

Forty-nine OSLDs were irradiated with 400 MU under SCRC on TU3 and a read routine was run thirty minutes later. The OSLDs were then used to continue the pilot study but only the results of this first read routine are pertinent to this investigation.

To investigate further, a video of the hub rotating without the carousel was recorded using a GT-I9000 "Galaxy S" smart phone (Samsung, Seoul, South Korea). Two snapshots were captured from the video approximately one half period of rotation apart using VLC media player* version 2.0.5 (VideoLAN Team). The two snapshots were overlaid as layers using the GNU Image Manipulation Program† version 2.6.11 (GIMP Development Team). A grid was added to give stationary reference points in both images. Two images were then created from the two layers showing movement in the hub as it rotates 180 degrees.

Mechanical repairs were carried out on the reader after the experiment described here in sub-section 9.2.1 but before the experiment described in sub-section 9.2.2. Amongst other things, the hub was replaced. These are the same repairs referred to in sub-section 8.2.1. After repairs, a Mitutoyo 2046FE dial indicator (Mitutoyo Corporation, Kawasaki-shi, Kanagawa, Japan) was used to measure the relative height of a point close to each carousel recesses as the hub was rotated (Figure 9.2).

Figure 9.2. Dial indicator measurements of the carousel wobble.

* http://www.videolan.org/
† http://www.gimp.org/

9.2.2. Quantitative investigation

To characterise the wobble, as many influence quantities, k_X, as possible were kept constant. If an influence quantity could not be kept constant, averaging was used to blur out its effect.

The influence quantities that could not remain constant were: the wobble of the hub (k_W); the natural distribution of sensitivities in the OSLDs (k_{ECF}); and the change in dose reported between read routines (k_T). All three effects are assumed to be independent.

Equation 2.3 was rearranged to give:

$$S = \frac{D_W}{N_{D,W} \prod k_X} = \frac{D_W}{N_{D,W}\ k_W\ k_{ECF}\ k_T} \tag{9.1}$$

For recess number i, read number j:

$$S(i,j) = \frac{D_W(i,j)}{N_{D,W}(i,j)\ k_W(i,j)\ k_{ECF}(i,j)\ k_T(i,j)} \tag{9.2}$$

Some of the variables above are constant with i, j or both. Therefore:

$$S(i,j) = \frac{D_W}{N_{D,W}\ k_W(i)\ k_{ECF}(i,j)\ k_T(j)} \tag{9.3}$$

The factor k_T is a combination of effects: fading, bleaching and positioning errors but these are assumed to affect all OSLDs equally. In this experiment k_T is normalised such that the mean is 1.

The factors $N_{D,W}$ and $k_{ECF}(i)$ are closely related and could be combined into one calibration factor for each OSLD but in this investigation it is preferable to use $k_{ECF}(i)$, where the average across all the OSLDs is 1.

Ideally, to quantify k_W, all other factors in equation 9.3 would be kept constant over i or j and any change in S would be attributable to k_W. Unfortunately k_{ECF} is not constant with i* and k_T is not constant with j.

* The index i and j are attached to k_{ECF} because the OSLDs are transferred to different recesses between read routines. k_{ECF} is dependent only on the OSLD number. The combination of read number and recess number allowed the OSLD number to be accessed from Table 9.1.

As an alternative, a first estimate of k_W was measured by rearranging equation 9.3 and averaging over all read routines. For recess number i:

$$\bar{k}_W(i) = \frac{1}{17} \sum_{j=1}^{17} \frac{D_W}{N_{D,W}\ k_T(j)\ k_{ECF}(i,j)\ S(i,j)} \tag{9.4}$$

To diminish the effect of k_{ECF} and k_T, seventeen read routines were conducted and the OSLDs were transferred to different recesses between read routines. By replacing k_{ECF} and k_T by their means (i.e. assuming $k_{ECF} = 1$ and $k_T = 1$), equation 9.4 becomes:

$$k_W(i) \approx \frac{D_W}{N_{D,W}\ 17} \sum_{j=1}^{17} S(i,j)^{-1} \tag{9.5}$$

Forty-nine OSLDs were given the numbers 1 to 49. Two hundred monitor units (approximately 2 Gy) was delivered to all the OSLDs on "TU3". The OSLDs were loaded into their matching numbered recesses in the carousel after 30 minutes and a read routine was run. All OSLDs except numbers 1, 11, 21, 31 and 41 were then transferred to another recess and another read routine was run.

A total of 17 read routines were conducted (total of 833 results) with the same forty-four OSLDs transferred to different recesses between each read routine (total of 704 movements). Table 9.1 lists the OSLD in each recess for each read. The mean of all 833 raw signal values was used as the value of the ratio of D_W and $N_{D,W}$.

Table 9.1. OSLD positions during each read routine. The numbers within the table refer to OSLDs. OSLDs numbered 1, 11, 21, 31 and 41 did not move.

	Read 1	Read 2	Read 3	Read 4	Read 5	Read 6	Read 7	Read 8	Read 9	Read 10	Read 11	Read 12	Read 13	Read 14	Read 15	Read 16	Read 17
Recess 1	1	1	1	1	1	1	1	1	1	1	1	1	1	1	1	1	1
Recess 2	2	40	30	20	10	49	39	29	19	9	48	38	28	18	8	47	37
Recess 3	3	42	32	22	12	2	40	30	20	10	49	39	29	19	9	48	38
Recess 4	4	43	33	23	13	3	42	32	22	12	2	40	30	20	10	49	39
Recess 5	5	44	34	24	14	4	43	33	23	13	3	42	32	22	12	2	40
Recess 6	6	45	35	25	15	5	44	34	24	14	4	43	33	23	13	3	42
Recess 7	7	46	36	26	16	6	45	35	25	15	5	44	34	24	14	4	43
Recess 8	8	47	37	27	17	7	46	36	26	16	6	45	35	25	15	5	44
Recess 9	9	48	38	28	18	8	47	37	27	17	7	46	36	26	16	6	45
Recess 10	10	49	39	29	19	9	48	38	28	18	8	47	37	27	17	7	46
Recess 11	11	11	11	11	11	11	11	11	11	11	11	11	11	11	11	11	11
Recess 12	12	2	40	30	20	10	49	39	29	19	9	48	38	28	18	8	47
Recess 13	13	3	42	32	22	12	2	40	30	20	10	49	39	29	19	9	48
Recess 14	14	4	43	33	23	13	3	42	32	22	12	2	40	30	20	10	49
Recess 15	15	5	44	34	24	14	4	43	33	23	13	3	42	32	22	12	2
Recess 16	16	6	45	35	25	15	5	44	34	24	14	4	43	33	23	13	3
Recess 17	17	7	46	36	26	16	6	45	35	25	15	5	44	34	24	14	4
Recess 18	18	8	47	37	27	17	7	46	36	26	16	6	45	35	25	15	5
Recess 19	19	9	48	38	28	18	8	47	37	27	17	7	46	36	26	16	6
Recess 20	20	10	49	39	29	19	9	48	38	28	18	8	47	37	27	17	7
Recess 21	21	21	21	21	21	21	21	21	21	21	21	21	21	21	21	21	21
Recess 22	22	12	2	40	30	20	10	49	39	29	19	9	48	38	28	18	8
Recess 23	23	13	3	42	32	22	12	2	40	30	20	10	49	39	29	19	9
Recess 24	24	14	4	43	33	23	13	3	42	32	22	12	2	40	30	20	10
Recess 25	25	15	5	44	34	24	14	4	43	33	23	13	3	42	32	22	12
Recess 26	26	16	6	45	35	25	15	5	44	34	24	14	4	43	33	23	13
Recess 27	27	17	7	46	36	26	16	6	45	35	25	15	5	44	34	24	14
Recess 28	28	18	8	47	37	27	17	7	46	36	26	16	6	45	35	25	15
Recess 29	29	19	9	48	38	28	18	8	47	37	27	17	7	46	36	26	16
Recess 30	30	20	10	49	39	29	19	9	48	38	28	18	8	47	37	27	17
Recess 31	31	31	31	31	31	31	31	31	31	31	31	31	31	31	31	31	31
Recess 32	32	22	12	2	40	30	20	10	49	39	29	19	9	48	38	28	18
Recess 33	33	23	13	3	42	32	22	12	2	40	30	20	10	49	39	29	19
Recess 34	34	24	14	4	43	33	23	13	3	42	32	22	12	2	40	30	20
Recess 35	35	25	15	5	44	34	24	14	4	43	33	23	13	3	42	32	22
Recess 36	36	26	16	6	45	35	25	15	5	44	34	24	14	4	43	33	23
Recess 37	37	27	17	7	46	36	26	16	6	45	35	25	15	5	44	34	24
Recess 38	38	28	18	8	47	37	27	17	7	46	36	26	16	6	45	35	25
Recess 39	39	29	19	9	48	38	28	18	8	47	37	27	17	7	46	36	26
Recess 40	40	30	20	10	49	39	29	19	9	48	38	28	18	8	47	37	27
Recess 41	41	41	41	41	41	41	41	41	41	41	41	41	41	41	41	41	41
Recess 42	42	32	22	12	2	40	30	20	10	49	39	29	19	9	48	38	28
Recess 43	43	33	23	13	3	42	32	22	12	2	40	30	20	10	49	39	29
Recess 44	44	34	24	14	4	43	33	23	13	3	42	32	22	12	2	40	30
Recess 45	45	35	25	15	5	44	34	24	14	4	43	33	23	13	3	42	32
Recess 46	46	36	26	16	6	45	35	25	15	5	44	34	24	14	4	43	33
Recess 47	47	37	27	17	7	46	36	26	16	6	45	35	25	15	5	44	34
Recess 48	48	38	28	18	8	47	37	27	17	7	46	36	26	16	6	45	35
Recess 49	49	39	29	19	9	48	38	28	18	8	47	37	27	17	7	46	36

A second estimate of k_W was made by correcting every raw signal value for changes in dose reported between read routines. k_T was calculated for each read routine by rearranging equation 9.3 and averaging over all recesses. For read routine number j:

$$\overline{k}_T(j) = \frac{1}{49} \sum_{i=1}^{49} \frac{D_W}{N_{D,W}\ k_W(i)\ k_{ECF}(i,j)\ S(i,j)} \qquad (9.6)$$

By replacing k_W and k_{ECF} by their means (i.e. assuming $k_W = 1$ and $k_{ECF} = 1$), equation 9.6 becomes:

$$k_T(j) \approx \frac{D_W}{N_{D,W}\ 49} \sum_{i=1}^{49} S(i,j)^{-1} \tag{9.7}$$

By substituting k_T into equation 9.4* and once again assuming $k_{ECF} = 1$:

$$k_W(i) \approx \frac{D_W}{N_{D,W}\ 17} \sum_{j=1}^{17} \left(\frac{1}{S(i,j)\ \frac{D_W}{N_{D,W}\ 49} \sum_{i=1}^{49} S(i,j)^{-1}} \right) \tag{9.8}$$

and simplified:

$$k_W(i) \approx \frac{49}{17} \sum_{j=1}^{17} \left(S(i,j)\ \sum_{i=1}^{49} S(i,j)^{-1} \right)^{-1} \tag{9.9}$$

The experimental estimates of k_W were plotted against i and a function was fitted to the data taking the form:

$$\overline{k}_W(i) = a \sin\left(i \frac{2\pi}{50} + b \right) + 1 \tag{9.10}$$

where a and b are fit parameters.

9.2.3. Checking k_W

To confirm the estimated values of k_W, Four read routines were run using three OSLDs that were previously irradiated to approximately 1 Gy† in recesses numbered 1, 3 and 20. After two read routines, the order of the OSLDs was reversed.

* k_T was used in this experiment to calculate k_W but in the normal use the two are independent.

† Exact knowledge of the dose delivered to the OSLDs and correction for k_{ECF} are not required because the no comparison is made here between different OSLs.

Table 9.2. OSLD positions during each read routine.

	Read 1	**Read 2**	**Read 3**	**Read 4**
Recess 1	OSLD 1	OSLD 1	OSLD 3	OSLD 3
Recess 3	OSLD 2	OSLD 2	OSLD 2	OSLD 2
Recess 20	OSLD 3	OSLD 3	OSLD 1	OSLD 1

Dosimeter readings, M, were calculated for each OSLD and read routine. The difference between the mean dosimeter reading for the forward and reversed order was also calculated for each OSLD. If the wobble correction is appropriate, the difference should be less than 1 %. For this experiment, equation 2.2 can be reduced to:

$$M = S \; k_W \; k_T \tag{9.11}$$

Values for k_T were calculated using equation 9.7 and substituting the mean of all twelve values of S for the ratio of D_W to $N_{D,W}$.

Raw signal values were plotted for each OSLD and read routine with no correction; read routine correction only; and with read routine and wobble correction.

9.3. Results

9.3.1. Qualitative investigation

The results of the single irradiation and read routine, as shown in Figure 9.3, exhibited a distinct pattern.

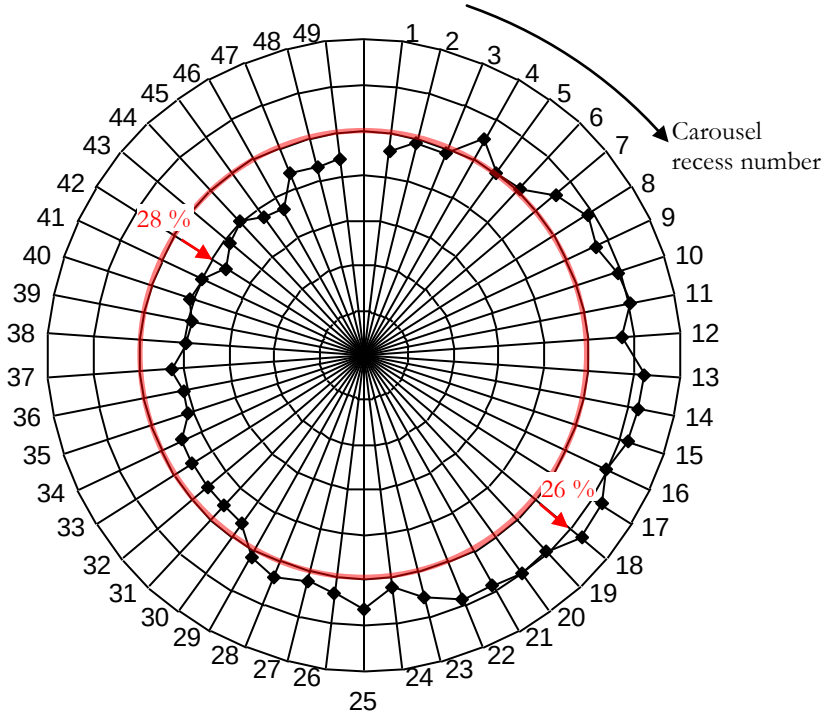

Figure 9.3. Radar plot shows the variation in OSL signal across 49 identically irradiated OSLDs. The distance from any dot to the centre of the plot is proportional to the OSL signal (arbitrary units) of the corresponding OSLD. The red line represents the mean of the OSL signals of all the OSLDs. The red arrows identify the highest and lowest OSL signals and their corresponding differences from the mean as a percentage of the mean.

The OSL signal is noticeably higher on one side of the carousel than the other. For the OSLD in recess number 18 the OSL signal is 26 % higher than the mean OSL signal. Almost directly opposite, the OSLD in recess number 42 has a OSL signal 28 % lower than the mean OSL signal.

The eccentricity in the hub as it rotates is demonstrated in Figure 9.4. The eccentricity is more obvious from the video but is difficult to represent in a static medium.

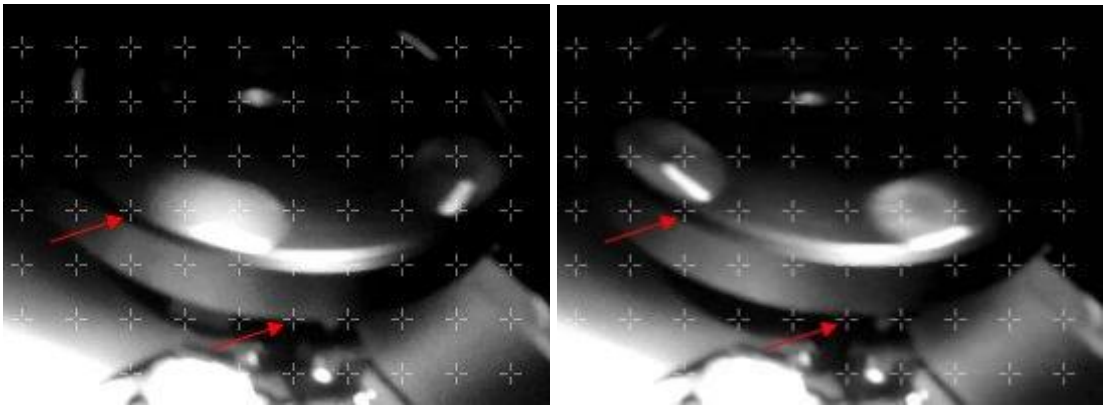

Figure 9.4. Two images separated by approximately 180° show the eccentricity in the hub as it rotates. The grey crosses mark out a grid which is identical on both images. The red arrows identify points where the change in the hub is most obvious.

After repairs, the dial indicator read 0.38 mm at the high side of the carousel and 1.05 mm at the low side.

9.3.2. Quantitative investigation

The first and second estimates of k_W agreed at all recess to within 0.0015 but the uncertainty as estimated by the experimental standard deviation of the mean (ESDM) (BIPM 2008) was much larger for the first estimate as shown in Figure 9.5.

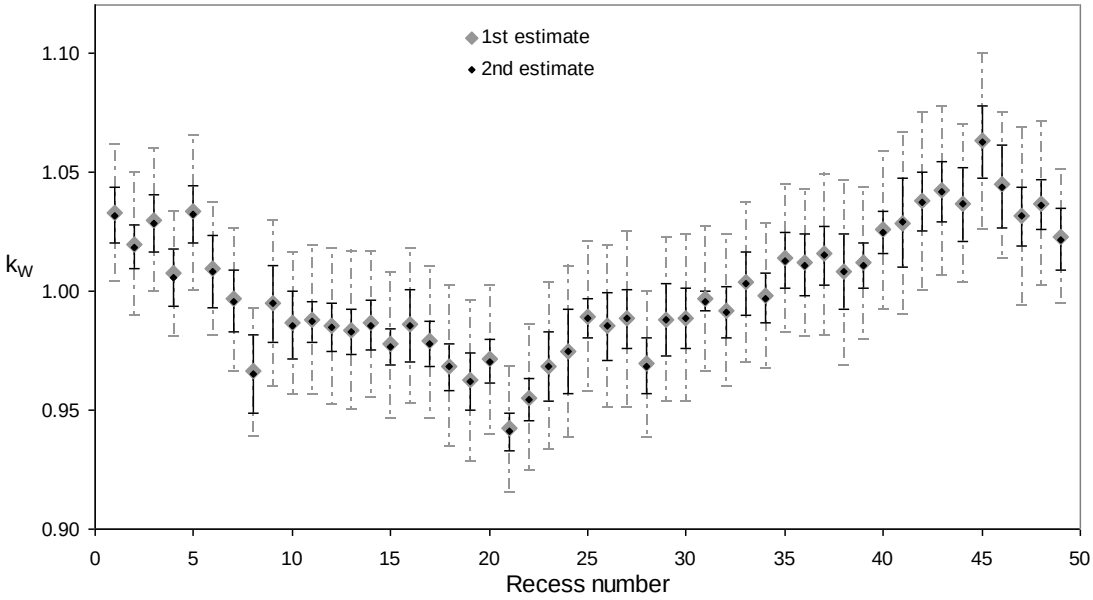

Figure 9.5. Measured estimates of k_W plotted against the recess number i. The grey markers and error bars are the first estimates and the black markers and error bars are the second estimates. The error bars represent the expanded uncertainty as calculated using the ISO Guide to the Expression of Uncertainty in Measurement. The expanded uncertainty is the interval that is estimated to contain the measurand with 95 % probability. The coverage factor for the interval is 2.

Values of $k_T(j)$ are plotted in Figure 9.6.

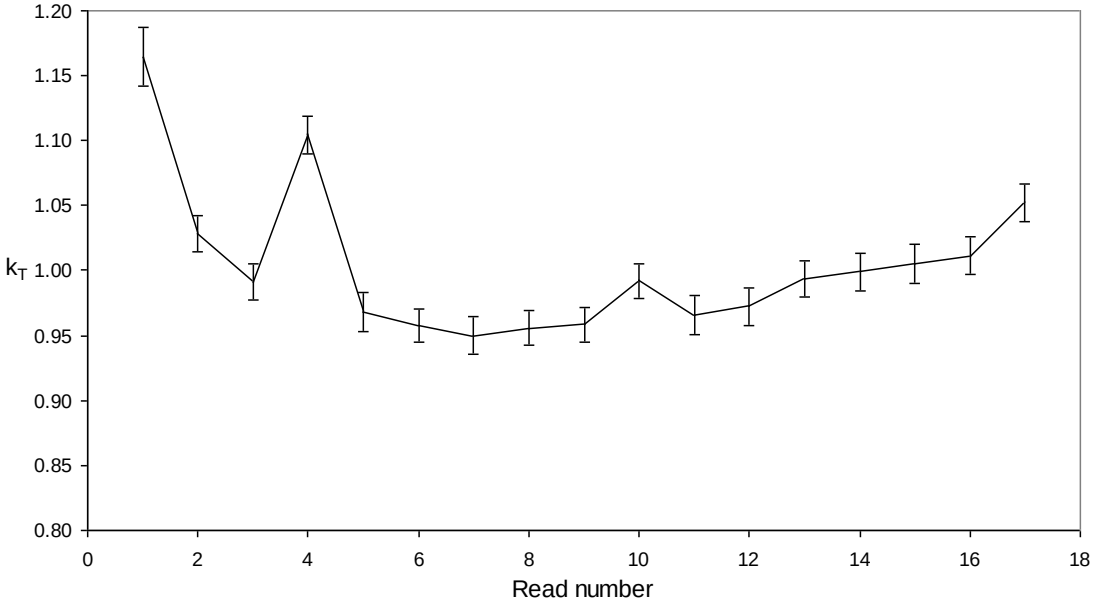

Figure 9.6. Measured values of k_T plotted against the recess number j. The error bars represent the expanded uncertainty as calculated using the ISO Guide to the Expression of Uncertainty in Measurement. The coverage factor for the interval is 2.

The fit parameters a and b equal 0.035 ± 0.004 and 2.16 ± 0.13 respectively. The interval is estimated to contain the measurand with 95 % probability. The coverage factor for the interval is 2. Equation 9.10 becomes:

$$k_W(i) = 0.035 \sin\left(i \frac{2\pi}{50} + 2.16\right) + 1 \qquad (9.12)$$

as shown in Figure 9.7. Values of k_W for recesses 1-49 are tabulated in Table 9.3.

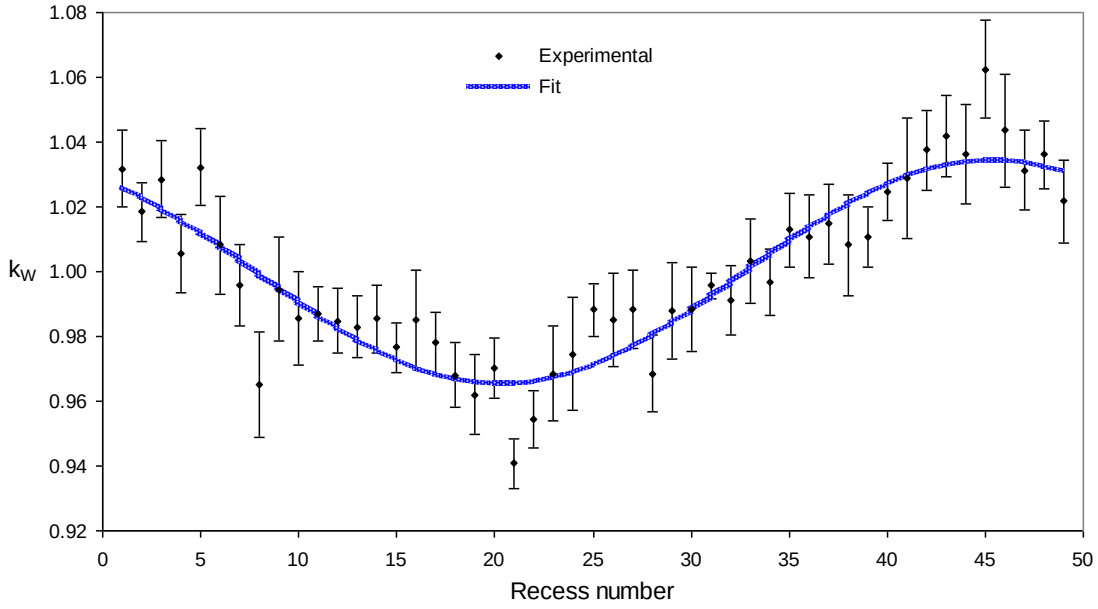

Figure 9.7. Measured estimates of k_W plotted against the recess number i. The error bars represent the expanded uncertainty as calculated using the ISO Guide to the Expression of Uncertainty in Measurement. The coverage factor for the interval is 2.

Table 9.3. Carousel recess number correction factor, k_W.

Recess	k_W	Recess	k_W	Recess	k_W	Recess	k_W
1	1.026	14	0.976	26	0.974	38	1.021
2	1.023	15	0.973	27	0.977	39	1.024
3	1.020	16	0.970	28	0.980	40	1.027
4	1.016	17	0.968	29	0.984	41	1.030
5	1.012	18	0.967	30	0.988	42	1.032
6	1.008	19	0.966	31	0.992	43	1.033
7	1.004	20	0.965	32	0.996	44	1.034
8	0.999	21	0.966	33	1.001	45	1.035
9	0.995	22	0.966	34	1.005	46	1.034
10	0.991	23	0.967	35	1.009	47	1.034
11	0.987	24	0.969	36	1.013	48	1.033
12	0.983	25	0.971	37	1.017	49	1.031
13	0.979						

9.3.3. Checking k_W

The dosimeter readings for each read routine are shown in Table 9.4. The difference between the means of the forward and reversed order as a percentage of the reversed order is very small.

Table 9.4. Dosimeter readings in counts, M, for each OSLD and read routine.

	Forward order		Reversed order		Difference
	Read 1	Read 2	Read 3	Read 4	
OSLD 1	114006	111956	112576	112660	−0.3%
OSLD 2	99942	99434	99408	99852	−0.1%
OSLD 3	103751	106160	105163	104627	−0.1%

Figure 9.8 shows reduction in the range of raw signal values obtained by applying read routine and wobble corrections. The range is not reduced for OSLD number 3 with the application of a wobble correction factor because this OSLD is always in the same recess.

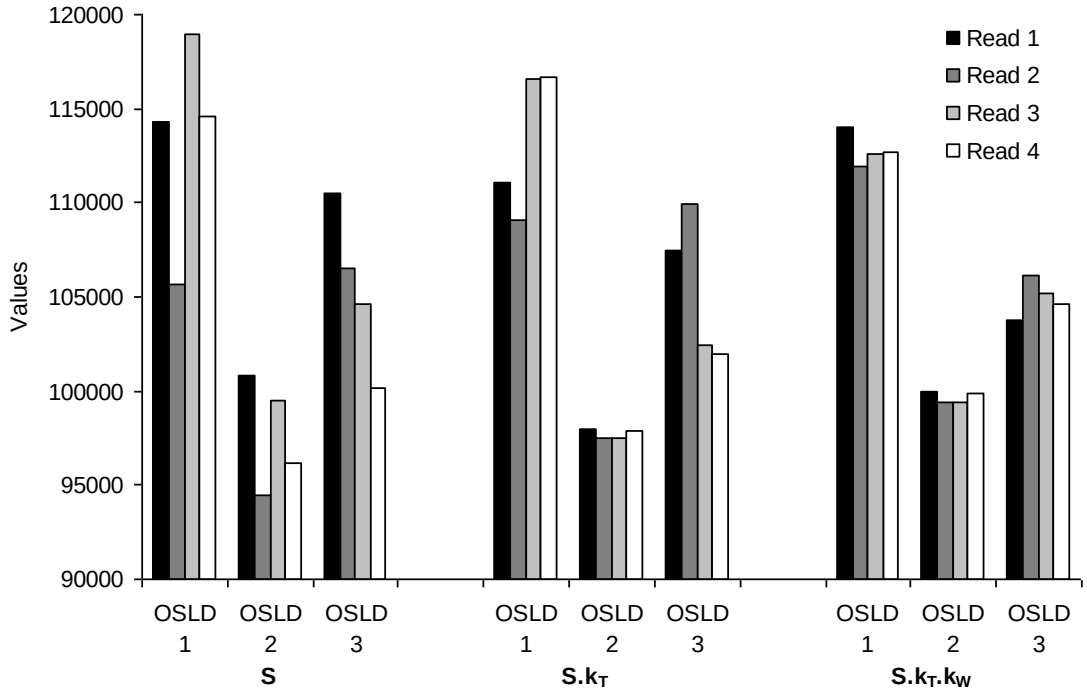

Figure 9.8. No correction (left); routine correction (centre); routine and wobble correction (right)

9.4. Discussion

Given the visible wobble in the hub, the logical explanation for differences in relative raw signal around the carousel is that the separation between the OSLD being stimulated and the PMT varies around the carousel.

After the repairs mentioned above, a point on the carousel near the recesses was found to move vertically by 0.335 mm from the mid point (i.e. variation in each direction, s_{var} = 0.335 mm). If the mean separation, s, is assumed to be approximately 20 mm and if the change in raw signal varies with the square of the separation then wobble correction is:

$$k_W(\text{low side}) = \left(\frac{s}{s - s_{var}}\right)^2 = 1.034 \qquad (9.13)$$

$$k_W(\text{high side}) = \left(\frac{s}{s + s_{var}}\right)^2 = 0.967 \qquad (9.14)$$

These values are very close (within 0.002) to the estimates of the highest and lowest k_W given above.

The cause of the wobble is likely to be a small misalignment of the hub on the spindle. Further reduction of the wobble may be possible if the hub is removed and refitted but such a reduction is limited because the three grub screws which hold the hub onto the spindle are in the same plane.

This investigation does not provide evidence that the wobble is stable. This experiment should be repeated regularly unless a more stable spindle and hub are developed.

9.5. Conclusions

The wobble correction factors given in Table 9.3 agree with those expected based on the dial indicator measurements. When the wobble factors are used to correct raw signal values, the effect of moving OSLDs to different recesses is removed. No wobble correction is required if a OSLD is always used in the same recess or if a comparison is made between the averages of groups of OSLDs in the same recesses.

A wobble is an inevitable feature with the current design of the reader. There is no evidence to show that the wobble is stable in the long term. Therefore parts of this investigation should be repeated annaully.

10. Accumulated dose since last bleaching

10.1. Introduction

Measurement is greatly simplified if the measurement device has a linear response to the quantity being measured. There are two approaches if the device is not linear: (1) select from several calibration factors across the range of doses delivered; or (2) apply a single calibration factor and then correct for non-uniformity. The later is proposed here.

Non-linearity in Al_2O_3:C dosimetry is reported in the literature (Yukihara & McKeever 2011; Dunn et al. 2013; Jursinic 2007; Yukihara et al. 2004). The ratio of delivered dose to raw signal anywhere on the response curve gives an indication of the local sensitivity. By normalising to a dose value within a range that is known to be linear, the raw signal may be "corrected" back to linear response.

The OSLDs and reader were considered together as the measurement device. An experiment was conducted to investigate the response of OSLDs and reader to accumulated dose delivered in 2 Gy steps up to 22 Gy. This range was chosen because the vendor recommended reusing the dosimeters without bleaching but subtracting previous irradiations. Even if the OSLDs are used several times, this range should be sufficient.

10.2. Materials and methods

Fifty OSLDs were divided into two equal sets. One set to determine response in the 2 Gy – 12 Gy range and the other to determine response in the 12 Gy – 22 Gy range. Set "1-25" was placed in one solid water phantom with depressions numbered 1 to 25 and the other set "26-50" was placed in a second solid water phantom with depressions numbered 26 to 50.

The dose correction factor (DCF) on TU2 was measured using an FC65-P ionisation chamber (SN: 2133). The number of monitor units required to deliver 2.00 Gy to the OSLDs was calculated. Both sets of OSLDs were irradiated with six 2.00 Gy steps. Each

step consisted of 2.00 Gy being delivered under SCRC on TU2 except the first step for set "26-50" which was 12.00 Gy.

A read routine was run 30 minutes after each dose step. A polynomial fit to the collected data was calculated using TableCurve™:

$$S = a + b\,D + c\,D^2 + d\,D^3 + e\,D^4 \tag{10.1}$$

Where S is the raw signal, D is the delivered dose and the lower-case letters a to e are the fit parameters determined using TableCurve™.

The response was converted into a non-linearity correction factor using equation 10.2. The non-linearity correction factor is normalised to 1 at the 2.00 Gy point.

$$k_L = \frac{D}{2}\frac{S_{2Gy}}{S} \tag{10.2}$$

Where k_L is the non-linearity correction factor normalised to 2 Gy, S_{2Gy} is the raw signal produced by 2 Gy delivered dose and D_{2Gy} is 2.00 Gy.

To allow easy interpolation, the non-linearity correction was plotted with respect to the raw signal and a curve of best fit was calculated using TableCurve™:

$$k_L = \frac{1}{f + g\,D^2} \tag{10.3}$$

Where the lower-case letters f and g are the fit parameters determined using TableCurve™.

10.3. Results

The DCF on TU2 was 1.000. Therefore each irradiation was 200 MU except for the first irradiation for set "26-50" which was 1200 MU. The LINAC's linear output with respect to MUs is checked annually with a tolerance of 1 %.

The read signal is plotted against the delivered dose in Figure 10.1. The fit to the collected data calculated using TableCurve™ had a coefficient of determination (r^2) of 0.9994 demonstrating good correlation between the fit and collected data.

The raw signal values for a delivered dose of 12.00 Gy from both sets agree closely. Their means are only 1755 counts (0.2 %) apart and a two-tailed t-test (paired samples) of the hypothesis that their means are equal by chance has a p-value of 0.78. Therefore there is no statistically significant difference between the two sets at 12.00 Gy and only one point need be considered.

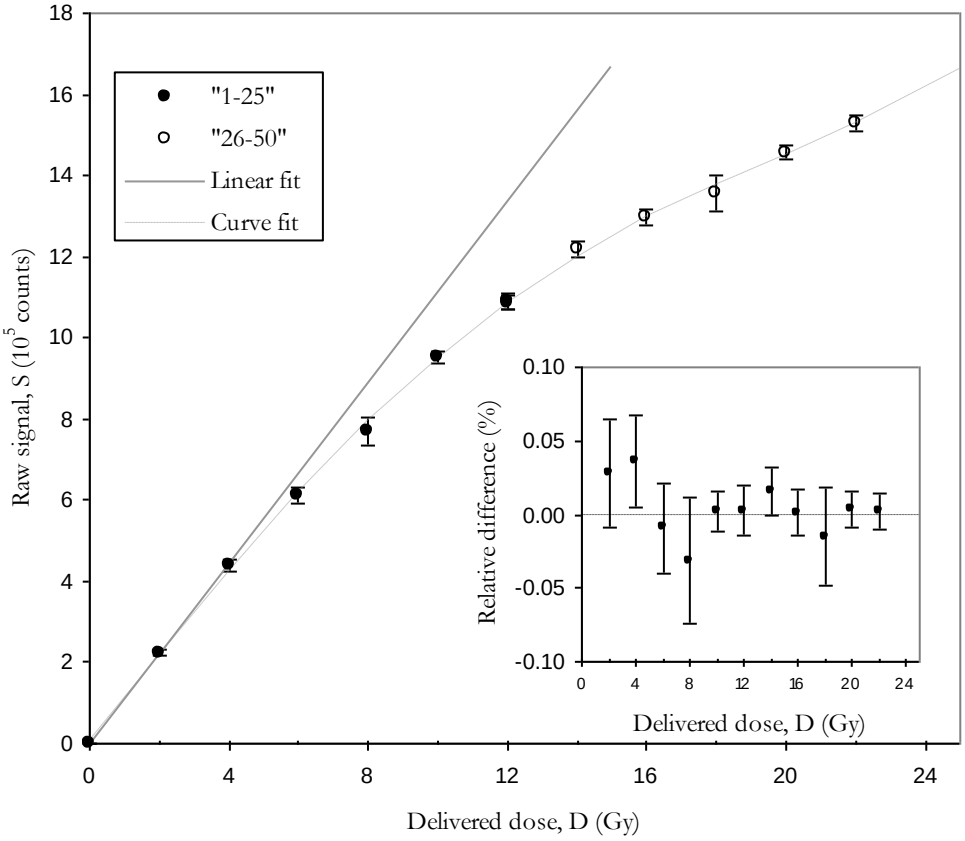

Figure 10.1. Response to delivered dose and difference between experimental data and fit (inset). The circles represent the mean raw signal of the set and the error bars represent one standard deviation of the raw signal values for each step. The 12.00 Gy point for set "26-50" is hidden by the 12.00 Gy point for set "1-25". The solid line is a linear fit to the 0 Gy and 2 Gy steps for set "1-25" extrapolated to 15 Gy. The dashed line is calculated using equation 10.1 and the following parameters: a = 6107.608848 counts, b = 105549.9794 counts/Gy^1, c = 360.7702434 counts/Gy^2, d = −195.974421 counts/Gy^3 and e = 4.739770889 counts/Gy^4. For the 12 Gy point only the difference for the "1-25" set is considered.

The non-linearity correction factor is plotted against the raw signal in Figure 10.2. The fit to the collected data calculated using TableCurve™ had a coefficient of determination of 0.9804 and passes within the combined standard uncertainty of each data point. The non-linearity correction factor for a range of raw signal values is given in Table 10.1.

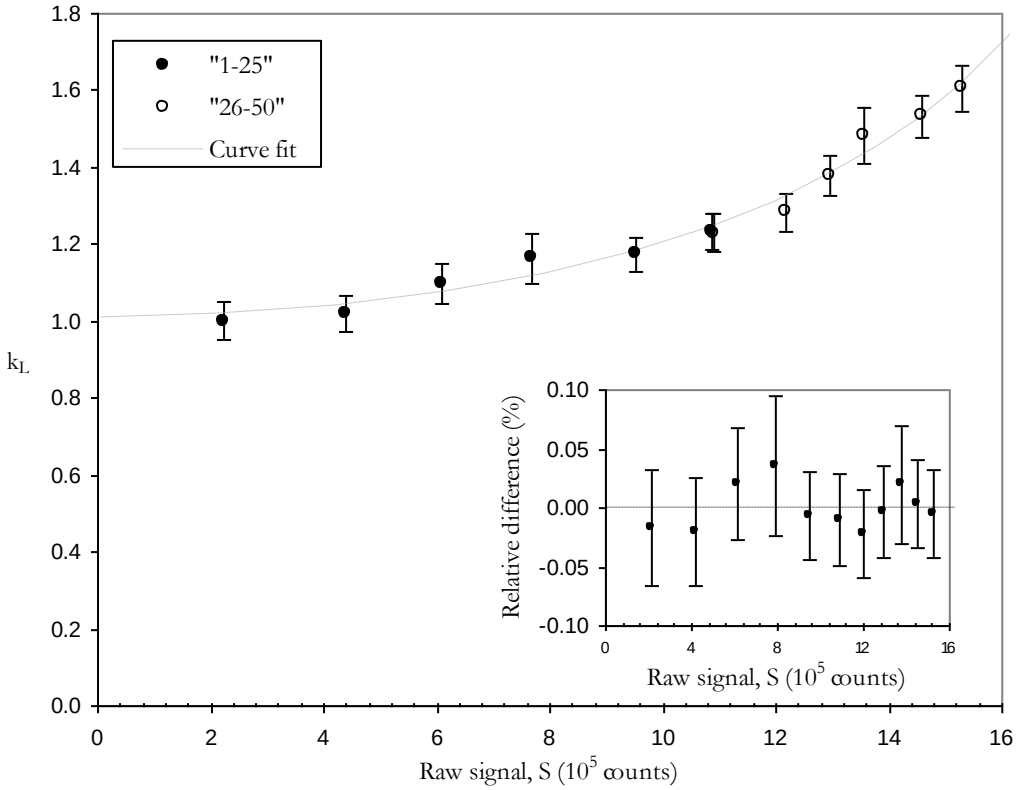

Figure 10.2. Non-linearity correction factor and the difference between experimental data and fit (inset). The circles represent the non-linearity correction calculated from equation 10.2 and the error bars represent the combined standard uncertainty for each dose step. The 12.00 Gy point for set "26-50" is partially hidden by the 12.00 Gy point for set "1-25". The dashed line is calculated using equation 10.3 and the following parameters: f = 0.990046197 and g = −0.001589 counts^{-2}. For the 12 Gy point only the difference for the "1-25" set is considered.

Table 10.1. Non-linearity correction factor for OSLDs.

Raw signal (10^5 counts)	0.5	1	2	4	6	8	10	12	14
k_L	1.01	1.01	1.02	1.04	1.07	1.13	1.20	1.31	1.47

10.4. Discussion

The above results show the response of OSLDs and reader to delivered dose to be linear below 4 Gy, i.e. the linear fit is within standard uncertainty of the mean response. The response becomes increasingly sub-linear above 4 Gy. The total dose range characterised above was investigated with two different sets of OSLDs but the response curve should be considered to be continuous because there is good agreement at the 12 Gy point.

Yukihara and McKeever (2011) state that the response of Al_2O_3:C is linear below approximately 10 Gy, supra-linear up to some value (approximately 40 Gy or 300 Gy depending on how the raw signal is produced) and then sub-linear. Dunn, Lye et al. (2013) reported supra-linearity over the range investigated (0 Gy to 11 Gy) for InLight® nanoDots™ (Landauer Inc., Glenwood, IL, USA) while Jursinic (2007) reported linearity below 3 Gy and supra-linearity between 3 Gy and 10 Gy while characterising InLight® OSL Dots (Landauer Inc., Glenwood, IL, USA).

McKeever and Chen (1997) attribute changes in sensitivity of TL/OSL materials to competition between traps of different depths for charge carriers excited by absorbed dose. Another possible cause of non-linear response may be the reader itself. The scintillation crystal, photomultiplier tube or counting circuitry may begin to saturate if the choice of any component is inappropriate for the level of luminescence from the OSLD.

It is evident that the results of this investigation are not consistent with those reported in the literature but this is not unexpected given the different equipment used. A satisfactory explanation for the difference is difficult without detailed knowledge of the components of the reader and the systems used by the above authors (all proprietary systems).

The reader software assumes linearity in its automatic conversion from raw signal to reader dose. The assumption of linearity becomes unacceptable above 4 Gy accumulated dose and therefore the WBRC work instruction proposes removal of the internal calibration and application of a non-lineary correction factor (k_L). The assumption that $k_L = 1$ is reasonable below 4 Gy.

The equations for the line of best fit of k_L described above can only be used for interpolation between measured values. No correlation between the fit and real response can be assumed above 22 Gy.

10.5. Conclusions

The relationship between raw signal and delivered dose for the OSLDs and reader is linear below 4 Gy and progressively more sub-linear above 4 Gy. A non-linearity

correction has been reported above can be applied to the raw signal of each Al_2O_3:C and users are advised to pay special attention to non-linear behaviour above 4 Gy.

11. Dose rate and irradiation angle

11.1. Introduction

Radiotherapy treatments make use of various LINAC dose rates (MU/min) for technological and biological reasons. The LINAC produces a pulsed beam; therefore the nominal dose rate is an average with time. The response of the OSLDs was expected to be independent of dose rate because the dose per pulse is constant.

When used as an in-vivo dosimeter, the angle between the source and the OSLD front face (irradiation angle) will vary depending on the shape of the patient's surface. The response of the OSLDs was expected to also be independent of irradiation angle.

11.2. Materials and methods

11.2.1. Average dose rate

To measure dose rate dependence, twenty-five OSLDs were separated into five groups. Each group was irradiated with 200 MU under SCRC on TU1 with a different dose rate (see Table 11.1).

Table 11.1. Five groups of OSLDs irradiated with a different dose rate.

Group	**OSLD** i =	**Dose rate** (MU/min)
1	1-5	160
2	6-10	320
3	11-15	480
4	16-20	640
5	21-25	800

The irradiations occurred over 20 minutes and a read routine was run 2 hours after the last irradiation. All raw signal values were corrected for carousel wobble using:

$$M(i) = S(i) \cdot k_W(i) \qquad (11.1)$$

where i is the OSLD or recess (same) and $k_W(i)$ is the values determined in chapter 9. The mean for each dose rate (DR) was calculated using:

$$\bar{M}_{DR} = \frac{1}{5}\sum_{i} M(i) \qquad (11.2)$$

All mean dosimeter readings were normalised to the mean dosimeter reading for group 1 (160 MU/min).

11.2.2. Irradiation angle

To measure the angular dependence of the OSLDs a Perspex™ blank in the shape of farmer-type ionisation chamber was machined. A cavity was milled so that a OSLD can be placed on the blank's central axis. A plug was also machined to hold the OSLD in place.

Figure 11.1. Perspex™ farmer-type shaped blank with cavity for OSLD and plug.

The experimental setup is depicted in Figure 11.2. Specialised slabs with cavities for farmer-type and CC13 ionisation chambers were stacked along with 1 cm thick slabs. A CC13 ionisation chamber (SN: 5676) placed in its slab on the beam's central axis.

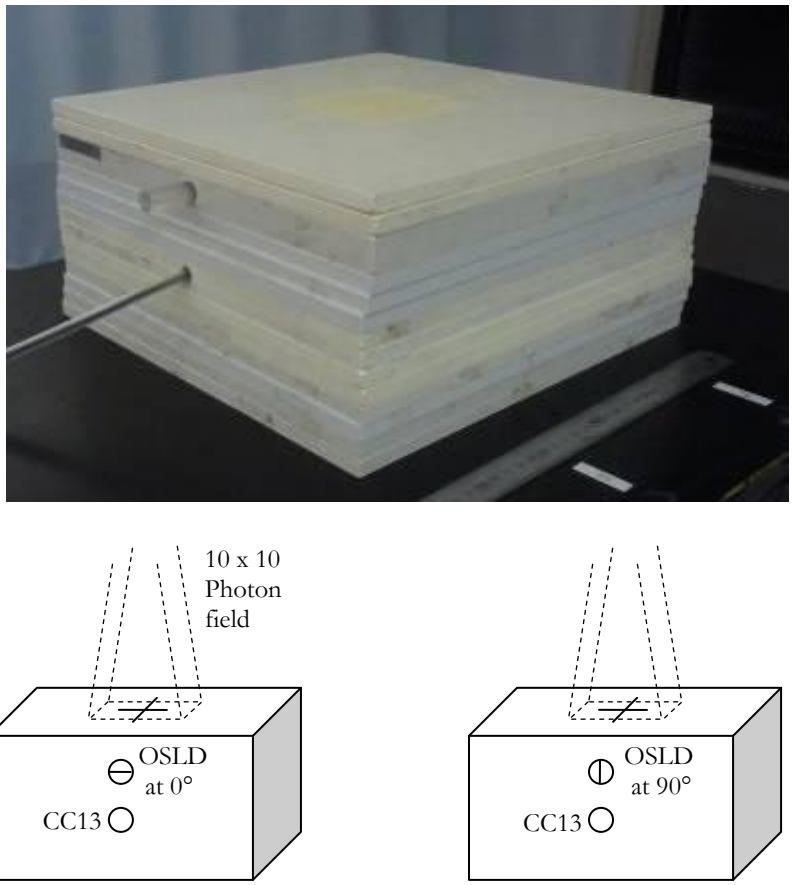

Figure 11.2. Experimental setup used to measure angular dependence.

The blank fit snugly into the cavity for the farmer-type ionisation chamber. The OSLD was held 2 cm from the beam's central axis; well within the flat region of the 10 cm x 10 cm field.

Twenty different OSLDs were irradiated in turn with 100 MU in the above experimental setup on LA4 over 1 hour. The blank was positioned alternatively at two different rotations around the blank's central axis. Even-numbered OSLDs were positioned perpendicular (0°) and odd-numbered OSLDs were positioned parallel (90°) to the beam's central axis. The irradiation angles were actually 1.1° and 88.9° due to the 2 cm offset from the beam's central axis.

The signal from the CC13 was used to confirm that LINAC output was stable across all irradiations. A read routine was run sixty minutes after the last irradiation with the OSLDs placed in order of irradiation. All raw signal values were corrected for carousel wobble using:

$$M(i) = S(i) \cdot k_W(i) \quad (11.3)$$

where i is the OSLD or recess (same) and $k_W(i)$ is the values determined in chapter 9.

11.3. Results

11.3.1. Average dose rate

Mean dosimeter readings for each dose rate group are presented in Figure 11.3. There is significant overlap in the expanded uncertainty range (95 % probability of containing measurand) for all dose rates.

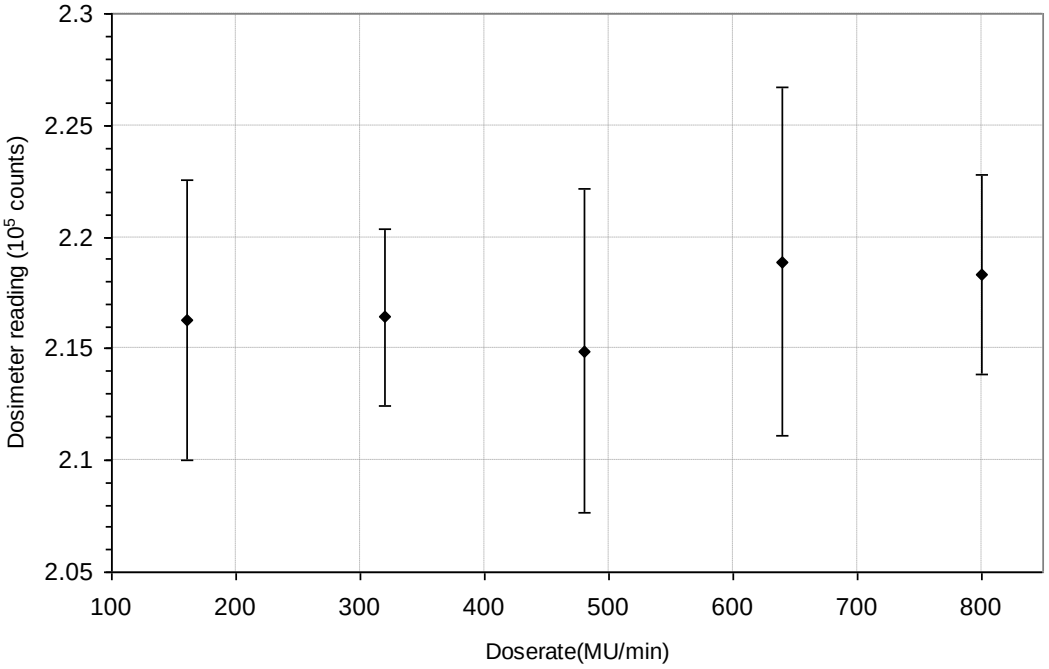

Figure 11.3. Dosimeter readings for OSLDs in five groups irradiated at different dose rates. The error bars represent the expanded uncertainty.

Calculated results for the five groups irradiated at different dose rates are presented in Table 11.2. The normalised mean dosimeter readings are within expanded uncertainty (95 % probability) of 1.00 at all dose rates. An analysis of variance test shows that there is no statistically significant differences between the five groups ($p = 0.82$).

Table 11.2. Calculated results for OSLDs in five groups irradiated at different dose rates. M_N is the normalised mean dosimeter reading and U is the expanded uncertainty in the normalised mean.

Group	Doserate (MU/min)	M_{DR} (counts)	M_N	U (M_N) k = 2.78
1	160	216283	1.00	0.03
2	320	216416	1.00	0.02
3	480	214893	0.99	0.03
4	640	218879	1.01	0.04
5	800	218336	1.01	0.02

11.3.2. Irradiation angle

The dosimeter reading values for all twenty OSLDs are presented in Figure 11.4

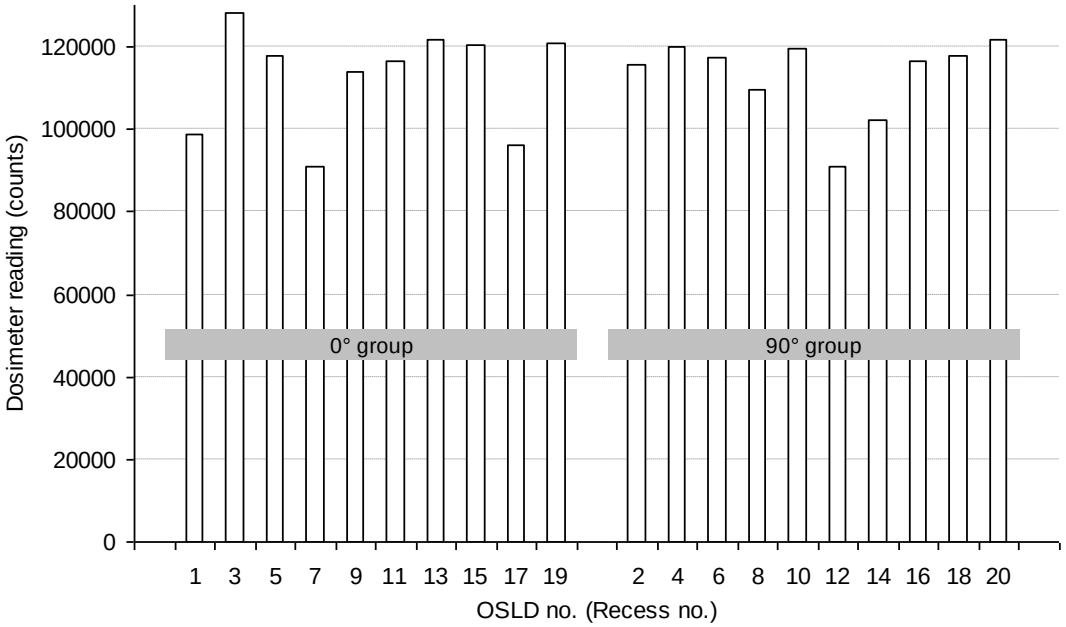

Figure 11.4. Dosimeter readings for OSLDs angled at either 0° or 90° to the beam's central axis.

The difference in the means of the two groups is 0.5 %. A two-tailed t-test (two-sample unequal variance) on the two groups showed that the difference in the means is not statistically significant (p = 0.90).

A chi-squared test showed that there was no statistically significant deviation in the CC13 readings from constant (p =1.00). Therefore the LINAC output was stable.

11.4. Conclusion

The response of the OSLDs has no statistically significant dependence on nominal dose rate or irradiation angle (significance level of 0.05).

12. Calibration and measurement method

12.1. Introduction

To fulfil the primary aim of this project, a method was devised to calculate the dose delivered to an OSLD using the reader dose values, S_{mrad}, reported by the reader. Equation 6.2 was substituted into equation 2.3 and the $\prod k_X$ term was expanded to reflect those influence quantities on which the raw signal, S, has been observed to depend:

$$D_{calc} = N_{D,W} \left(\frac{S_{mrad} + S_{offset}}{f_{cal}} \right) k_{ECF} \; k_L \; k_W \; k_T \qquad (12.1)$$

Correction factors were estimated in the above investigations for carousel wobble, k_W, (Table 9.3 and equation 9.12) and accumulated dose since last bleaching, k_L, (Table 10.1 and equation 10.3). Irradiation angle and dose rate were demonstrated to have no effect. The absorbed dose to water calibration factor, $N_{D,W}$, and element correction factor, k_{ECF}, were established during calibration.

Correction factors for photon energy, dose signal fading at room temperature, and dose history could not be determined accurately. Pilot experiments were conducted but these influence quantities were small compared to the read routine inconsistency.

The read routine correction factor k_T, is a combination of effects such as fading, bleaching and positioning errors that are common to all OSLDs in the same read routine. In chapter 8, hub slippage was concluded to be the most likely cause of inconsistent values of k_T.

Estimation of k_T was impossible because it was unpredictable. In sub-sections 8.3.1 and 9.3.2 the factor (k_T) was calculated in order to correct for the mean change in raw signal with repeated read routines during experiments. Figure 12.1 shows the average raw signal for each repeated read routine in these two experiments (normalised to the maximum average raw signal).

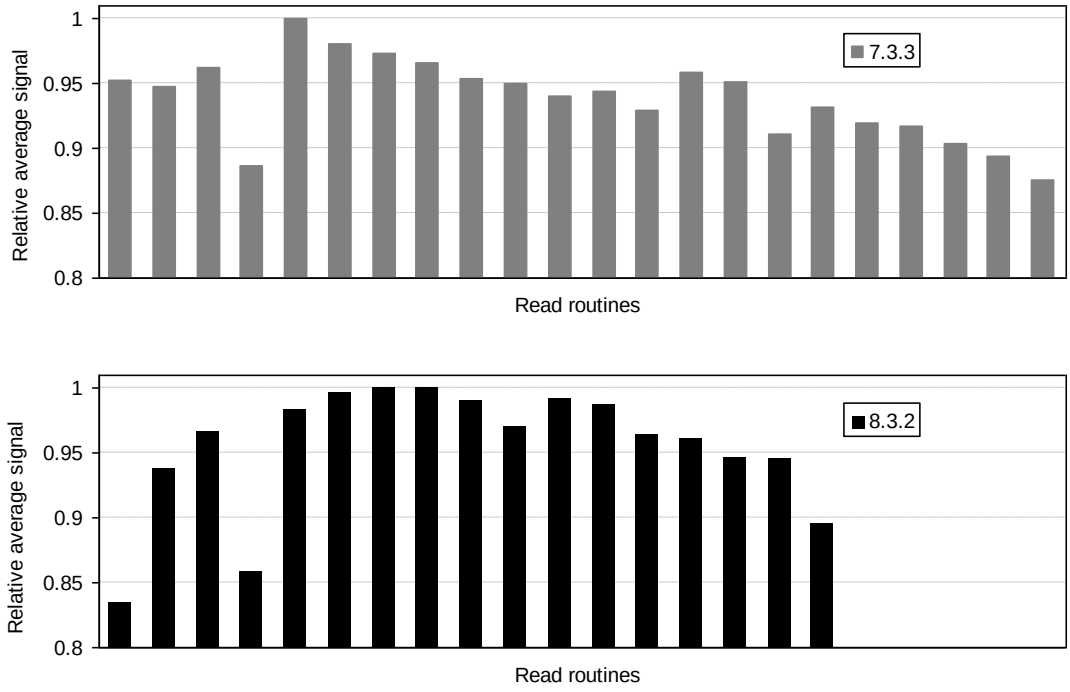

Figure 12.1. The average raw signal from repeated read routines in two experiments. The averages are normalised to the highest average in each experiment.

When used for in vivo dosimetry, having no value for k_T may lead to an error in the calculated dose of more than 15 %. Therefore a method must be developed to predict or observe the relative response for each read routine.

12.2. Method

A typical in vivo dosimetry measurement may include two or four OSLDs (i.e. one or two sites, OSLDs paired for redundancy). The proposed method employs extra reference OSLDs which were calibrated with the dosimetry OSLDs but not irradiated on the patient (in this case a solid water phantom). At the measurement read routine, the reference OSLDs were included. Their relative raw signal values were used to estimate k_T.

For this method, a superscript C refers to the calibration (known irradiation and read routine) and the superscript M refers to the in vivo measurement (unknown irradiation and read routine). Subscript "R" indicates a reference OSLD and i is the OSLD number for the dosimetry OSLDs.

12.2.1. Calibration

A small known dose (e.g. 0.5 Gy) was given to all the OSLDs and a read routine was run. The ratio of the average wobble-corrected raw signal to each individual wobble-corrected raw signal is used to calculate $k_{ECF,i}$ for each dosimetry OSLD:

$$k_{ECF,i} = \frac{\sum_i (S_i^C \, k_{W,i})}{S_i^C \, k_{W,i}} \tag{12.2}$$

The above assumes that the average sensitivity of the OSLDs is 1. The overall calibration is calculated from the average dosimeter reading:

$$N_{D,W} = \frac{D_W^C}{\frac{1}{n}\sum_i M_i^C} = \frac{D_W^C}{\frac{1}{n}\sum_i (S_i^C \, k_{W,i} \, k_{ECF,i})} \tag{12.3}$$

No correction is made for dose since last bleaching because OSLD response is linear at 0.5 Gy. k_T is assumed to be 1 for the calibration read routine.

12.2.2. Measurement

The two or four calibrated OSLDs were used in an in vivo dosimetry measurement while the reference OSLDs were stored in the dark. A read routine was run containing all OSLDs.

12.2.3. Calculation of k_T

The ratio of raw signal values for the reference OSLDs in the calibration and measurement read routines was used to correct for any change in response of the reader:

$$k_T = \frac{\sum S_R^C}{\sum S_R^M} \tag{12.4}$$

The calibration dosimeter reading was subtracted from the measurement dosimeter reading.

$$D_{calc,i} = N_{D,W} \, (M_i^M - M_i^C) \tag{12.5}$$

Therefore:

$$D_{calc} = N_{D,W}\ k_{ECF,i}\ k_{W,i} \left[\left(\frac{S_{mrad}^{M} + S_{offset}}{f_{cal}} \right) k_L\ k_T \right) - \left(\frac{S_{mrad}^{C} + S_{offset}}{f_{cal}} \right) \right] \quad (12.6)$$

12.3. Example

The following example (Table 12.1) was simulated using Microsoft® Office Excel 2003 and the characteristics of the OSLDs determined in this project. A known dose of 0.5 Gy was delivered to six OSLDs and the expected raw signal calculated assuming an effect of the carousel wobble consistent with sub-section 9.3.2 and a randomly generated OSLD sensitivity (sampled from a normal population with mean = 112000 counts/Gy, σ = 2800 counts/Gy).

The unknown dose delivered and the change in reader response were randomly generated (D_W^M sampled from a normal population with mean = 1.0 Gy, σ = 0.05 Gy; and k_T^{-1} sampled from a normal population with mean = 1.0, σ = 0.15).

Table 12.1. Simulation of an example of the above method. The far-right column indicates the source of the values given in each row. "1" indicates a number strategically chosen; "2" indicates a randomly generated value; "3" indicates a value looked up in a table; and "4" indicates a value calculated using the equations in this chapter.

	OSLD 1 (reference)	**OSLD 2**	**OSLD 3**	**OSLD 4**	**OSLD 5**	**OSLD 6** (reference)	**Source**
D_W^C (Gy)	0.50	0.50	0.50	0.50	0.5	0.5	1
S^C (cts)	54979	57171	54965	55284	54935	56095	2
k_W		1.023	1.020	1.016	1.012		3
k_{ECF}		0.967	1.009	1.007	1.018		4
M^C (cts)		56576	56576	56576	56576		4
$N_{D,W}$ (Gy/cts)	0	8.84 x10^{-6}	8.84 x10^{-6}	8.84 x10^{-6}	8.84 x10^{-6}		4
D_W^M (Gy)	0.000	1.003	1.003	1.003	1.003	0.000	2
S^M (cts)	53630	167692	161220	162157	161134	54718	
k_T	1.025	1.025	1.025	1.025	1.025	1.025	2
M^M (cts)	0	170123	170123	170123	170123	0	4
$M^M - M^C$		113547	113547	113547	113547		4
D_{cal}^M (Gy)		1.003	1.003	1.003	1.003		4

The simulation correctly calculated the unknown delivered dose (i.e. $D_W^M = D_{calc}^M$) for many sets of randomly generated values. The simulation assumes infinitely precise delivered dose and correction factors. A simulation was demonstrated here because the real results were less certain and therefore obscured the suitability of the method.

12.4. Uncertainty in k_T

The uncertainty in the correction factor k_T (and subsequently D_{calc}) is related to the number of reference OSLDs as shown by Figure 12.2. The results of the repeated reads described in sub-section 9.3.2 were revisited. These results and Equation 12.4 were used to calculate values of k_T for each read routine based on two, four, twenty and forty-nine OSLDs.

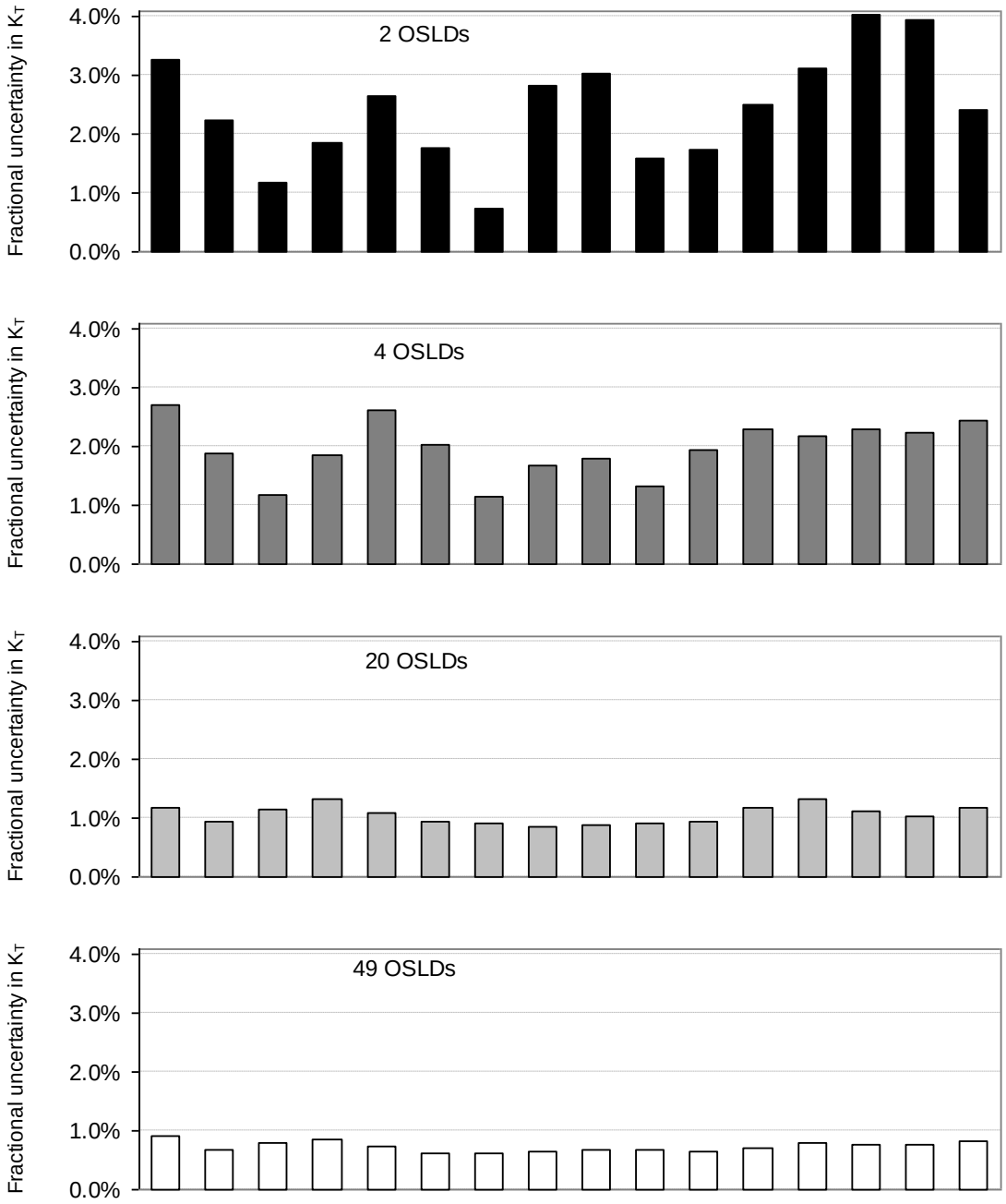

Figure 12.2. The factional standard uncertainty in k_T decreases with the number of OSLDs used.

12.5. Discussion

The above method for measuring an unknown dose with the OSLDs doesn't account for dose signal fading at room temperature. Some fading will occur between the two read routines and will lead to an overestimation of k_T. The inconstant response makes quantification of room temperature dose signal fading very difficult so currently fading must be ignored.

A larger number of reference OSLDs will reduce the uncertainty in k_T but using 20+ reference OSLDs for each in vivo measurement is prohibitive.

12.6. Conclusions

A method has been devised to calculate the dose delivered to an OSLD using the reader dose values, S_{mrad}, reported by the reader.

The proposed method provides a more certain calculated dose than the dose reported by the reader but the uncertainty in the wobble correction and read routine correction factors are still significant. Therefore the OSL system should not be used clinically until the issues of read routine inconsistency and carousel wobble can be fully resolved.

13. Conclusions

13.1. Project summary

This project documents the attempted implementation of a new optically stimulated luminescence (OSL) system comprising aluminium oxide OSL dosimeters (OSLDs) and a reader. The primary aim was to move from the reader's simple internal dose calculation method to a method that considers all the OSLD system's influence quantities. The secondary aim of this project was to uncover the practical considerations, such as the effect of ambient light, which would guide the safe and accurate use of the OSLD system in the clinic.

Scanning electron microscope images and energy dispersive spectroscopy provided insight into the composition and structure of the OSLDs. The OSLDs are likely to be unsuitable for water phantom measurements due to possible infiltration by water or contaminants into the unsealed edges.

The lack of Al_2O_3:C crystals on the OSLD surface may need to be considered if using the OSLDs to measure surface dose or if measuring very low energy radiation. The distribution of Al_2O_3:C crystals suggests that if the OSLDs were cut down to a smaller size or another shape, there may be a greater sensitivity difference between OSLDs.

Exposure to typical office or laboratory lighting can have a significant effect. A two minute exposure to room light can introduce up to a 5 % underestimation of the calculated dose. This finding has lead to the recommendation that OSLDs should not be handled in a room with the lights turned on.

An inexpensive black plastic was found to be suitable to preserve the dose information stored in the OSLDs. There was no statistically significant difference between OSLDs stored in the dark and OSLDs covered by a single layer of black plastic and exposed to room light for two hours. Light-tight packages were made with this plastic and an impulse sealer to enable easy handling by staff in light-filled treatment rooms.

The relationship between the reader dose reported by the system and the raw signal from the photomultiplier tube was found to be linear. The gradient can be found in the dose report for each read routine, the intercept must be found via observing a read routine in engineering mode. The gradient and intercept will need to be remeasured in the event of recalibration being required due to a software upgrade or failure.

By restricting irradiation to specific zones on several OSLDs it was observed that approximately 33 % of the OSL originated from within 0.5 mm of the edge of the gap through which the OSLD was stimulated. A portion of the OSL was lost if the OSLD was not positioned exactly above the stimulating laser.

A potential future application of the OSLDs is to cut them down to 1 mm diameter circles in order to reduce dose gradient averaging in very small fields. Approximately 18 % of the OSL was observed to originate in the central 1 mm diameter circle. Therefore cutting down the OSLDs will decrease the raw signal by a factor of five.

Inconsistent raw signal values were observed in repeated read routines for a group of uniformly irradiated OSLDs. The dominant cause of the inconsistency was concluded to be slippage of the hub on the spindle. The inconstancy was reduced but not completely eliminated after replacement of the original hub. Further repairs or preferably spindle redesign will be required because hub slippage introduces errors that may change at any time.

Factors to correct for the wobble of the reader's carousel were estimated from raw signal values and are consistent with dial indicator measurements if raw signal is assumed to be inversely proportionate to the square of the distance to the photomultiplier tube in the reader. The wobble factors have been shown to give the same dosimeter reading (after corrections are applied) in two different recesses. At least some wobble is an inevitable feature of the current reader. There is no evidence to show that the wobble is stable in the long term. Therefore a measurement of the wobble should be repeated annually.

The relationship between raw signal and delivered dose for the OSL system is linear below 4 Gy and progressively more sub-linear above 4 Gy. A non-linearity correction has been estimated and can be applied to the raw signal of each OSLD. The response of the

OSL system has no statistically significant dependence on nominal dose rate or irradiation angle.

Fading and energy corrections were found to be unimportant compared to the read routine inconsistency. Any need for dose history correction was eliminated in the proposed calibration method, as it is recommended that all OSLDs be calibrated before each use.

A method was devised which allows the calculation of an unknown dose from the values reported by the reader and incorporates a number of necessary corrections. Patient doses calculated via the OSL system's internal method or with the more comprehensive set of corrections devised in this project have significant uncertainty and may potentially lead to incorrect dose monitoring. An error in an in vivo dosimetry estimate may lead to an ill-informed clinical decision.

Therefore the OSL system should not be used clinically until the issues of read routine inconsistency and carousel wobble can be fully resolved. This recommendation and the above conclusions apply only to the specific devices used at WBRC and do not necessarily apply to other products by the same manufacturer or others.As of March 2014, WBRC will soon begin a trail of first treatment in vivo for all external beam photon patients with diodes.

13.2. Future work

As the project progressed, it became apparent that there was considerable noise in the results. Therefore most experiments in this project involved irradiations of 2 Gy because this dose was thought to lead to a preferable signal-to-noise ratio. Measurements at lower dose levels or smaller increments should be conducted when the reader is more stable.

Further work is required to fill the gaps in the SEM investigation. Such work might include SEM examination of both faces (top and bottom) of the OSLD; EDS mapping; or transmission electron microscopy (TEM) imaging to attempt to quantitatively describe the distribution of Al_2O_3:C crystals in both size and spacing. Additionally, an investigation of Al_2O_3:C dosimeters from several vendors would be most interesting.

Appendix A. Uncertainty budget

A.1. Components

A.1.1. Absorbed dose to water calibration factor, $N_{D,W}$ and element correction factor, k_{ECF}

The uncertainty in the sensitivity of an individual OSLD is shared between $N_{D,W}$ and k_{ECF}. The calibration factor is a single value for a batch of OSLDs and is chosen so that the average value of k_{ECF} is 1. In order to estimate the uncertainty, the three hundred OSLD raw signal readings, S, were collected. Corrections k_L, k_W and k_T were applied then each resulting dosimeter readings, M, were divided by the known delivered dose. The standard uncertainty of the mean was 3.5 % of the mean.

A.1.2. Raw signal from the PMT, S

The manufacturer has not provided an uncertainty specification for the reader. The raw signal from the PMT for a 1 Gy irradiation is approximately 100,000 counts and is given with a precision of 1 count. Therefore a type B evaluation of uncertainty would be very small (10^{-3} %). There will be statistical fluctuations in the performance of the PMT but these are hidden behind bigger sources of uncertainty so the uncertainty in S was ignored.

A.1.3. Non-linearity correction factor, k_L

The curve fit for the non-linearity correction factor in chapter 10 had an average standard uncertainty of 2.2 %.

A.1.4. Wobble correction factor, k_W

The curve fit for the wobble correction factor in chapter 9 had an average standard uncertainty of 1.1 %.

A.1.5. The read routine correction factor, k_T

If two reference OSLDs are used in every clinical measurement then the standard uncertainty in k_T is 2.4 %.

A.1.6. Signal loss from light exposure

The experiments in this project were conducted under more idealised conditions that eliminated exposure of the OSLDs to ambient light. Clinical use of the OSLDs will inevitably result in exposure during packaging, unpacking and loading because the

OSLDs are very hard to see in a darkened room. Light will be required to prevent loss or inadvertent substitution of OSLDs. Two minutes of ambient light exposure can lead to a 3.3 % loss in stored dose signal.

A.1.7. Excluded influence quantities

Several known influence quantities were excluded from this project because they could not be accurately estimated (see Appendix B). The lack of knowledge of these influence quantities increases the uncertainty in the calculated dose but by an unknown amount.

A.2. Combined

The uncertainty components are independent and therefore were combined by taking the square-root of the some of their squares.

Table A.1. Calculated results for OSLDs in five groups irradiated at different dose rates. M_N is the normalised mean dosimeter reading and U is the expanded uncertainty in the normalised mean.

Source	Component
$N_{D,W}$ & k_{ECF}	3.5 %
S	0 %
k_L	2.2 %
k_W	1.1 %
k_T	2.4 %
Ambient light	3.3 %
Excluded factors	?
TOTAL	> 5.9 %

Appendix B. Excluded influence quantities

B.1. Readout signal depletion

As some dose information is lost from an OSLD when stimulated then a correction should be made to any subsequent reads. The obvious test for signal depletion with each read routine is to conduct a sequence of many repeated readout routines on the same OSLD. The results of one such sequence is shown in Figure B.1 as taken from the experiment in subsection 8.3.3. The mean raw signal, S, of five uncollimated OSLDs shows a downward trend but the correlation with a linear fit very weak, $R^2 = 0.40$. Therefore a correction should not be derived from this data.

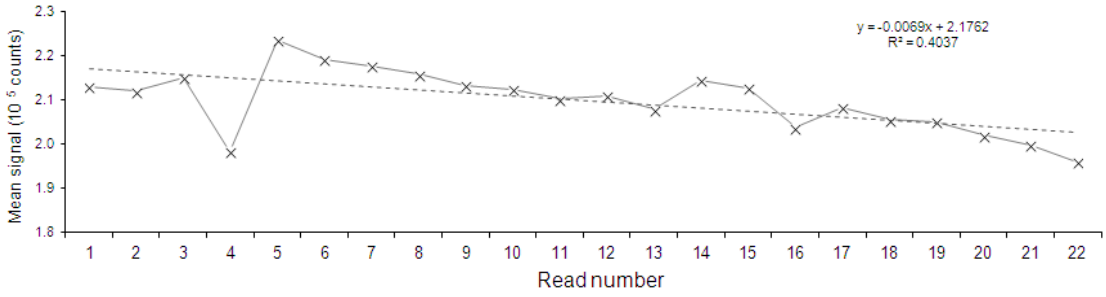

Figure B.1. Mean raw signal for each of twenty-two repeated read routines.

Using the information in Figure 8.8, the read routines were grouped by the estimated overshoot (left dominance; $DOM_{LR} < 0$) or undershoot (right dominance; $0 < DOM_{LR} < 1$) of the spindle for the read routine (Figure B.2). Some of the stimulation may have been blocked by the carousel in the "right very dominant" group ($DOM_{LR} > 1$).

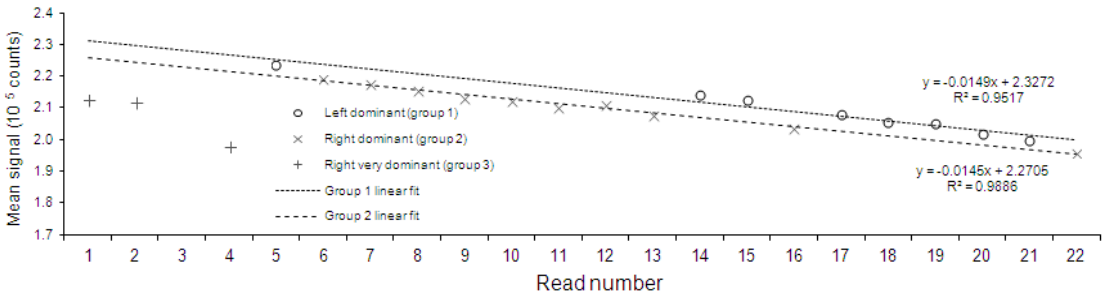

Figure B.2. Mean raw signal for each of twenty-two repeated read routines separated into three groups. Linear fits are shown for two groups (left dominant; $DOM_{LR} < 0$) and (right dominant; $0 < DOM_{LR} < 1$).

The correlation with the linear fit within both the left and right dominant groups is strong, $R^2 > 0.95$.The gradient is 0.6 % of the mean signal axis intercept for both groups.

If different parts of the OSLD are being stimulated when the spindle overshoots or undershoots then this 0.6 % value may be an estimate of the signal depletion with each read routine. Unfortunately, without collimating the stimulating laser for several OSLDs in every future read routine, as in subsection 8.2.3, any overshoot or undershoot is unknown. Additionally, when the overshoot or undershoot is extreme, the stimulation may be blocked and the raw signal may be unexpectedly lower.

Therefore no distinct readout signal depletion correction was possible within this project.

B.2. Fading and afterglow

The raw signal output by the reader for a given dose delivered to an OSLD will change with time since irradiation due to afterglow and fading. The only mechanisms within this project to address these effects were fixing the time between irradiation and readout and the read routine correction factor k_T. Both mechanisms worked to cancel out any time effects but there was no attempt made to quantify them.

To quantify the time effects, an experiment could be designed in which a large set of OSLDs are identically irradiated and then read out in smaller sub-sets at different time intervals. Reference OSLDs would be required to estimate k_T in order to correct for hub slippage (overshoot and undershoot) which is thought to cause instability in the output of the reader. If the reference OSLDs are irradiated with the large set, then the factor kT will also correct away the time effects. If they are irradiated at a constant time before each sub-set in read out, then the k_T will not eliminate the reader instability.

Unfortunately, there is no way to accurately quantify fading and afterglow while the much larger effect of reader instability remains.

B.3. Change in sensitivity after bleaching

An experiment was conducted to observe any changes in the response of the OSLDs when used (irradiated, read out and bleached) several times but this experiment instead

revealed the reader instability. Change in sensitivity after bleaching was subsequently ignored because its effect would be masked by the instability. A useful future experiment would be to repeat the linearity experiment four or five times using the same OSLDs – bleached before each repeat.

References

ARPANSA 2011, *National Directory for Radiation Protection, Radiation Protection Series Publication No. 6,* Australian Radiation Protection and Nuclear Safety Agency, Canberra, Australia.

Aznar, MC, Andersen, CE, Bøtter-Jensen, L, Bäck, SÅJ, Mattsson, S, Kjær-Kristoffersen, F & Medin, J 2004, 'Real-time optical-fibre luminescence dosimetry for radiotherapy: physical characteristics and applications in photon beams', *Physics in Medicine and Biology,* vol. 49, pp. 1655-1669.

Barrett, A, Dobbs, J, Morris, S & Roques, T 2009, *Practical radiotherapy planning,* 4th edn, Hodder Arnold, London, UK.

Beddar, AS, Law, S, Suchowerska, N & Rockwell Mackie, T 2003, 'Plastic scintillation dosimetry: Optimization of light collection efficiency', *Physics in Medicine and Biology,* vol. 48, no. 9, pp. 1141-1152.

Bentley, RE 2003, *Uncertainty in Measurement: The ISO Guide,* National Measurement Laboratory, Linfield, Australia.

BIPM 2006, *The International System of Units (SI),* 8th edn, Bureau International des Poids et Mesures, Sèvres, France.

BIPM 2008, *Evaluation of measurement data - Guide to the expression of uncertainty in measurement,* Bureau International des Poids et Mesures, Sèvres, France.

Boag, A, Hughes, AE, Glenn, AM, Muster, TH & McCulloch, D 2011, 'Corrosion of AA2024-T3 Part I: Localised corrosion of isolated IM particles', *Corrosion Science,* vol. 53, no. 1, pp. 17-26.

Brady, Z 2012, 'Radiation Doses and Risks from Paediatric Computed Tomography', PhD thesis, RMIT University, Melbourne, Australia.

Bucciolini, M, Buonamici, FB, Mazzocchi, S, De Angelis, C, Onori, S & Cirrone, GAP 2003, 'Diamond detector versus silicon diode and ion chamber in photon beams of different energy and field size', *Medical Physics,* vol. 30, no. 8, pp. 2149-2154.

Bushberg, JT, Seibert, JA, Jr, EML & Boone, JM 2002, *The essential physics of medical imaging,* 2nd edn, Lippincott, Williams & Wilkins, Philadelphia, USA.

Butson, MJ, Yu, PKN, Cheung, T & Metcalfe, P 2003, 'Radiochromic film for medical radiation dosimetry', *Materials Science and Engineering,* vol. 41, pp. 61-120.

Charles, PH, Crowe, SB, Kairn, T, Kenny, J, Lehmann, J, Lye, J, Dunn, L, Hill, B, Knight, RT, Langton, CM & Trapp, JV 2012, 'The effect of very small air gaps on small field dosimetry', *Physics in Medicine and Biology,* vol. 57 no. 2012, pp. 6947-6960.

Danzer, J, Dudney, C, Seibert, R, Robison, B, Harris, C & Ramsey, C 2007, *Optically Stimulated Luminescence of Aluminum Oxide Detectors for Radiation Therapy Quality Assurance* AAPM.

Dark, GG 2013, *Oncology at a glance,* Wiley-Blackwell, Hoboken, USA.

Department of Health 2011, *Victorian clinical governance policy framework*, Department of Health, Victoria, Australia, viewed 2013-04-16, http://docs.health.vic.gov.au/docs/doc/4C6559130DA88FD5CA257902000D5EFA/$FILE/clin_gov_pol_framework.pdf.

Dunn, L, Lye, J, Kenny, J, Lehmann, J, Williams, I & Kron, T 2013, 'Commissioning of optically stimulated luminescence dosimeters for use in radiotherapy', *Radiation measurements,* vol. 51-52, pp. 31-39.

Dutreix, A, Bjärngard, BE, Bridier, A, Mijnheer, B, Shaw, JE & Svensson, H 1997, *Monitor Unit Calculation for High Energy Photon Beams* ESTRO, Brussels, Belgium.

Faull, C, de Caestecker, S, Nicholson, A & Black, F (Eds) 2012, *Handbook of Palliative Care* Wiley-Blackwell, Hoboken, USA.

Hall, EJ & Giaccia, AJ 2006, *Radiobiology for the radiologist,* 6th edn, Lippincott Williams & Wilkins, Philadelphia, USA.

Halliday, D, Resnick, R & Walker, J 2001, *Fundamentals of physics,* 6th edn, John Wiley and Sons, New York, USA.

Hill, R, Kuncic, Z & Baldock, C 2010, 'The water equivalence of solid phantoms for low energy photon beams', *Medical Physics,* vol. 37, no. 8, pp. 4355-4363.

Holmes-Siedle, A 1974, 'The space-charge dosimeter', *Nuclear Instruments and Methods,* vol. 121, pp. 169-179.

Hoskin, P Ed. 2012, *Radiotherapy in Practice: External Beam Therapy,* 2nd edn, Oxford University Press, Cary, USA.

Howard, M n.d., *Introduction to Crystallography and Mineral Crystal Systems* Bob's Rock Shop, viewed 2013-04-15, http://www.rockhounds.com/rockshop/xtal/index.shtml.

Huyskens, D, Bogaerts, R, Verstraete, J, Loof, M, Nystrom, H, Fiorino, C, Broggi, S, Jornet, N, Ribas, M & Thwaites, DI 2001, *Practical guide for the implementation of in vivo dosimetry with diodes in external radiotherapy photon beams (entrance dose),* ESTRO, Brussels, Belgium.

IAEA 1996, *International basic safety standards for protection against ionizing radiation and for the safety of radiation sources, IAEA Safety Series Number 115,* International Atomic Energy Agency, Vienna, Austria.

IAEA 2000a, *Absorbed dose determination in external beam radiotherapy: an International Code of Practice for dosimetry based on standards of absorbed dose to water, IAEA Technical Report Series 398* International Atomic Energy Agency, Vienna, Austria.

IAEA 2000b, *Lessons learned from accidental exposures in radiotherapy, IAEA Safety Report Series 17* International Atomic Energy Agency, Vienna, Austria.

Ismail, A, Giraud, J-Y, Lu, GN, Sihanath, R, Pittet, P, Galvan, JM & Balosso, J 2009, 'Radiotherapy quality insurance by individualized in vivo dosimetry: State of the art', *Cancer/Radiothérapie,* vol. 13, pp. 182–189.

Johnson, RA & Bhattacharayya, GK 1992, *Statistics Principles and Methods,* 2nd edn, John Wiley & Sons, Inc., New York, USA.

Jursinic, PA 2007, 'Characterization of optically stimulated luminescent dosimeters, OSLDs, for clinical dosimetric measurements', *Medical Physics,* vol. 34, no. 12, pp. 4594-4604.

Karzmark, CJ, Nunan, CS & Tanabe, E 1993, *Medical electron accelerators,* McGraw-Hill, New York, USA.

Khan, FM 2003, *The physics of radiation therapy,* 3rd edn, Lippincott Williams & Wilkins, Philadelphia, USA.

Kim, DW, Chung, WK, Shin, DO, Yoon, M, Hwang, U-J, Rah, J-E, Jeong, H, Lee, SY, Shin, D, Lee, SB & Park, SY 2012, 'Dose response of commercially available optically stimulated luminescent detector, Al_2O_3:C for megavoltage photons and electrons', *Radiation Protection Dosimetry,* vol. 149, no. 2, pp. 101-108.

Klein, EE, Hanley, J, Bayouth, J, Yin, F-F, Simon, W, Dresser, S, Serago, C, Aguirre, F, M, L, Arjomandy, B & Liu, C 2009, 'Task Group 142 report: Quality assurance of medical accelerators', *Medical Physics,* vol. 36, no. 9, pp. 4197-4212.

Klevenhagen, SC, Aukett, RJ, Harrison, RM, Moretti, C, Nahum, AE & Rosser, KE 1996, 'The IPEMB code of practice for the determination of absorbed dose for X-rays below 300 kV generating potential (0.035 mm Al-4 mm Cu HVL; 10-300 kV generating potential)', *Physics in Medicine and Biology,* vol. 41, no. 12, pp. 2605-2625.

Leng, Y 2009, *Materials Characterization: Introduction to Microscopic and Spectroscopic Methods,* 1st edn, Wiley, Chicester, UK.

Marks, LB, Yorke, ED, Jackson, A, Ten Haken, RK, Constine, LS, Eisbruch, A, Bentzen, SM, Nam, J & Deasy, JO 2010, 'Use of Normal Tissue Complication Probability Models in the Clinic', *International Journal of Radiation Oncology*Biology*Physics,* vol. 76, no. 3, Supplement, pp. S10-S19.

McKeever, SWS & Chen, R 1997, 'Luminescence models', *Radiation measurements,* vol. 27, no. 5/6, pp. 625–661.

Metcalfe, P, Kron, T & Hoban, P 2007, *The Physics of Radiotherapy X-rays and Electrons,* Medical Physics Publishing, Madison, USA.

Millar, M, Cramb, J, Das, R, Ackerly, T, Brown, G & Webb, D 1996, *Recommendations for the safe use of external beams and sealed brachytherapy sources in radiation oncology,* Australasian College of Physical Scientists and Engineers in Medicine, Mascot, Australia.

Mould, RF 1989, *Introductory Medical Statistics.,* Adam Hilget, Bristol, UK.

New York City department of health and mental hygiene - office of radiological health 2005, *ORH information notice 2005-01*, New York State Department of Health, viewed 2013-01-02, http://www.health.ny.gov/environmental/radiological/radon/radioactive_material_licensing/docs/berp2005_1.pdf.

Niroomand-Rad, A, Blackwell, CR, Coursey, BM, Gall, KP, Galvin, JM, McLaughlin, WL, Meigooni, AS, Nath, R, Rodgers, JE & Soares, CG 1998, 'Radiochromic film dosimetry: Recommendations of AAPM Radiation Therapy Committee Task Group 55', *Medical Physics,* vol. 25, no. 11, pp. 2093-2115.

Oldham, M 2007, 'Radiation sensitive film and gels', in Mayles, P, Nahum, A & Rosenwald, J-C (Eds), *Handbook of Radiotherapy Physics: Theory and Practice,* Taylor & Francis, London, UK, pp. 321-331.

Piermattei, A, Fidanzio, A, Stimato, G, Azario, L, Grimaldi, L, D'Onofrio, G, Cilla, S, Balducci, M, Gambacorta, MA, Di Napoli, N & Cellini, N 2006, 'In vivo dosimetry by an aSi-based EPID', *Medical Physics,* vol. 33, no. 11, pp. 4414-4422.

RANZCR 2011, *Tripartite Radiation Oncology Practice Standards,* Royal Australian and New Zealand College of Radiologists, Sydney, Australia.

Reft, CS 2009, 'The energy dependence and dose response of a commercial optically stimulated luminescent detector for kilovoltage photon, megavoltage photon, and electron, proton, and carbon beams', *Medical Physics,* vol. 36, no. 5, pp. 1690-1699.

Roberts, KB, Chen, Z & Seropian, S 2008, 'Total-body and Hemibody irradiation', in Halperin, EC, Perez, CA & Brady, LW (Eds), *Perez and Brady's principles and practice of radiation oncology,* 5th edn, Lippincott Williams & Wilkins, Philadelphia, USA, pp. 364-377.

Rosenfeld, AB 2011, 'Advanced Semiconductor Dosimetry in Radiation Therapy', *AIP Conference Proceedings,* vol. 1345, pp. 48-74.

Scarboro, SB, Followill, DS, Kerns, JR, White, RA & Kry, SF 2012, 'Energy response of optically stimulated luminescent dosimeters for non-reference measurement locations in a 6 MV photon beam', *Physics in Medicine and Biology,* vol. 57, pp. 2505-2515.

Schembri, V & Heijmen, BJM 2007, 'Optically stimulated luminescence (OSL) of carbon-doped aluminum oxide (AI_2O_3:C) for film dosimetry in radiotherapy', *Medical Physics,* vol. 34, no. 6, pp. 2113-2118

Seco, J & Evans, PM 2006, 'Assessing the effect of electron density in photon dose calculations', *Medical Physics,* vol. 33, no. 2, pp. 540-552.

Şerifaki, K, Böke, H, Yalçın, Ş & İpekoğlu, B 2009, 'Characterization of materials used in the execution of historic oil paintings by XRD, SEM-EDS, TGA and LIBS analysis', *Materials Characterization,* vol. 60, no. 4, pp. 303-311.

Shin, B 2012, *OSL Bluelight Software User's & Service Manual version 1.2,* Gammasonics Institute of Medical Research Pty. Ltd., Five Dock, Australia.

Van Dam, J & Marinello, G (Eds) 2006, *Methods for in vivo dosimetry in external radiotherapy,* ESTRO, Brussels, Belgium.

Van Dyk, J, Barnett, RB & Battista, JJ 1999, 'Computerized radiation treatment planning systems', in Van Dyk, J Ed. *The modern technology of radiation oncology,* Medical Physics Publishing, Madison, USA, pp. 231-286.

Van Dyk, J & Taylor, JS 1999, 'CT simulators', in Van Dyk, J Ed. *The modern technology of radiation oncology,* Medical Physics Publishing, Madison, USA, pp. 131-168.

Vladár, AE & Postek, MT 2008, 'The Scanning Electron Microscope', in Orloff, J Ed. *Handbook of Charged Particle Optics, Second Edition,* CRC Press, Boca Raton, USA, pp. 437-496.

WBRC Patient Information Committee 2013, *Patient Information Booklet - External Beam Radiotherapy,* Alfred Health, Melbourne, Australia.

Williams, M & Metcalfe, P 2010, 'Radiochromic Film Dosimetry and its Applications in Radiotherapy', manuscript, *4th Summer School on Solid State Dosimetry,* Wollongong, Australia.

Wong, CJ, Ackerly, T, He, C, Patterson, W, Powell, CE, Ho, A, Qiao, G, Solomon, DH, Meder, R & Geso, M 2007, 'High-resolution measurements of small field beams using polymer gels', *Applied Radiation and Isotopes,* vol. 65, no. 10, pp. 1160-1164.

Yoe, C 2011, *Principles of Risk Analysis,* CRC Press, Boca Raton, USA.

Yukihara, EG, Gasparian, PBR, Sawakuchi, GO, Ruan, C, Ahmad, S, Kalavagunta, C, Clouse, WJ, Sahoo, N & Titt, U 2010, 'Medical applications of optically stimulated luminescence dosimeters (OSLDs)', *Radiation measurements,* vol. 45, pp. 658–662.

Yukihara, EG & McKeever, SWS 2011, *Opically stimulated luminescence funimentals and applications,* John Wiley & Sons Ltd., Chichester, UK.

Yukihara, EG, Whitley, VH, McKeever, SWS, Akselrod, AE & Akselrod, MS 2004, 'Effect of high-dose irradiation on the optically stimulated luminescence of Al_2O_3:C', *Radiation measurements,* vol. 38, pp. 317–330.